

Structure-Based Design of Grp94-Selective Inhibitors

By

Sanket Mishra

Submitted to the graduate degree program in Medicinal Chemistry and the Graduate Faculty of The University of Kansas in partial fulfillment of the requirements for the degree of Master of Science.

Committee Members:

Brian Blagg, Ph.D.
Chairperson

Apurba Dutta, Ph.D.

Michael Clift, Ph.D.

Date Defended: December 17, 2014

The thesis committee for Sanket Mishra
certifies that this is the approved version of the following dissertation:

Structure-Based Design of Grp94-Selective Inhibitors

Brian Blagg, Ph.D.

Chairperson

Date:

Date approved:.....

Abstract

Heat shock protein 90 KDa (Hsp90) belongs to family of proteins called molecular chaperone that are associated with protein folding and maturation. Hsp90 clients play a critical role in the pathogenesis of diseases such as cancer, neurodegeneration and infection. Currently, clinical trials are underway for various Hsp90 inhibitors, however, all of these inhibitors exhibit pan-inhibition of all four Hsp90 isoforms, which could be the cause of side effects observed with these inhibitors, including, hepatotoxicity, cardiotoxicity, and renal toxicity. Hence, the development of isoform selective Hsp90 inhibitor is needed to delineate the role each Hsp90 isoform plays towards the pathogenesis of these toxicities. One such isoform is the ER residing glucose regulated protein (Grp94), which is important for cellular communication and adhesion.

Co-crystallization studies of radamide, an Hsp90 pan-inhibitor developed in our lab established that there exists a unique hydrophobic pocket found only in Grp94. To probe this pocket, two approaches have been investigated; 1) des-quinone analogs of radamide and 2) employing cis-amide isosteres.

The co-crystal structure of cis-amide isostere compound BnIm bound to Grp94 and Hsp90 led to the discovery of a novel pocket in Grp94 due to ligand induced conformational change. This pocket has been probed by the modification of SNX 2112, a *pan*-inhibitor of Hsp90 that is currently undergoing clinical evaluation. These modifications have resulted in the identification of ACO1, which exhibits good potency and high selectivity towards Grp94. Rationale for the design of ACO analogs is discussed alongside their inhibition activities.

Acknowledgments

The work described in this thesis would not have been possible without the guidance, criticism and help from my colleagues.

First of all, I would like to express my gratitude to my advisor, Dr. Brian Blagg for mentoring and support throughout my research. I am also grateful to the members of the Blagg's group who have been helpful in shaping this thesis, in particular Jinbo, Anuj, Vince and Aaron, Mercy and Gaurav.

I am thankful to committee members Dr. Apurba Dutta and Dr. Michael Clift for their valuable time and their guidance.

Support from family and friends has been critical in providing me with strength to face the challenges presented during the span this work.

Finally, I would like to thank the Department of Medicinal Chemistry and the funding agencies for providing me with resources to complete my research work.

Table of Contents

List of Sections:

Chapter 1

Hsp90 Structure, Function and Therapeutic Potential

1. Introduction.....	2
2. Hsp90 Structure.....	3
3. Hsp90 Function.....	4
4. Hsp90 Therapeutic Potentials	5
4.1. Cancer	7
4.2. Neurodegenerative diseases.....	8
4.3. Infectious diseases.....	10
5. Hsp90 Inhibitors.....	10
5.1 N-terminal Inhibitors.....	11
5.1.1 Natural products and their semi-synthetic derivatives.....	11
5.1.2 Synthetic small molecule inhibitors.....	12
5.2 C-terminal Inhibitors.....	15
5.2.1 Novobiocin and Related Natural Products.....	15
5.2.2 Epigallocatechin-3-Gallate.....	16
5.2.3 Cisplatin.....	16
5.3. Co-chaperone/Hsp90 disrupters.....	17
6. Conclusion and Future Directions.....	18

Chapter 2

Structure Activity Relationship Studies of Radamide and Its *cis*-amide isostere Analogues to Develop Grp94-Selective Inhibitors.

1. Introduction.....	28
2. Structure Activity Relationship (SAR) studies on RDA and BnIm Analogues	32
2.1. <i>des</i> -quinone approach.....	32
2.2 <i>cis</i> -amide isostere approach.....	40
3. Conclusions and Future Directions.....	47
4. Experimental Section.....	48
5. References.....	75

Chapter 3

Discovery of ACO, A Novel Scaffold for Grp94-Selective Inhibition

1. Introduction.....	79
2. Rationale for Design.....	81
3. Synthesis and Evaluation.....	85
4. Conclusion and Future Directions.....	96
5. Experimental Section.....	97
6. References.....	140

List of Figures:

Chapter 1

Figure 1.1 The Crystal structure of yeast Hsp90.....	2
Figure 1.2 The Hsp90-chaperone cycle.....	5
Figure 1.3 Proposed mechanism of Hsp90 inhibition for cancer treatment.....	7
Figure 1.4 Proposed mechanism of induction of heat shock response with Hsp90 N-terminal inhibitors.....	10
Figure 1.5 Structures of Geldanamycin (GDA) and its derivatives 17-AAG and 17-DMAG.....	11
Figure 1.6. Structure of radicicol and related analogues.....	12
Figure 1.7 Structures of purine based analogues.....	13
Figure 1.8 Structures of resorcinolic and benzamide Hsp90 NTD inhibitors.....	14
Figure 1.10 Structures of A4, KU32, DHN2 and NA-2.....	16
Figure 1.11 Structures of EGCG, cisplatin, celastrol, gedunin and Sansalvamide A.....	17

Chapter 2

Figure 2.1 Structures of natural product Hsp90 inhibitors GDA and RDC, and chimeric inhibitor RDA.....	30
Figure 2.2 (A) Co-crystal structures of RDA bound to Hsp90 and Grp94 (B) primary amino acid sequence alignment of Grp94 and Hsp90.....	31

Figure 2.3 A) Synthetic scheme and B) Biological evaluation of the linker RDA analogs using fluorescence polarization assay.....	33
Figure 2.4 A) Synthetic scheme for compounds 5-10 B) Biological evaluation of the 2-substituted RDA analogs using fluorescence polarization assay C) Compounds 6 docked in the Grp94	34
Figure 2.5 A) Synthetic scheme for compounds 11-15 B) Biological evaluation of the 3-substituted RDA analogs using fluorescence polarization assay C) Compounds 12 docked in the Grp94.....	35
Figure 2.6 A) Synthetic scheme for compounds 16-27 B) Biological evaluation of the 4-substituted RDA analogs using fluorescence polarization assay C) Compounds 18 docked in the Grp94 protein.....	36
Figure 2.7 Inhibition of MDA-MB-231 cell migration by compounds 6 and 18	39
Figure 2.8 A) Determination of the binding affinity of the compounds 38-45 towards Grp94 by fluorescence polarization assay using B) Docked pose of BnIm in Grp94 C) Compound 40 docked into Grp94.....	44
Figure 2.9 Crystal structure of BnIm bound to Hsp90 and Grp94.....	45
Figure 2.10 A) Synthetic scheme for the ester analogs of BnIm B) Determination of binding affinity of the compounds 29, 46-48	46

Chapter 3

- Figure 3.1** A) BnIm bound to Hsp90 B) BnIm bound to Grp94 C) Overlay of the Hsp90 and Grp94 crystal structures, showing the movement of the PHE 138 and TYR 139. D) ATP lid movement in Grp94 and Hsp90 bound to BnIm.....81
- Figure 3.2** A) Overlay of BnIm bound to Grp94 and SNX 2112 bound to Hsp90 B) structures of BnIm and SNX 2112 C) Overlay of SNX 2112 with BnIm in Grp94 D) the steric clash between SNX 2112 and induced conformation of Grp94 circled with red.....83
- Figure 3.3** A) Proposed compound for Grp94 selective inhibition. B) Overlay of Grp94 and Hsp90 along with the docked ACO compound. C) Grp94 binding site residues illustrated.....84
- Figure 3.4** A) Apparent K_d for compound **4a**. B) Dose response curve for compound **4a** binding to Grp94 and Hsp90.....87
- Figure 3.5** A) K_d values for linker compounds **16** using fluorescence polarization assay. B) Docking image compound **4a** in Grp94 depicting the cavity around ASN 107.....94
- Figure 3.6** A) Inhibition of MDA-MB-231 cell migration by compounds **15a** and **7e**. B) percent viability of MDA-MB-231 cells determined using MTS assay.....95

List of Schemes:

Chapter 2

Scheme 2.1 Proposed approaches for design of Grp94 selective inhibitors.....32

Scheme 2.2 *cis*-amide constraint employed on the RDA scaffold.....41

Scheme 2.3 Synthesis of the *cis*-amide isostere analogs.....42

Chapter 3

Scheme 3.1. Retrosynthetic analysis of compound **ACO**.....85

Scheme 3.2 Synthetic scheme for compounds **4a-j**.....86

Scheme 3.3 Synthetic scheme for compound **7a-n**.....89

Scheme 3.4 Synthetic scheme for compound **11**.....90

Scheme 3.5 Synthetic route for compounds **15a-c**.....93

List of Tables:

Chapter 1

Table 1.1 Co-chaperones and co-activators that regulate Hsp90 chaperone cycle.....	6
Table-1.2 Six hallmarks of cancer associated with Hsp90 client proteins.....	8

Chapter 2

Table-2.1 Grp94 clients and their role in disease pathogenesis.....	29
Table 2.2 Kd values determined using fluorescence polarization assay for listed compounds using Grp94 and Hsp90.....	38
Table 2.3 Percent viability of MDA-MB-231 cells determined using MTS assay	40
Table 2.4 Determination of binding affinity of compounds 29-33	42
Table 2.5 Determination of binding affinity of the compounds 34-37	43
Table 2.6 Kd Values for BnIm and Compound 40 determined using fluorescence polarization assay towards Grp94 and Hsp90.....	45

Chapter 3

Table 3.1 Determined K_d values for compounds 4b-j	88
Table 3.2 Kd values for linker compounds 7a and 11	91
Table 3.3 Kd values for linker compounds 7b-i	92
Table 3.4 Table 3.4 Kd values for compounds 15a-c and 7m using fluorescence polarization assay.....	94

Abbreviations:

17-AAG = 17-(allylamino)-17-demethoxygeldanamycin

17-DMAG = 17-(2-dimethylaminoethylamino)-17-desmethoxygeldanamycin

ADP = adenosine diphosphate

Aha1 = activator of Hsp90 ATPase homologue-1

Akt = serine/threonine protein kinase

ATP = adenosine triphosphate

Boc = butyloxy carbonyl

CDK4 = cyclin-dependent kinase-4

CHIP = carboxy terminus of Hsp70 interacting protein Heat shock protein 90 (Hsp90)

DMAP = 4-(Dimethyl) aminopyriine

DMSO= dimethyl sulfoxide

DPPF= 1,1'-Bis(diphenylphosphino)ferrocene

EGF-R = epidermal growth factor receptor

ER = Endoplasmic Reticulum

EDCI = 1-ethyl-3-(3-dimethylaminopropyl)carbodiimide

FITC = Fluorescein isothiocyanate

Grp94 = glucose regulated protein 94

GHKL= Family of ATPases consisting of DNA Gyrase, Hsp90, Histidine Kinase, and Mut L

GDA = geldanamycin

GSK3 β = glycogen synthase kinase-3 β

Her2 = human epidermal growth factor receptor-2 (erbB2 synonym)

HOP = Hsp70/Hsp90 organizing protein

Hsc70 = Heat shock cognate isoform of Hsp70

HSF1 = Heat shock factor 1 (Hsp transcription factor)

Hsp = Heat shock protein

IGF I/II = Insulin like growth factor I/II:

KDa = kilodalton

K_d = Dissociation constant

K_i = inhibitory constant

LRP6 = low density lipoprotein receptor-related protein 6

MARK2 = microtubule affinity regulating kinase-2

MCF-7 = Michigan Cancer Foundation – 7 (breast cancer cell line)

MTS= [3-(4,5-dimethylthiazol-2-yl)-5-(3-carboxymethoxyphenyl)-2-(4-sulfophenyl)-2H-tetrazolium, inner salt]

SKBr3 = Sloan-Kettering breast cancer cell line

p23 = chaperone associated protein 23 kDa

p53 = tumor protein 53

ROS = Reactive oxygen species

RDA= radamide

RDC = radicicol

SAR = structure activity relationship

Trap-1/Hsp75 = tumor necrosis factor associated protein

TBAF = tetrabutylammonium fluoride

TPR= tetratricopeptide-containing repeat

TLC= thin layer chromatography

Chapter 1

Hsp90 Structure, Function and Therapeutic Potential

Chapter 1

Introduction

Molecular chaperones such as Heat shock protein 90 (Hsp90) play a key role in protein synthesis by folding nascent polypeptides into their functional conformation, thereby inducing maturation and providing stability to client proteins.^{1,2} Cellular stress such as increased temperature, presence of heavy metals, and oxidative stress cause the denaturation of proteins. In order to rescue these proteins, cells respond with increased levels of Hsp90.^{3,4} Hsp90 is one of the most abundant proteins within the cell and exists as four isoforms; Hsp90 α (inducible) and Hsp90 β (constitutively expressed) are present in cytosol, whereas the Endoplasmic Reticulum (ER) residing glucose regulated protein 94 (Grp94/gp96/endoplasmic reticulum chaperone) and mitochondrial isoform tumor necrosis factor associated protein (Trap-1/Hsp75) are present in a distinct organelle.^{5,6} More than 200 client proteins have been identified that are dependent upon the Hsp90 machinery for their maturation and activation.⁷ These client proteins are critical for cell growth as they are associated with signal transduction, chromatin remodeling, protein trafficking and cell survival. Two classes of Hsp90 client proteins are best characterized, namely, the steroid hormone receptors and protein kinases. In fact, >2/3 of protein kinases, many transcription factors and some E3-ligases, have been found dependent on Hsp90.⁸ Hsp90 clients are mutated and/or overexpressed in many cancers, therefore, inhibition of Hsp90 represents a unique multipronged chemotherapeutic approach to treat cancer by interfering with multiple pathways simultaneously, which forces these client proteins to undergo proteasomal degradation.^{8,9} While inhibition of Hsp90 has been shown to be effective in cancer treatment, induction of Hsp90 however, has been proposed as an approach to treat diseases such as Parkinson's, Alzheimer's, Huntington's, and prion-related diseases caused by the aggregation of proteins.^{2,4}

2. Hsp90 Structure

The Hsp90 molecular chaperone is a member of the GHKL (Gyrase, Hsp90, Histidine Kinase and MutL) subgroup of ATPases, which contain a Bergerat fold.¹⁰ Hsp90 exists as a homodimer with each homodimer comprising three structural domains; A 25 kDa highly conserved N-terminal ATP-binding domain (NTD), a 35 kDa flexible middle domain (MD), and a 12 kDa C-terminal dimerization domain (CTD) (Figure 1.1).³

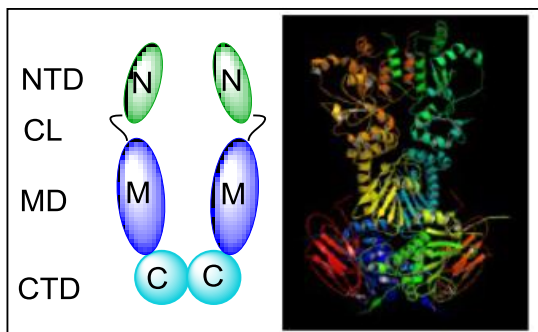


Figure 1.1. The Crystal structure of yeast Hsp90; PDB 2CG9.

ATP binds the NTD ATP-binding site in a unique and bent conformation, which is a characteristic feature exhibited by members of GHKL superfamily.¹¹ The Bergerat fold present in NTD comprises four β - sheets and three α -helices with an ATP-binding pocket located in the middle.¹²⁻¹⁴ Also, in the NTD, a few conserved residues of the Bergerat fold form an “ATP lid” that is closed when ATP is bound, but is open when ADP is bound.¹⁵ The NTD is the major site of ATP hydrolysis in Hsp90 and represents the most druggable binding pocket of Hsp90, which is evident by 17 N-terminal inhibitors in clinical trials.¹ The MD is connected to the NTD by a flexible, highly charged linker (CL), and is required for interactions with co-chaperones and client proteins (e.g. Aha1).¹⁶ This domain also regulates ATP hydrolysis in the NTD by interacting with the γ -phosphate of ATP.¹⁷

The CTD is the site for homodimerization of Hsp90¹², and contains MEEVD motif that recognizes the tetratricopeptide-containing repeat (TPR) found in various co-chaperones such as the Hsp70-Hsp90 organizing protein (HOP) and the immunophilins. In eukaryotic Hsp90, opening of the CTD is anticorrelated to closing of the NTD.¹⁸ The CTD has an alternative ATP binding site that allosterically regulates NTD ATPase activity.¹⁹ Natural products such as Novobiocin and EGCG have been found to bind to the CTD ATP binding site and affect the Hsp90 protein folding process.²⁰⁻²²

3. Hsp90 Function

Hsp90 is a multifaceted protein, with functions ranging from folding nascent polypeptides into mature proteins, to solubilizing and refolding aggregated or denatured proteins²³⁻²⁵. In unstressed cells, Hsp90 represents about 1-2 % of total cellular protein, whereas, under stress or in a state of unregulated growth such as cancer, the levels of Hsp90 can rise to 4-6 %, as there is an increased demand for Hsp90 client proteins.²⁴ The Chaperoning cycle involves processing of newly synthesized polypeptides via a heteroprotein complex before its release as a conformationally mature protein (Figure 1.2). Although, Complete elucidation of the Hsp90-mediated protein folding mechanism is yet to be achieved, we now know that it involves various co-chaperones, immunophilins and partner proteins.²⁶ A newly synthesized protein exits the ribosomal machinery as a long linear polypeptide, Hsp70 binds to and stabilizes these polypeptide chains, preventing their aggregation before transferring them to Hsp90, which subsequently folds them into their biologically active conformation.²⁷ The Hsp90 chaperone cycle begins with the association of nascent polypeptides to a complex comprising of Hsp70, Hsp40 and ADP. It is then followed by the binding of Hsp70 interacting protein (HIP), which stabilizes it further.²⁸ The immature protein is then transferred from Hsp70 to Hsp90 via Hsp90-Hsp70 organizing protein (HOP), as HOP can bind to both Hsp70 and the Hsp90 CTD via the TPR domain.²⁹ Co-

chaperones, immunophilins (FKBP51, FKBP52) and partner proteins, also bind the Hsp90 homodimer to form an activated

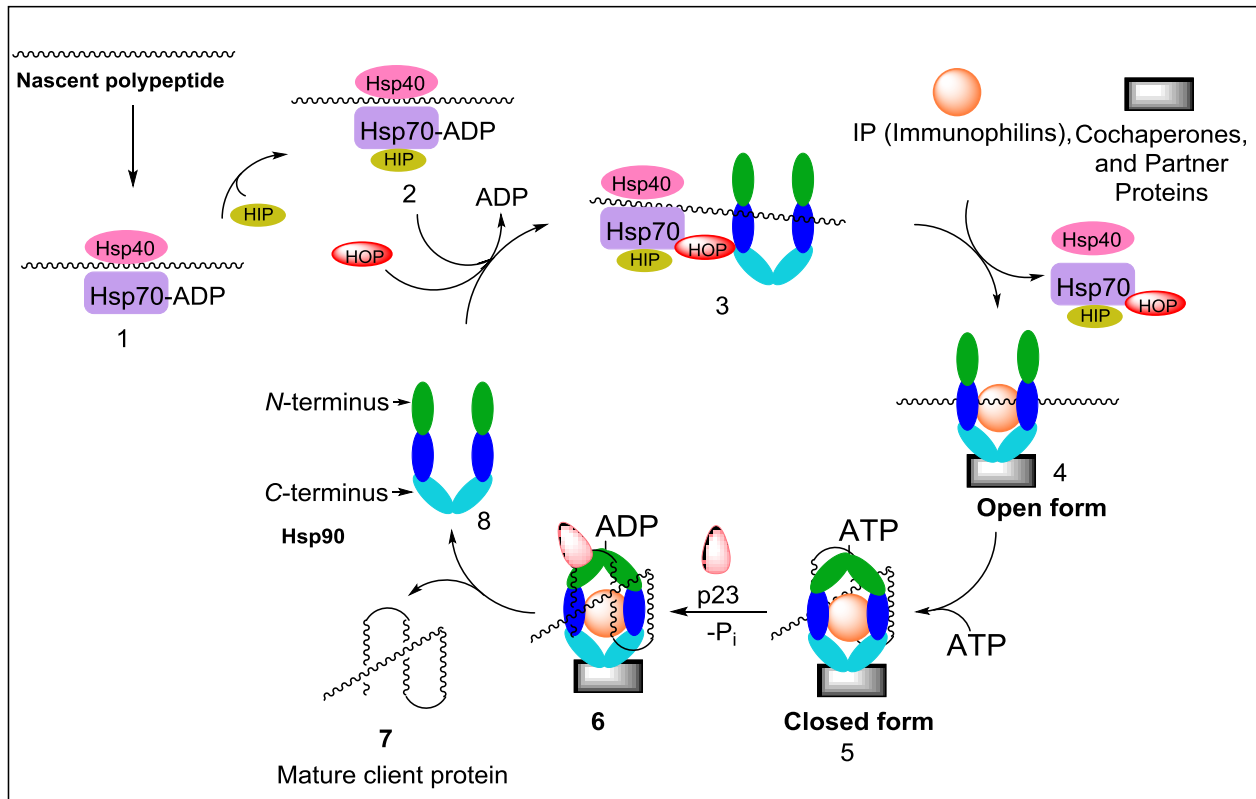


Figure 1.2. The Hsp90-chaperone cycle

heteroprotein complex that simultaneously releases Hsp40, Hsp70, Hip and HOP. After formation of the activated complex, ATP binds to the open NTD and promotes formation of the closed conformation of Hsp90 and clamps around the bound client protein³¹. Small molecules compete with ATP for binding to NTD, and subsequently prevent formation of the closed conformation that makes Hsp90 a catalyst for client protein degradation via the ubiquitin-proteasome pathway³. However, in the presence of ATP, the co-chaperone p23 is recruited to the complex, and further stabilizes the closed Hsp90 complex and inducing ATP hydrolysis, which represents the source of the energy required for client protein maturation³². The mature protein is finally released from the complex along with the dissociation of immunophilins and co-chaperones from the heteroprotein complex.

The Hsp90 chaperone cycle is regulated by a number of co-chaperones and post-translational modifications.⁷ These co-chaperones work in conjunction with Hsp90 to modulate the rate of chaperoning cycle (Table 1.1).^{26, 33} Post-translational modifications to Hsp90 include acetylation, phosphorylation, S-nitrosylation and methylation that control Hsp90 chaperone activity by modulating its affinity for co-chaperones and/or client proteins.³⁴

4. Hsp90 Therapeutic Potentials

Indirect functional disruption of Hsp90 client proteins via inhibition of Hsp90 can represent a useful therapeutic approach for various diseases, as these client proteins carry out a wide range of functions that are critical in disease etiology. For example, client proteins such as signaling tyrosine kinases and steroid hormones receptors are responsible for the progression of various cancers.³⁵ Inhibitors of Hsp90 are being sought for the treatment of cancer, neurodegenerative, and infectious diseases.³⁶

Co-chaperone or Co-activator	Function
Aha1	Stimulates ATPase activity
Cdc37	Mediates activation of protein kinase substrates
CHIP	Involved in degradation of unfolded client proteins
Cyclophilin-40	Peptidyl propyl isomerase
FKBP51 and 52	Peptidyl propyl isomerase
Hop	Mediates interaction between Hsp90 and Hsp70
Hsp40	Stabilizes and delivers client proteins to Hsp90 complex
Hsp70	Stabilizes and delivers client proteins to Hsp90 complex
p23	Stabilizes closed, clamped substrate bound conformation
HIP	Inhibits ATPase activity of Hsp70
PP5	Protein phosphatase 5
Sgt1	Client adaptor, involved in client recruitment
Tom70	Facilitates translocation of pre-proteins into mitochondrial matrix

WISp39	Regulates p21 stability
--------	-------------------------

Table 1.1: Co-chaperones and co-activators that regulate Hsp90 chaperone cycle.

Rapidly growing cancer cells require oncoproteins at increased levels, many of which are Hsp90 dependent clients. Therefore, inhibition of Hsp90 provides an alternate approach to traditional chemotherapy for the treatment of cancer.^{4, 37} While Hsp90 inhibition is beneficial for the treatment of cancer, induction of the pro-survival heat shock response is desired for neurodegenerative disorders in which protein aggregates accumulate. An overall increase in Hsps, causes de-aggregation and solubilization of neurotoxic protein aggregates.³⁸ Hence, drugs that induce Hsp90 at non-toxic levels can serve as a potential treatment for neurodegenerative disorders.

4.1. Cancer

Cancer is a group of diseases that involve uncontrolled cell growth which results from the dysregulation of signaling pathways.³⁹ Recent advances in cancer chemotherapy have focused on perturbing functions of specific proteins involved in these signaling pathways, but resistance often develops via compensatory mechanisms. However, we now know that malignant transformations require multiple interconnected signaling pathways. Therefore, combination therapy has evolved as a useful approach for cancer treatment. Alternatively, inhibition of Hsp90 can provides a combinatorial disruption of multiple client proteins, providing effective anticancer therapy with a single agent. Figure 1.3 explains how client proteins are directed towards degradation after Hsp90 inhibition. Hsp90 inhibitors bind the Hsp90 multiprotein complex and

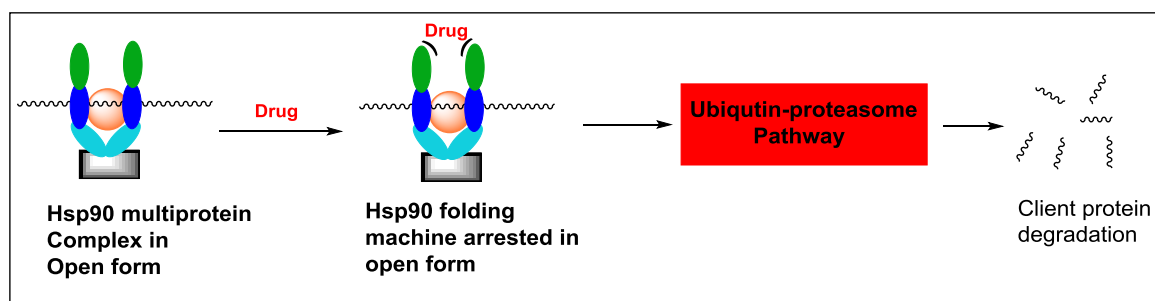


Figure 1.3. Proposed mechanism of Hsp90 inhibition for cancer treatment.

prevent formation of the closed Hsp90 conformation that is needed for the maturation of client proteins. As a result, the complex is directed toward the ubiquitin-proteasome pathway, which leads to degradation of these clients.

Increased Hsp90 expression stabilizes client proteins that are key drivers of malignancy in tumor cells. Hsp90 thereby promotes the maturation of clients distributed amongst all six hallmarks of cancer, such as Her2, Raf1, Akt, and CDK4 (Table-1.2),^{5, 37} which affect signal transduction pathways, tumor-cell survival, proliferation, immortalization, angiogenesis and metastasis.⁴⁰

Hallmarks of Cancer	Client Protein
Evasion of Apoptosis	Akt,Rip,P53,Survivin, Apaf-1,Bcl2, IGF-IR
Sustained Angiogenesis	VEGFR, HIF1,Akt, FAK,Src
Limitless replicative potential	Telomerase
Tissue invasion and metastasis	MMP-2, c-MET
Self-sufficiency in growth signals	EGFR, Raf, Bcr-Abl, ErbB-2, Src, Akt, MEK
Insensitivity to anti-growth signals	Plk-1,Cdk4,Cdk6, Myt-1,cyclin D

Table-1.2. Six hallmarks of cancer associated with Hsp90 client proteins.⁵

There have been apprehensions about the selectivity manifested by Hsp90 inhibitors towards tumor cells, since Hsp90 is present ubiquitously across cell types. However, increasing evidence suggests that Hsp90 inhibitors accumulate to a greater extent in tumor cells than in normal cells. Hence, manifesting differential selectivity towards tumor vs normal cells, thus providing a large

therapeutic window.^{41, 42} Kamal and co-workers demonstrated that the accumulation of Hsp90 inhibitors in tumor cells results from the heteroprotein complex present in cancer cells, whereas in normal cells Hsp90 exists as a homodimer.⁴³ In cancer cells, Hsp90 exists in an activated multiprotein complex with enhanced affinity for ATP or inhibitors. Clinical trials with the Hsp90 inhibitor, 17-AAG, have shown promising results in both phase I and II studies with HER2 over expressing breast cancer patients, serving as a proof-of-concept for Hsp90 inhibition with therapeutic benefits⁶⁴.

4.2. Neurodegenerative diseases

Neurodegenerative diseases are characterized by chronic and progressive dysfunction or loss of neurons. Examples include Alzheimer's (AD), Parkinson (PD), Huntington (HD), Polyglutamine (PGD) and Prion diseases.^{2, 4} Neurodegenerative diseases can be caused by various reasons, however, the accumulation of misfolded/aberrant proteins leading to neuronal toxicity, is a common characteristic observed in most neurodegenerative diseases.⁴⁴ Consequently, prevention of protein aggregation in neuron may serve as a therapeutic strategy for the treatment of these diseases. It has been shown that the binding of NTD inhibitors to Hsp90 causes the release of a transcription factor called heat shock factor-1 (HSF-1) from the Hsp90 multiprotein complex.⁴⁵ Upon release, HSF-1 is trimerized, phosphorylated and translocated to the nucleus, wherein, it induces the heat shock response, which is the overexpression of molecular chaperones, including Hsp27, Hsp40, Hsp70 and Hsp90 (Figure 1.4).⁴⁶ Induction of the heat shock response provides neuroprotection by preventing protein aggregation, resolubilizing aggregated proteins, and promoting the degradation of misfolded and aggregated proteins.⁴⁷ Interestingly, aberrant proteins such as Tau and α -synuclein are also degraded after heat shock induction.^{48, 49} This finding presents a new paradigm for development of drugs against AD and PD. AD is a disease that results from protein misfolding (proteopathy),

and subsequent formation of β -amyloid ($A\beta$) plaques in the brain. In AD, *Tau* hyperphosphorylation results in aggregation of filamentous structures that organize into neurofibrillary tangles.⁵⁰ Hsp90 client proteins cyclin-dependent protein kinase 5 (Cdk5), glycogen synthase kinase-3 β (GSK3 β) and microtubule affinity regulating kinase-2 (MARK2) are known *Tau* kinases. These kinases are dysregulated in AD and hyperphosphorylate *Tau*, leading to neuronal toxicity³³. Another Hsp90 client protein, α -synuclein, has been found to aggregate and form Lewy bodies in neurons causing PD. Administration of the Hsp90 inhibitor, GDA, has been shown to alleviate PD-like symptoms in a transgenic mouse model.⁵¹ Recent studies have found that Hsp90 forms a strong complex with toxic oligomeric α -synuclein and prevents further aggregation in an ATP-independent manner.⁵² Future investigation into the role played by Hsp90 in neurodegenerative diseases may prove useful in development of a therapeutic approach with dual advantage of inhibiting client proteins and simultaneous induction of the prosurvival heat shock response.

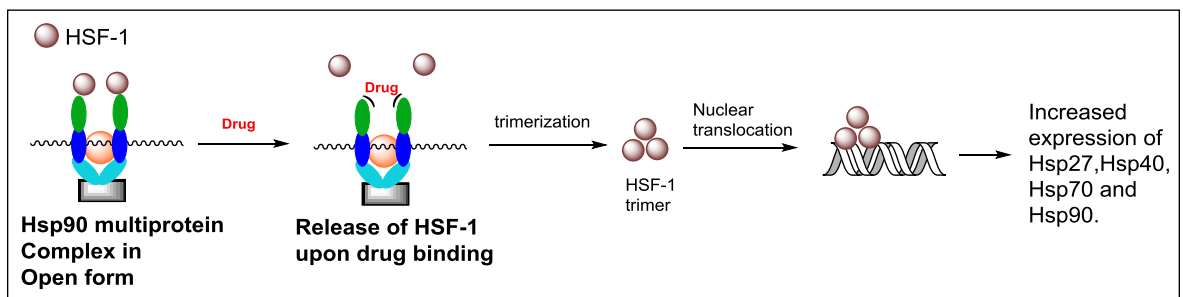


Figure 1.4. Proposed mechanism of induction of heat shock response with Hsp90 N-terminal inhibitors.

4.3. Infectious diseases

Hsp90 is essential for the pathogenesis of many infectious diseases caused by viruses, bacteria, and fungus.^{36, 53} Viruses exploit the protein folding machinery of the host and thus depend upon molecular chaperones, such as Hsp90 for replication. Therefore, inhibition of Hsp90 provides an alternative strategy for the treatment of viral diseases such as hepatitis B, hepatitis C, polio, herpes

simplex and influenza.⁵⁴ Interestingly, Hsp90 inhibitors have been found to be inhibiting viral replication at levels that are not toxic.⁵⁵ Similar to viral infections, Hsp90 client proteins have been associated with the virulence of fungal pathogens, including *Candida albicans*, *Aspergillus fumigatus* and *teereus* and hence, could be targeted for development of antifungal agents.⁵⁶⁻⁵⁷

5. Hsp90 Inhibitors

There has been considerable progress towards the development of Hsp90 inhibitors in past few years, beginning with first generation compounds that were derived from natural products to second generation small molecules based on rational design. These inhibitors interrupt Hsp90 chaperone activity by competing with ATP or by binding Hsp90 to regulate ATPase activity and Hsp90 co-chaperone interactions. Hsp90 inhibitors are broadly divided into three categories; (1) N-terminal inhibitors, (2) C-terminal inhibitors, and (3) others, which will be discussed below.

5.1. N-terminal Inhibitors

5.1.1. Natural products and their semi-synthetic derivatives

The natural product, geldanamycin (GDA) was the first Hsp90 inhibitor identified and is a benzoquinone ansamycin isolated from fermentation broth of *Streptomyces hygroscopicus* in 1970.⁵⁸ GDA was thought to manifest anti-proliferative activity through inhibition of the v-Src oncogene,⁵⁹ until Whitesell and Neckers revealed that GDA exerted its activity through the inhibition of Hsp90 in 1994.⁶⁰ Finally, by attainment of co-crystal, it was established that GDA is a competitive inhibitor of the N-terminal ATP binding site, and upon binding, restrains Hsp90 in its ADP bound form, and disrupts the chaperone cycle.^{61, 62} Although GDA exhibits promising anticancer activities against various cell lines *in vitro*, it failed as a clinical candidate, primarily as a result its poor solubility, *in vivo* stability, and hepatotoxicity.⁶³ However, it has

been used as a chemical probe to identify Hsp90 client proteins and to study the role of Hsp90 during malignant transformations. Subsequent structure-activity relationship studies on semisynthetic derivatives of GDA led to the development of 17-(allylamino)-17-demethoxygeldanamycin (17-AAG) and 17-(2-dimethylaminoethylamino)-17-desmethoxygeldanamycin (17-DMAG), which manifest an improved toxicity profile and are currently undergoing clinical investigation.^{64, 65}

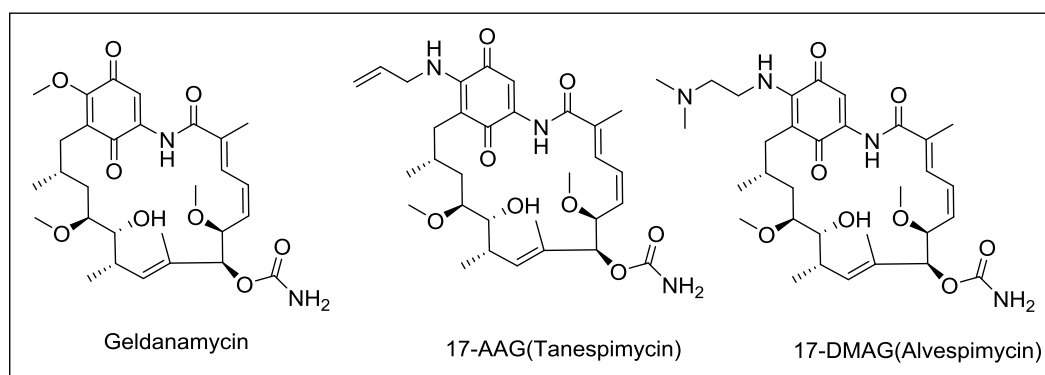


Figure 1.5. Structures of Geldanamycin (GDA) and its derivatives 17-AAG and 17-DMAG

Radicalol (RDC) is a macrocyclic lactone isolated from the fungi, *Monocillium nordinii* and *Monosporium bonorden*, as an antifungal agent in 1953⁶⁶. RDC was believed to be a tyrosine kinase inhibitor, but later studies confirmed it as an inhibitor of the Hsp90 N-terminus (Kd= 14nM).⁶⁷

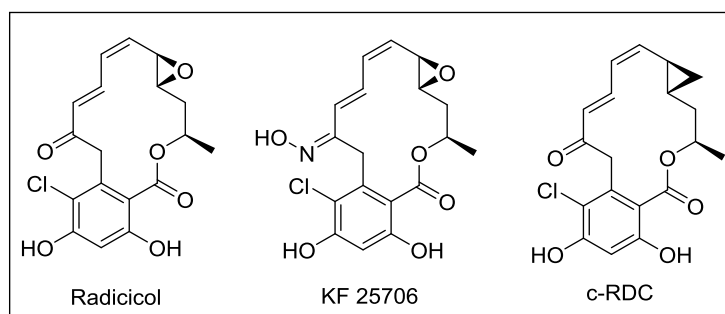


Figure 1.6. Structure of radicalol and related analogues.

RDC exhibits promising anticancer activity *in vitro*, but not *in vivo*, likely due to the $\alpha,\beta,\gamma,\delta$ -unsaturated ketone and epoxide, which make it prone to rapid metabolism.⁶⁸ Therefore, SAR studies have focused on the identification of analogues with improved *in vivo* stability. Modifications such as the oxime in KF 25706, have led to the development of derivatives that manifest potent inhibitory activity *in vitro* as well as in human tumor xenograft models.⁶³ Furthermore, replacement of the labile allylic epoxide with a cyclopropyl ring (cycloproparadicicol, c-RDC) was shown to not compromise its inhibitory activity.⁶⁹ Although, RDC and its derivatives could be potential candidates, there are no clinical reports for the use of this class of natural product compounds yet.

5.1.2 Synthetic small molecule inhibitors

Limited availability, challenging synthetic accessibility, and the toxicity associated with these natural products necessitated the discovery of new small molecule inhibitors. In 2001, Chiosis and co-workers used X-ray crystallographic analysis and molecular modeling to design PU3, which contained a purine scaffold and became the first known synthetic inhibitor of Hsp90. PU3 manifested low micromolar affinity ($K_d = 15\text{-}20\ \mu\text{M}$) for the Hsp90 N-terminus and moderate anti-proliferative activity ($IC_{50} = 50\ \mu\text{M}$) against MCF-7 breast cancer cells.⁷⁰ Modifications to the purine scaffold led to identification of PU24FC1, which exhibits improved anticancer activity both in *in vitro* and *in vivo*.⁷¹ CNF2024/BIIB021 is an optimized purine-based molecule that was identified in 2005 and became the first purine-based inhibitor to enter clinical trials.⁷² Debio 0932 represents another molecule derived from the purine scaffold that has subsequently entered clinical trials for the treatment of solid tumors and lymphomas.⁶⁴

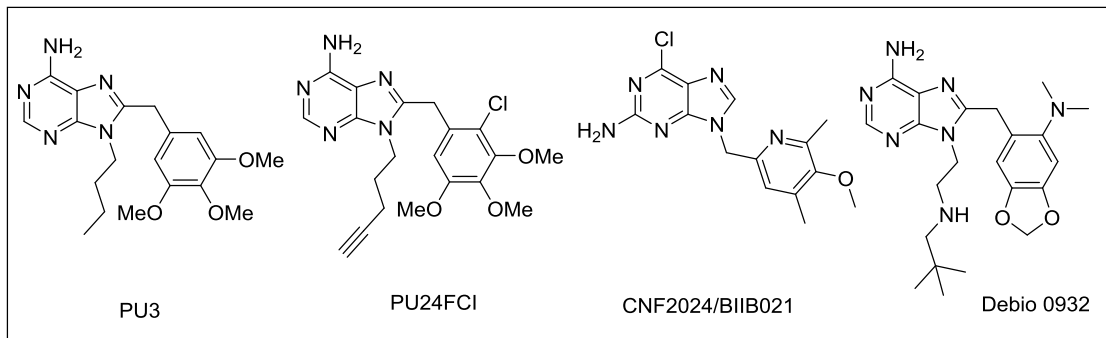


Figure 1.7. Structures of purine based analogues.

After it was determined that small molecules could effectively inhibit Hsp90 function, pharmacophore hit discovery efforts were initiated by the pharmaceutical industry and high throughput screening (HTS) campaigns were launched. One such HTS led to the identification of the 3,4-diarylpyrazole scaffold containing compound CCT018159, which manifested potent ATPase inhibitory activity against yeast Hsp90 (IC₅₀ = 7.1 μM).⁷³ It was confirmed through protein crystallographic studies that CCT018159 binds deep into the ATP pocket of the Hsp90 N-terminal domain, and that the resorcinol ring and pyrazole nitrogen engage in water-mediated hydrogen bonding interactions.⁷⁴ In another such HTS effort, Novartis Research Foundation screened a library of 1,000,000 compounds and identified two lead compounds, G3129 and G3130, which also contained the resorcinol pharmacophore. Co-crystal structures of G3129 bound to Hsp90⁷⁵ helped Dymock and co-workers to develop, VER49009 (ATPase IC₅₀ = 0.14 μM), which contains an amide group that provides additional interactions with Gly97 within the Hsp90 N-domain.⁷⁶

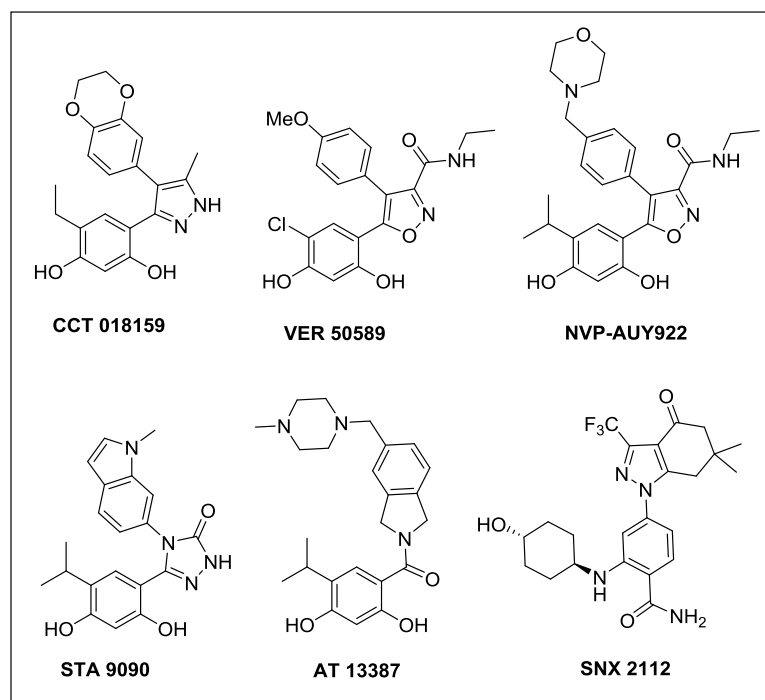


Figure 1.8. Structures of resorcinolic and benzamide Hsp90 NTD inhibitors.

Further exploration involved the replacement of the pyrazole with an isoxazole which led to VER50589, a compound that exhibited both higher affinity and increased cellular uptake ($K_d = 4.5 \text{ nM}$).⁷⁷ Finally, an optimized isoxazole analog, VER52296/NVP-AUY922, entered clinical trials in 2008 and is currently being evaluated in phase I/II for the treatment of solid malignancies.⁷⁸ STA-9090 is another resorcinol derived compound, and manifest Hsp90 inhibition with a K_d of 10 nM, and is currently under clinical evaluations for metastatic breast cancer⁷⁹. A fragment based approach resulted in the discovery of AT13387, a resorcinol containing compound with a dihydroisoindole amide. AT13387 shows anticancer activity comparable to 17-AAG and is currently in clinical trials for refractory gastrointestinal stromal tumors.⁸⁰ Benzamides represent another interesting class of Hsp90 N-terminal inhibitors, such as SNX-2112, which was identified through an affinity purification technique, SNX-2112 manifests a K_d of 3 nM against Hsp90 α and β , and has re-entered clinical trials after being withdrawn due to ocular toxicity.^{81, 82}

5.2. C-terminal Inhibitors

5.2.1. Novobiocin and Related Natural Products

The coumarin containing antibiotics such as novobiocin (NB), chlorobiocin, and coumermycin A1 are known inhibitors of enzyme DNA gyrase and have been utilized extensively as anti-infectious agents for multi-resistant gram-positive bacterial infections.⁸³ In 2000, Neckers and co-workers found that NB was a weak inhibitor of the Hsp90 C-terminal nucleotide binding site ($IC_{50} = 700 \mu\text{M}$ in SKBr3 cells), and induced the degradation of Hsp90 dependent client proteins, including v-src, Raf-1 and Erb2.^{20, 84} Interestingly, NB did not induce the pro-survival heat shock response, which is a major concern associated with Hsp90 N-terminal inhibitors. Encouraged by the initial findings, the NB scaffold was investigated for SAR studies and to improve its inhibitory activity against Hsp90. Initial studies done by Blagg and co-workers revealed key structural features of NB required for its binding to Hsp90.⁸⁵ Compound A4 (Figure 1.10), which lacks the 4-hydroxyl on the coumarin ring and contains an N-acyl side chain in lieu of the aryl group, was found to induce Hsp90 client protein degradation at ~70 fold lower concentrations than NB ($IC_{50} = 10 \mu\text{M}$). Surprisingly, compound A4 induced Hsp90 levels at much lower concentrations (~1000 fold) than that required for client protein degradation. This observation generated interest in A4 and its further exploration as a neuroprotective agent.

Eventually KU32, a variant of A4, showed greater induction of Hsp90 compared to A4 and is currently under investigation for the treatment of neurodegenerative diseases.⁸⁷ Further studies investigated the carbamoyl side chain in KU32 to switch the activity from anti-proliferative to cytoprotective.⁸⁷ Incorporation of a benzamide side chain onto KU32 was shown to restore the anti-proliferative activity without induction of the heat shock response, and identified DHN1. Further SAR studies on this class of compounds led to the development of

highly efficacious compounds, such as NA-2, which manifests mid nanomolar activity in anti-proliferative assays against various cancer cell lines.⁸⁸⁻⁹⁰

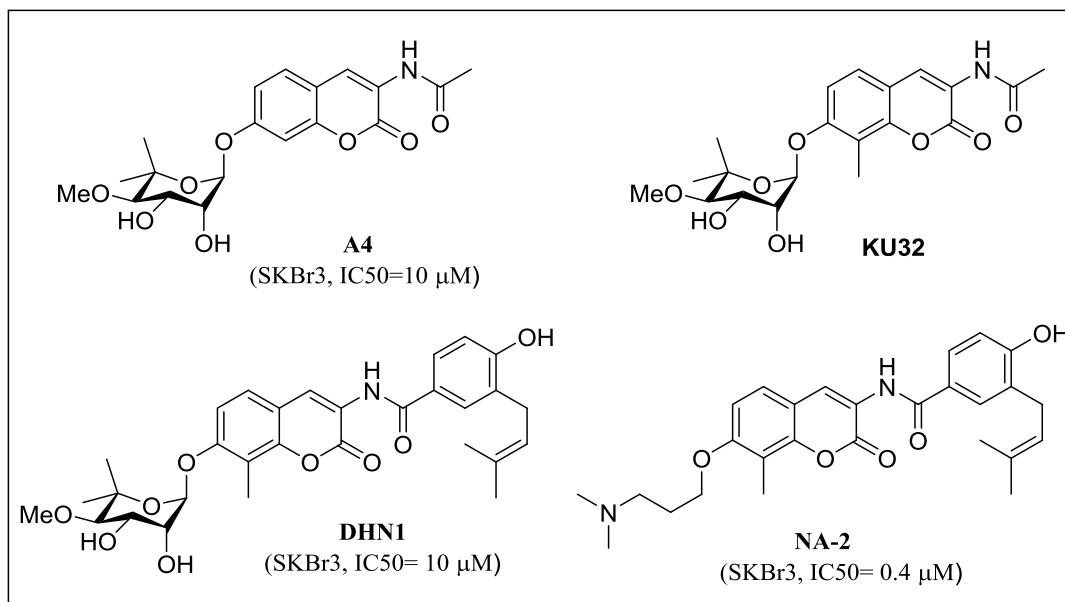


Figure 1.10 Structures of A4, KU32, DHN1 and NA-2.

5.2.2. Epigallocatechin-3-Gallate (EGCG)

EGCG is a polyphenolic compound extracted from green tea that elicits functional inhibition of wide range of proteins, including telomerase, aryl hydrocarbons receptor (AhR), several kinases and transcription factors, all of which are known Hsp90 dependent client proteins.⁹¹ In 2005, Palermo and co-workers used affinity chromatography to show that EGCG exhibits its antagonistic behavior against AhR through Hsp90 inhibition.⁹² Subsequent SAR studies revealed the phenols to be essential for anti-proliferative activity manifested by EGCG.⁹³ Studies are currently underway to improve the Hsp90 inhibitory activity exhibited by EGCG analogues.

5.2.3. Cisplatin

Cisplatin is a platinum-containing anti-cancer chemotherapeutic agent that binds DNA covalently and is used to treat a range of solid tumors⁹⁴. Cisplatin has been found to bind Hsp90 and interfere with its chaperone activity.⁹⁵ Subsequent studies have suggested that cisplatin binds

both the CTD and NTD, having different effects on these two domains. Cisplatin induces a conformational change in NTD, but not CTD.⁹⁶

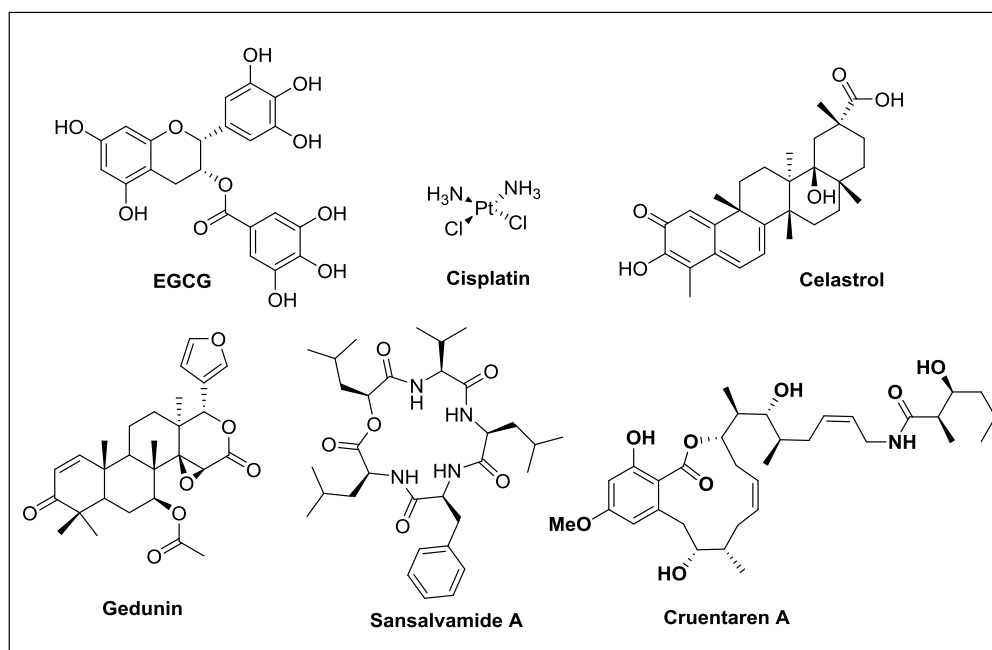


Figure 1.11 Structures of EGCG, cisplatin, celastrol, gedunin and Sansalvamide A.

5.3. Co-chaperone/Hsp90 disruptors

Agents that disrupt protein-protein interactions between Hsp90 and its co-chaperones can have similar consequences as those inhibitors that directly inhibit Hsp90.⁹⁸ Natural products such as celastrol and gedunin have been identified as disruptors of such interactions of Hsp90.^{98, 99} The Hsp90 co-chaperone, Cdc37, is required for the recruitment and maturation of several oncogenic kinases such as BRAF and EGFRvIII. Celastrol has been shown to disrupt Hsp90-Cdc37 interactions, subsequently inducing the degradation of the Cdc37-dependent Hsp90 clients.^{98, 100} Another natural product that disrupts the Hsp90/co-chaperone interaction is gedunin, a tetracyclic triterpenoid natural product that traditionally is used for the treatment of malaria and other infectious diseases.⁹⁹ Gedunin exhibits potent anti-proliferative activity against various cancer cell lines. Patwardhan and co-workers determined that gedunin exhibits its anticancer

activity by disruption of Hsp90-p23 interactions, which causes cell death through the activation of caspases.¹⁰¹ Sansalvamide A (San A) is a cyclic pentapeptide that binds Hsp90 NTD/MD and allosterically effects the CTD. San A disrupts CTD specific protein-protein interactions with IP6K2 and FKBP102 within CTD, and its derivatives exhibit 1 nM IC50 against pancreatic tumor cells.¹⁰³ Recently, Cruentaren A, a resorcinolic natural product with EC50 of 0.2-0.8 nM against breast and lung cancer cells, was shown to disrupt interactions between Hsp90 and F1Fo ATP synthase (FAS) without induction of the heat shock response.¹⁰⁴ As our understanding of the Hsp90 interactome grows, these compounds will find new applications and will help validate disruption of specific Hsp90/co-chaperone/client interaction.

6. Conclusion and Future Directions

The discovery of natural products that bind to Hsp90 led to the establishment that Hsp90 is a druggable target, which laid the foundation for the eventual design of synthetic small molecules inhibitors. It has now been validated that Hsp90 is a crucial mediator of oncogene addiction and disruption of the Hsp90 chaperone machine can shift the paradigm of cancer chemotherapeutics. Hsp90 as an anti-cancer target has an attractive advantage of simultaneous depletion of multiple oncogenic proteins. However, the inhibitors of Hsp90 that are being investigated in clinical trials have manifested side effects, such as cardiotoxicity and hepatotoxicity which are believed to be caused as a result of pan-inhibition of all Hsp90 isoforms. As a consequence, alternative strategies are desired for future development of Hsp90 inhibitors that are isoform selective, to expand our understanding of contributions of individual isoforms towards disease pathogenesis. In particular, the less explored isoforms such as Grp94 and Trap-1

Although, Hsp90 C-terminal inhibitors present as an attractive alternative for Hsp90 inhibition by not exhibiting heat shock induction, lack of a crystal structure of Hsp90 C-terminus

bound to an inhibitor, has proved to be a roadblock for structure based design of isoform selective C-terminus inhibitor. In conclusion, as the of Hsp90 biology advances, it will help us gain better insight about the role of each isoform of Hsp90 in pathogenesis, of not only cancer but other diseases. This knowledge can then be used collectively towards rational design of a drug that has improved pharmaceutical properties and tolerance.

References

1. Taipale, M.; Jarosz, D. F.; Lindquist, S., HSP90 at the hub of protein homeostasis: emerging mechanistic insights. *Nat. Rev. Mol. Cell Biol.* **2010**, *11*, 515-528.
2. Macario AJ, Conway de Macario E. Sick chaperones, cellular stress, and disease. *N Engl J Med* **2005**, *353*, 1489–501.
3. Donnelly, A.; Blagg, B. S. J., Novobiocin and Additional Inhibitors of the Hsp90 C-Terminal Nucleotide-binding Pocket. *Curr. Med. Chem.* **2008**, *15*, 2702-2717.
4. Powers MV, Workman P. Inhibitors of the heat shock response :biology and pharmacology. *FEBS Lett* **2007**, *581*, 3758–69.
5. Blagg, B. S. J.; Kerr, T. D., Hsp90 inhibitors: Small molecules that transform the Hsp90 protein folding machinery into a catalyst for protein degradation. *Med. Res. Rev.* **2006**, *26*, 310-338.
6. Wang X, Song X, Zhuo W, Fu Y, Shi H, Liang Y. Tong M, Chang G, Luo Y. The regulatory mechanism of Hsp90 alpha secretion and its function in tumor malignancy. *Proc Natl Acad Sci U S A* **2009**, *106*, 21288-93.
7. Trepel, J.; Mollapour, M.; Giaccone, G.; Neckers, L., Targeting the dynamic HSP90 complex in cancer. *Nat. Rev. Cancer* **2010**, *10*, 537-549.
8. Picard D, Khursheed B, Garabedian MJ, Fortin MG, Lindquist S, Yamamoto KR. Reduced levels of hsp90 compromise steroid receptor action in vivo. *Nature* **1990**, *348*, 166-8.
9. Stancato LF, Chow YH, Hutchison KA, Perdew GH, Jove R, Pratt WB. Raf exists in a native heterocomplex with hsp90 and p50 that can be reconstituted in a cell-free system. *J Biol Chem* **1993**, *268*, 21711-6.
10. Taipale M, Krykbaeva I, Koeva M, Kayatekin C, Westover KD, Karras GI & Lindquist S Quantitative analysis of hsp90–client interactions reveals principles of substrate recognition. *Cell* **2012**, *150*, 987–1001.
11. Dutta, R.; Inouye, M., GHKL, an emergent ATPase/kinase superfamily. *Tren. biochem. sci.* **2000**, *25*, 24-28.
12. Pearl, L. H.; Prodromou, C., Structure and Mechanism of the Hsp90 Molecular Chaperone Machinery. *Annu. Rev. Biochem.* **2006**, *75*, 271-294.
13. Prodromou, C.; Roe, S. M.; O'Brien, R.; Ladbury, J. E.; Piper, P. W.; Pearl, L. H., Identification and Structural Characterization of the ATP/ADP-Binding Site in the Hsp90 Molecular Chaperone. *Cell* **1997**, *90*, 65-75.
14. Stebbins, C. E.; Russo, A. A.; Schneider, C.; Rosen, N.; Hartl, F. U.; Pavletich, N. P., Crystal Structure of an Hsp90 Geldanamycin Complex: Targeting of a Protein Chaperone by an Antitumor Agent. *Cell* **1997**, *89*, 239-250.
15. Ali MM, Roe SM, Vaughan CK, Meyer P, Panaretou B, Piper PW, Prodromou C, Pearl LH., Crystal structure of an Hsp90-nucleotide-p23/Sba1 closed chaperone complex. *Nature* **2006**, *440*,1013-7.
16. Huai, Q.; Wang, H.; Liu, Y.; Kim, H.-Y.; Toft, D.; Ke, H., Structures of the N-Terminal and Middle Domains of E. coli Hsp90 and Conformation Changes upon ADP Binding. *Structure* **2005**, *13*, 579-590.

17. Meyer, P.; Prodromou, C.; Hu, B.; Vaughan, C.; Roe, S. M.; Panaretou, B.; Piper, P. W.; Pearl, L. H., Structural and Functional Analysis of the Middle Segment of Hsp90: Implications for ATP Hydrolysis and Client Protein and Cochaperone Interactions. *Molecular Cell* **2003**, *11*, 647-658.
18. Ratzke C, Mickler M, Hellenkamp B, Buchner J, Hugel T., Dynamics of heat shock protein 90 C-terminal dimerization is an important part of its conformational cycle. *Proc Natl Acad Sci U S A* **2010**, *107*, 1610-16.
19. Prodromou, C.; Siligardi, G.; O'Brien, R.; Woolfson, D. N.; Regan, L.; Panaretou, B.; Ladbury, J. E.; Piper, P. W.; Pearl, L. H., Regulation of Hsp90 ATPase activity by tetratricopeptide repeat (TPR)-domain co-chaperones. *EMBO J* **1999**, *18*, 754-62.
20. Marcu, M. G.; Chadli, A.; Bouhouche, I.; Catelli, M.; Neckers, L. M., The Heat Shock Protein 90 Antagonist Novobiocin Interacts with a Previously Unrecognized ATP-binding Domain in the Carboxyl Terminus of the Chaperone. *J. Biol. Chem.* **2000**, *275*, 37181-37186.
21. Yin, Z.; Henry, E. C.; Gasiewicz, T. A., (-)-Epigallocatechin-3-gallate Is a Novel Hsp90 Inhibitor†. *Biochemistry* **2008**, *48*, 336-345.
22. Byrd, C. A.; Bornmann, W.; Erdjument-Bromage, H.; Tempst, P.; Pavletich, N.; Rosen, N.; Nathan, C. F.; Ding, A., Heat shock protein 90 mediates macrophage 23 activation by Taxol and bacterial lipopolysaccharide. *Proc. Natl. Acad. Sci. USA* **1999**, *96*, 5645-5650.
23. Pearl, L. H.; Prodromou, C.; Workman, P., The Hsp90 molecular chaperone: an open and shut case for treatment. *Biochem. J.* **2008**, *410*, 439-453.
24. Picard, D., Heat-shock protein 90, a chaperone for folding and regulation. *CMLS, Cell. Mol. Life Sci.* **2002**, *59*, 1640-1648.
25. Sidera, K.; Patsavoudi, E., Extracellular HSP90: An Emerging Target for Cancer Therapy. *Curr. Signal Transd. T.* **2009**, *4*, 51-58.
26. Peterson, L. B.; Blagg, B. S. J., To fold or not to fold: modulation and consequences of Hsp90 inhibition. *Future Med. Chem.* **2009**, *1*, 267-283.
27. Walter, S.; Buchner, J., Molecular Chaperones—Cellular Machines for Protein Folding. *Angew. Chem. Int. Ed. Engl.* **2002**, *41*, 1098-1113.
28. Chaudhury, S.; Welch, T. R.; Blagg, B. S. J., Hsp90 as a Target for Drug Development. *ChemMedChem* **2006**, *1*, 1331-1340.
29. Murphy, P. J. M.; Kanelakis, K. C.; Galigniana, M. D.; Morishima, Y.; Pratt, W. B., Stoichiometry, Abundance, and Functional Significance of the hsp90/hsp70-based Multiprotein Chaperone Machinery in Reticulocyte Lysate. *J. Biol. Chem.* **2001**, *276*, 30092-30098.
30. Kosano, H.; Stensgard, B.; Charlesworth, M. C.; McMahon, N.; Toft, D., The Assembly of Progesterone Receptor-hsp90 Complexes Using Purified Proteins. *J. Biol. Chem.* **1998**, *273*, 32973-32979.
31. Prodromou, C.; Panaretou, B.; Chohan, S.; Siligardi, G.; Brien, R.; Ladbury, J. E.; Roe, S. M.; Piper, P. W.; Pearl, L. H., The ATPase cycle of Hsp90 drives a molecular 'clamp' via transient dimerization of the N-terminal domains. *EMBO J.* **2000**, *19*, 4383-4392.
32. Ali MM, Roe SM, Vaughan CK, Meyer P, Panaretou B, Piper PW, Prodromou C, Pearl LH., Crystal structure of an Hsp90-nucleotide-p23/Sba1 closed chaperone complex. *Nature* **2006**, *440*, 1013-17.
33. Garcia-Carbonero, R.; Carnero, A.; Paz-Ares, L., Inhibition of HSP90 molecular chaperones: moving into the clinic. *Lancet Oncol* **2013**, *14*, 358-69.
34. Mollapour M, Neckers L., Post-translational modifications of Hsp90 and their contributions to chaperone regulation. *Biochim Biophys Acta* **2012**, *1823*, 648-55.
35. Miyata, Y.; Nakamoto, H.; Neckers, L., The therapeutic target Hsp90 and cancer hallmarks. *Curr. pharmaceu. desi.* **2013**, *19*, 347-65.

36. Solit, D. B.; Chiosis, G., Development and application of Hsp90 inhibitors. *Drug Discovery Today* **2008**, *13*, 38-43.
37. Koga, F.; Kihara, K.; Neckers, L., Inhibition of Cancer Invasion and Metastasis by Targeting the Molecular Chaperone Heat-shock Protein 90. *Anticancer Res.* **2009**, *29*, 797-807.
38. Paul, S.; Mahanta, S., Association of heat-shock proteins in various neurodegenerative disorders: is it a master key to open the therapeutic door? *Mol. Cell Biochem.* **2014**, *386*, 45-61.
39. Neckers, L.; Workman, P., Hsp90 Molecular Chaperone Inhibitors: Are We There Yet? *Clin. Cancer Res.* **2012**, *18*, 64-76.
40. Grem JL, Morrison G, Guo XD, et al. Phase I and pharmacologic study of 17-(allylamino)-17-demethoxygeldanamycin in adult patients with solid tumors. *J Clin Oncol* **2005**, *23*, 1885–93.
41. Neckers L., Heat shock protein 90: the cancer chaperone. *JBiosci* **2007**, *32*, 517-530.
42. Chiosis G, Neckers L., Tumor selectivity of Hsp90 inhibitors the explanation remains elusive. *ACS Chem Biol* **2006**, *1*, 279–284.
43. Kamal, A.; Thao, L.; Sensintaffar, J.; Zhang, L.; Boehm, M. F.; Fritz, L. C.; Burrows, F. J., A high-affinity conformation of Hsp90 confers tumour selectivity on Hsp90 inhibitors. *Nature* **2003**, *425*, 407-410.
44. Meriin, A. B.; Sherman, M. Y., Role of molecular chaperones in neurodegenerative disorders. *Int. J. Hyperthermia* **2005**, *21*, 403-419.
45. Ali A, Bharadwaj S, O'Carroll R, Ovsenek N HSP90 interacts with and regulates the activity of heat shock factor 1 in Xenopus oocytes. *Mol Cell Biol* **1998**, *18*, 4949-4960.
46. Dickey, C. A.; Eriksen, J.; Kamal, A.; Burrows, F.; Kasibhatla, S.; Eckman, C. B.; Hutton, M.; Petrucelli, L., Development of a high throughput drug screening assay for the detection of changes in tau levels -- proof of concept with HSP90 inhibitors. *Curr. Alzheimer res.* **2005**, *2*, 231-8.
47. Muchowski, P. J.; Wacker, J. L., Modulation of neurodegeneration by molecular chaperones. *Nat. Rev. Neurosci.* **2005**, *6*, 11-22.
48. Dickey CA, Kamal A, Lundgren K, Klosak N, Bailey RM, Dunmore J, Ash P, Shoraka S, Zlatkovic J, Eckman CB, Patterson C, Dickson DW, Nahman NS Jr, Hutton M, Burrows F, Petrucelli L., The high-affinity HSP90-CHIP complex recognizes and selectively degrades phosphorylated tau client proteins. *J Clin Invest* **2007**, *117*, 648-658.
49. Hashimoto, M.; Rockenstein, E.; Crews, L.; Masliah, E., Role of protein aggregation in mitochondrial dysfunction and neurodegeneration in Alzheimer's and Parkinson's diseases. *Neuromol. Med.* **2003**, *4*, 21-35.
50. Alonso, A. d. C.; Zaidi, T.; Novak, M.; Grundke-Iqbal, I.; Iqbal, K., Hyperphosphorylation induces self-assembly of τ into tangles of paired helical filaments/straight filaments. *Proc. Natl. Acad. Sci. USA* **2001**, *98*, 6923-6928.
51. Kim, H.-Y.; Heise, H.; Fernandez, C. O.; Baldus, M.; Zweckstetter, M., Correlation of Amyloid Fibril β -Structure with the Unfolded State of α -Synuclein. *ChemBioChem* **2007**, *8*, 1671-1674.
52. Daturpalli, S.; Waudby, C. A.; Meehan, S.; Jackson, S. E., Hsp90 inhibits alpha-synuclein aggregation by interacting with soluble oligomers. *J Mol Biol* **2013**, *425*, 4614-28.
53. Neckers, L., Tatu, U., Molecular Chaperones in Pathogen Virulence: Emerging New Targets for Therapy. *Cell host & microbe* **2008**, *4*, 519-527.
54. Pearl, L. H.; Prodromou, C.; Workman, P., The Hsp90 molecular chaperone: an open and shut case for treatment. *Biochem. J.* **2008**, *410*, 439-453.

55. Geller, R.; Vignuzzi, M.; Andino, R.; Frydman, J., Evolutionary constraints on chaperone-mediated folding provide an antiviral approach refractory to development of drug resistance. *Genes & Development* **2007**, *21*, 195-205.
56. Cowen, L. E.; Lindquist, S., Hsp90 Potentiates the Rapid Evolution of New Traits: Drug Resistance in Diverse Fungi. *Science* **2005**, *309*, 2185-2189.
57. Cowen, L. E.; Singh, S. D.; Kohler, J. R.; Collins, C.; Zaas, A. K.; Schell, W. A.; Aziz, H.; Mylonakis, E.; Perfect, J. R.; Whitesell, L.; Lindquist, S., Harnessing Hsp90 function as a powerful, broadly effective therapeutic strategy for fungal infectious disease. *Proc Natl Acad Sci USA* **2009**, *106*, 2818-23.
58. DeBoer C, Meulman PA, Wnuk RJ, Peterson DH., Geldanamycin, a new antibiotic. *J Antibiot* **1970**, *23*, 442-7.
59. Jove, R.; Hanafusa, H., Cell transformation by the viral src oncogene. *Annu. rev. cell biol.* **1987**, *3*, 31-56.
60. Whitesell, L.; Mimnaugh, E. G.; De Costa, B.; Myers, C. E.; Neckers, L. M., Inhibition of heat shock protein HSP90-pp60v-src heteroprotein complex formation by benzoquinone ansamycins: essential role for stress proteins in oncogenic transformation *Proc. Natl. Acad. Sci. USA* **1994**, *91*, 8324-8.
61. Mimnaugh EG, Chavany C, Neckers L. Polyubiquitination and proteasomal degradation of the p185c-erbB-2 receptor proteintyrosine kinase induced by geldanamycin. *J Biol Chem* **1996**, *271*, 22796-801.
62. Stebbins CE, Russo AA, Schneider C, Rosen N, Hartl FU, Pavletich NP., Crystal structure of an Hsp90-geldanamycin complex: Targeting of a protein chaperone by an antitumor agent. *Cell* **1997**, *89*, 239-50.
63. Messaoudi, S.; Peyrat, J. F.; Brion, J. D.; Alami, M., Recent advances in Hsp90 inhibitors as antitumor agents. *Anti-cancer agents med. chem.* **2008**, *8*, 761-82.
64. Sidera, K.; Patsavoudi, E., HSP90 inhibitors: current development and potential in cancer therapy. *Recent Pat Anticancer Drug Discov* **2014**, *9*, 1-20.
65. Modi S, Stopeck A, Linden H, Solit D, Chandarlapaty S, Rosen N, D'Andrea G, Dickler M, Moynahan ME, Sugarman S, Ma W, Patil S, Norton L, Hannah AL, Hudis C., HSP90 inhibition is effective in breast cancer: A Phase II trial of tanespimycin (17-AAG) plus trastuzumab in patients with HER2-positive metastatic breast cancer progressing on trastuzumab. *Clin Cancer Res* **2011**, *17*, 5132-9.
66. Delmotte, P.; Delmotte-Plaquee, J., A New Antifungal Substance of Fungal Origin. *Nature* **1953**, *171*, 344-344.
67. Soga S, Shiotsu Y, Akinaga S, Sharma SV. Development of radicicol analogues. *Curr Cancer Drug Targets* **2003**, *3*, 359-69.
68. Geng, X.; Yang, Z.-Q.; Danishefsky, S. J., Synthetic Development of Radicicol and cycloproparadicicol: Highly Promising Anticancer Agents Targeting Hsp90. *Synlett* **2004**, *8*, 1325-1333.
69. Yang, Z.-Q.; Geng, X.; Solit, D.; Pratilas, C. A.; Rosen, N.; Danishefsky, S. J., New Efficient Synthesis of Resorcinylic Macrolides via Ynolides: Establishment of Cycloproparadicicol as Synthetically Feasible Preclinical Anticancer Agent Based on Hsp90 as the Target. *J. Am. Chem. Soc.* **2004**, *126*, 7881-7889.
70. Chiosis, G.; Timaul, M. N.; Lucas, B.; Munster, P. N.; Zheng, F. F.; Sepp-Lorenzino, L.; Rosen, N., A small molecule designed to bind to the adenine nucleotide pocket of Hsp90 causes Her2 degradation and the growth arrest and differentiation of breast cancer cells. *Chem. biol.* **2001**, *8*, 289-299.

71. Chiosis, G.; Lucas, B.; Shtil, A.; Huezo, H.; Rosen, N., Development of a Purine-Scaffold Novel Class of Hsp90 Binders that Inhibit the Proliferation of Cancer Cells and Induce the Degradation of Her2 Tyrosine Kinase. *Bioorg. Med. Chem.* **2002**, *10*, 3555-3564.
72. Kasibhatla, S. R.; Hong, K.; Biamonte, M. A.; Busch, D. J.; Karjian, P. L.; Sensintaffar, J. L.; Kamal, A.; Lough, R. E.; Brekken, J.; Lundgren, K.; Grecko, R.; Timony, G. A.; Ran, Y.; Mansfield, R.; Fritz, L. C.; Ulm, E.; Burrows, F. J.; Boehm, M. F., Rationally Designed High-Affinity 2-Amino-6-halopurine Heat Shock Protein 90 Inhibitors That Exhibit Potent Antitumor Activity. *J. Med. Chem.* **2007**, *50*, 2767-2778.
73. Rowlands, M. G.; Newbatt, Y. M.; Prodromou, C.; Pearl, L. H.; Workman, P.; Aherne, W., High-throughput screening assay for inhibitors of heat-shock protein 90 ATPase activity. *Anal. Biochem.* **2004**, *327*, 176-183.
74. Cheung, K.-M. J.; Matthews, T. P.; James, K.; Rowlands, M. G.; Boxall, K. J.; Sharp, S. Y.; Maloney, A.; Roe, S. M.; Prodromou, C.; Pearl, L. H.; Aherne, G. W.; McDonald, E.; Workman, P., The identification, synthesis, protein crystal structure and in vitro biochemical evaluation of a new 3,4-diarylpyrazole class of Hsp90 inhibitors. *Bioorg. Med. Chem. Lett.* **2005**, *15*, 3338-3343.
75. Kreuzsch, A.; Han, S.; Brinker, A.; Zhou, V.; Choi, H.-s.; He, Y.; Lesley, S. A.; Caldwell, J.; Gu, X.-j., Crystal structures of human HSP90 α -complexed with dihydroxyphenylpyrazoles. *Bioorg. Med. Chem. Lett.* **2005**, *15*, 1475-1478.
76. Dymock, B. W.; Barril, X.; Brough, P. A.; Cansfield, J. E.; Massey, A.; McDonald, E.; Hubbard, R. E.; Surgenor, A.; Roughley, S. D.; Webb, P.; Workman, P.; Wright, L.; Drysdale, M. J., Novel, Potent Small-Molecule Inhibitors of the Molecular Chaperone Hsp90 Discovered through Structure-Based Design. *J. Med. Chem.* **2005**, *48*, 4212-4215.
77. Sharp, S. Y.; Prodromou, C.; Boxall, K.; Powers, M. V.; Holmes, J. L.; Box, G.; Matthews, T. P.; Cheung, K.-M. J.; Kalusa, A.; James, K.; Hayes, A.; Hardcastle, A.; Dymock, B.; Brough, P. A.; Barril, X.; Cansfield, J. E.; Wright, L.; Surgenor, A.; Foloppe, N.; Hubbard, R. E.; Aherne, W.; Pearl, L.; Jones, K.; McDonald, E.; Raynaud, F.; Eccles, S.; Drysdale, M.; Workman, P., Inhibition of the heat shock protein 90 molecular chaperone in vitro and in vivo by novel, synthetic, potent resorcinyl pyrazole/isoxazole amide analogues. *Mol. Cancer Ther.* **2007**, *6*, 1198-1211.
78. Brough, P. A.; Aherne, W.; Barril, X.; Borgognoni, J.; Boxall, K.; Cansfield, J. E.; Cheung, K.-M. J.; Collins, I.; Davies, N. G. M.; Drysdale, M. J.; Dymock, B.; Eccles, S. A.; Finch, H.; Fink, A.; Hayes, A.; Howes, R.; Hubbard, R. E.; James, K.; Jordan, A. M.; Lockie, A.; Martins, V.; Massey, A.; Matthews, T. P.; McDonald, E.; Northfield, C. J.; Pearl, L. H.; Prodromou, C.; Ray, S.; Raynaud, F. I.; Roughley, S. D.; Sharp, S. Y.; Surgenor, A.; Walmsley, D. L.; Webb, P.; Wood, M.; Workman, P.; Wright, L., 4,5-Diarylisoaxazole Hsp90 Chaperone Inhibitors: Potential Therapeutic Agents for the Treatment of Cancer. *J. Med. Chem.* **2007**, *51*, 196-218.
79. Lin TY, Bear M, Du Z, Foley KP, Ying W, Barsoum J, London C., The novel HSP90 inhibitor STA-9090 exhibits activity against Kitdependent and-independent malignant mast cell tumors. *Exp Hematol* **2008**, *36*, 1266-77.
80. Woodhead AJ, Angove H, Carr MG, Chessari G, Congreve M, Coyle JE, et al. Discovery of (2,4-dihydroxy-5-isopropylphenyl)- [5-(4-methylpiperazin-1-ylmethyl)-1,3-dihydrois oindol-2-yl] methanone (AT13387), a novel inhibitor of the molecular chaperone Hsp90 by fragment based drug design. *J Med Chem* **2010**, *53*, 5956-69.
81. Huang, K.H., Hughes, P., Ma, W., Ommen, A., Woodward, A., Veal, J., Barta, T. Tetrahydroindolone and tetrahydroindazolone derivatives. WO2008024970, Oct 23, **2008**.

82. Rajan A, Kelly RJ, Trepel JB, Kim YS, Alarcon SV, Kummar S, Gutierrez M, Crandon S, Zein WM, Jain L, Mannargudi B, Figg WD, Houk BE, Shnaidman M, Brega N, Giaccone G., A Phase I study of PF-04929113 (SNX-5422), an orally bioavailable heat shock protein 90 inhibitor, in patients with refractory solid tumor malignancies and lymphomas. *Clin Cancer Res* **2011**, *17*, 6831-9.
83. Yu, X. M.; Shen, G.; Blagg, B. S. J., Synthesis of (-)-Noviose from 2, 3-O-Isopropylidene-d-erythronolactol. *J. Org. Chem.* **2004**, *69*, 7375-7378.
84. Marcu, M. G.; Schulte, T. W.; Neckers, L., Novobiocin and Related Coumarins and Depletion of Heat Shock Protein 90-Dependent Signaling Proteins. *J. Natl. Cancer Inst.* **2000**, *92*, 242-248.
85. Yu, X. M.; Shen, G.; Neckers, L.; Blake, H.; Holzbeierlein, J.; Cronk, B.; Blagg, B. S. J., Hsp90 Inhibitors Identified from a Library of Novobiocin Analogues. *J. Am. Chem. Soc.* **2005**, *127*, 12778-12779.
86. Farmer, K.; Williams, S. J.; Novikova, L.; Ramachandran, K.; Rawal, S.; Blagg, B. S. J.; Dobrowsky, R.; Stehno-Bittel, L., KU-32, a Novel Drug for Diabetic Neuropathy, Is Safe for Human Islets and Improves In Vitro Insulin Secretion and Viability. *Exp. Diabetes Res.* **2012**, *2012*, 11.
87. Burlison, J. A.; Neckers, L.; Smith, A. B.; Maxwell, A.; Blagg, B. S. J., Novobiocin: Redesigning a DNA Gyrase Inhibitor for Selective Inhibition of Hsp90. *J. Am. Chem. Soc.* **2006**, *128*, 15529-15536.
88. Zhao, H.; Donnelly, A. C.; Kusuma, B. R.; Brandt, G. E. L.; Brown, D.; Rajewski, R. A.; Vielhauer, G.; Holzbeierlein, J.; Cohen, M. S.; Blagg, B. S. J., Engineering an Antibiotic to Fight Cancer: Optimization of the Novobiocin Scaffold to Produce Anti-proliferative Agents. *J. Med. Chem.* **2011**, *54*, 3839-3853.
89. Donnelly, A. C.; Mays, J. R.; Burlison, J. A.; Nelson, J. T.; Vielhauer, G.; Holzbeierlein, J.; Blagg, B. S. J., The Design, Synthesis, and Evaluation of Coumarin Ring Derivatives of the Novobiocin Scaffold that Exhibit Antiproliferative Activity. *J. Org. Chem.* **2008**, *73*, 8901-8920.
90. Zhao, H.; Reddy Kusuma, B.; Blagg, B. S. J., Synthesis and Evaluation of Noviose Replacements on Novobiocin That Manifest Antiproliferative Activity. *ACS Med. Chem. Lett.* **2010**, *1*, 311-315.
91. Yin, Z.; Henry, E. C.; Gasiewicz, T. A., (-)-Epigallocatechin-3-gallate Is a Novel Hsp90 Inhibitor *Biochemistry* **2008**, *48*, 336-345.
92. Palermo, C. M.; Westlake, C. A.; Gasiewicz, T. A., Epigallocatechin Gallate Inhibits Aryl Hydrocarbon Receptor Gene Transcription through an Indirect Mechanism Involving Binding to a 90 kDa Heat Shock Protein. *Biochemistry* **2005**, *44*, 5041-5052.
93. Khandelwal, A.; Hall, J. A.; Blagg, B. S. J., Synthesis and Structure–Activity Relationships of EGCG Analogues, a Recently Identified Hsp90 Inhibitor. *J. Org. Chem.* **2013**, *78*, 7859-7884.
94. Galanski, M., Recent developments in the field of anticancer platinum complexes. *Recent pat. anti-cancer drug discovery* **2006**, *1*, 285-95.
95. Sreedhar, A. S.; Soti, C.; Csermely, P., Inhibition of Hsp90: a new strategy for inhibiting protein kinases. *Biochim Biophys Acta* **2004**, *1697*, 233-42.
96. Ishida, R.; Takaoka, Y.; Yamamoto, S.; Miyazaki, T.; Otaka, M.; Watanabe, S.; Komatsuda, A.; Wakui, H.; Sawada, K.; Kubota, H.; Itoh, H., Cisplatin differently affects amino terminal and carboxyl terminal domains of HSP90. *FEBS Lett* **2008**, *582*, 3879-83.
97. Gray PJ, Jr., Prince T, Cheng J, Stevenson MA, Calderwood SK. Targeting the oncogene and kinome chaperone CDC37. *Nat Rev Cancer* **2008**, *8*, 491-5.

98. Sreeramulu, S.; Gande, S. L.; Göbel, M.; Schwalbe, H., Molecular Mechanism of Inhibition of the Human Protein Complex Hsp90–Cdc37, a Kinome Chaperone–Cochaperone, by Triterpene Celastrol. *Angew. Chem. Int. Ed. Engl.* **2009**, *48*, 5853-5855.
99. Brandt, G. E. L.; Schmidt, M. D.; Prisinzano, T. E.; Blagg, B. S. J., Gedunin, a Novel Hsp90 Inhibitor: Semisynthesis of Derivatives and Preliminary Structure–Activity Relationships. *J. Med. Chem.* **2008**, *51*, 6495-6502.
100. Roe, S. M.; Ali, M. M. U.; Meyer, P.; Vaughan, C. K.; Panaretou, B.; Piper, P. W.; Prodromou, C.; Pearl, L. H., The Mechanism of Hsp90 Regulation by the Protein Kinase-Specific Cochaperone p50cdc37. *Cell* **2004**, *116*, 87-98.
101. Patwardhan, C. A.; Fauq, A.; Peterson, L. B.; Miller, C.; Blagg, B. S. J.; Chadli, A., Gedunin Inactivates the Co-chaperone p23 Protein Causing Cancer Cell Death by Apoptosis. *J. Biol. Chem.* **2013**, *288*, 7313-7325.
102. Vasko RC, Rodriguez RA, Cunningham CN, Ardi VC, Agard DA, McAlpine SR. Mechanistic studies of Sansalvamide A-amide: An allosteric modulator of Hsp90. *ACS Med Chem Lett* **2010**, *1*, 4-8.
103. Davis MR, Styers TJ, Rodriguez RA, Pan PS, Vasko RC, McAlpine SR. Synthesis and cytotoxicity of a new class of potent decapeptide macrocycles. *Org Lett* **2008**, *10*, 177-80.
104. Hall, J. A.; Kusuma, B. R.; Brandt, G. E. L.; Blagg, B. S. J., Cruentaren A Binds F1F0 ATP Synthase To Modulate the Hsp90 Protein Folding Machinery. *ACS Chemical Biology* **2014**, *9*, 976-985.

Chapter 2

Structure Activity Relationship Studies of Radamide and Its cis-amide isotere Analogs to Develop Grp94-Selective Inhibitors.

Chapter 2

1. Introduction

Heat shock protein 90KDa (Hsp90) is a molecular chaperone that facilitates the conformational maturation of approximately 200 client proteins, thereby, playing an important role in cellular trafficking, signaling, protein folding and the maintenance of client protein levels.^{1,2} Hsp90 is a homodimer with each monomer comprising three domains; the N- and C-termini and the middle domain. The N-terminus contains an ATP-binding site that binds and hydrolyzes ATP to provide the energy required for protein folding.³⁻⁹ During cancerous transformation, Hsp90 is overexpressed and provides matured client proteins associated with the rapid growth and proliferation of cancer cells. Therefore, Hsp90 has emerged as an attractive therapeutic target, since disruption of Hsp90 can simultaneously affect multiple pathways required for cancer cell growth.¹⁰⁻²²

Hsp90 inhibition has been shown to be an effective therapeutic strategy and 17 Hsp90 inhibitors have progressed into clinical trials for the treatment of various cancers. These inhibitors, however, have been found to manifest side effects including cardiovascular, ocular, and/or hepatotoxicity, resulting in narrow therapeutic window for administration of these inhibitors.²³⁻²⁴ Therefore, it is necessary to study the effects of individual Hsp90 isoforms and to delineate the contribution of each isoform towards the pathogenesis of these diseases as well as their side effects. Recently, it was found that Hsp90 α is responsible for the maturation of the hERG

channel, and therefore could be responsible for the clinically observed cardiotoxicity.²⁵ Unfortunately, the development of isoform selective inhibitors has been challenging since the N-terminal ATP-binding site is >85% identical across all four Hsp90 isoforms; cytosolic Hsp90 α and β , the endoplasmic reticulum-localized isoform, Grp94, and the mitochondrial chaperone, Trap1.²⁶

In comparison to cytoplasmic isoforms Hsp90 α and β , the biological role for the ER residing isoform, glucose regulated protein-94 kDa (Grp94) has not been studied extensively.¹⁶ Grp94 chaperones various secreted proteins that are critical for intercellular communication and adhesion (Table 2.1).²⁷ For example, Grp94 regulates cellular metastasis indirectly via the integrins, making it a potential target for the development of anti-metastatic agents.²⁸ This is further supported by a recent finding that Grp94 knockdown leads to inhibition of cell proliferation, migration and metastasis in highly metastatic breast cancer cell line MDA-MB-231 and reactive oxygen species (ROS) resistant MCF-7 cells.²⁹ Due to its role in the clearance of mutant myocilin, Grp94 has also been implicated for the treatment of glaucoma.³⁰ In addition, Grp94 is required for the maturation of Wnt co-receptor, LRP6, which is overexpressed in multiple myeloma,³¹⁻³³ and as hypothesized, Grp94 inhibition results in reduced proliferation of multiple myeloma cells.³⁴

Grp94 client protein	Pathogenesis
IGF I/II	Regulates cell mitosis (Cancer)
EGF-R/ ErbB2	Cell growth (Cancer)
Insulin receptor	Cell growth (Cancer)
Integrins (CD11a, CD18, CD49d, α 4, β 7, α L, β 2)	Cell adhesion and communication (Cancer)
Toll-like receptors (TLR1,TLR2,TLR4and TLR9)	Inflammation and autoimmunity
LRP6	Co-receptor for Wnt receptor (Cancer)
Mutant myocilin	Glaucoma

Table-2.1 Grp94 clients and their role in disease pathogenesis.^{35, 30}

The Grp94 primary sequence differs from other Hsp90 isoforms in that it contains a five-amino acid (QEDGQ) sequence that is inserted between residues 182 and 186, which translates into topographic differences between the binding pockets of Grp94 and Hsp90.³⁶ This small perturbation creates a unique hydrophobic environment within the Grp94 N-terminal ATP-binding site, and provides an opportunity for selective inhibition.³⁶⁻³⁷ In 2009, co-crystal structures of radamide (RDA), radicicol/geldanamycin chimeric inhibitor bound to Hsp90 and Grp94 were solved, revealing that in the case of Hsp90, RDA bound exclusively in the *trans* conformation of the amide bond, whereas in Grp94, RDA existed in a 50:50 conformational abundance of *cis:trans* amide bond (Figure 2.1).³⁸⁻⁴² The *cis* amide bond in the case of Grp94 was found to occupy a unique pocket that is absent in Hsp90. Also, the quinone moiety of RDA was found to participate in polar interactions with Hsp90, and to a lesser extent with Grp94 (Figure 2.2). Therefore, modifications were sought to modify the RDA scaffold that specifically target the unique hydrophobic pocket of Grp94. The first approach involved replacement of the quinone with a phenyl ring that can be easily substituted to explore the unique pocket. While the second approach focused on constraining the amide bond into the *cis* conformation, utilizing

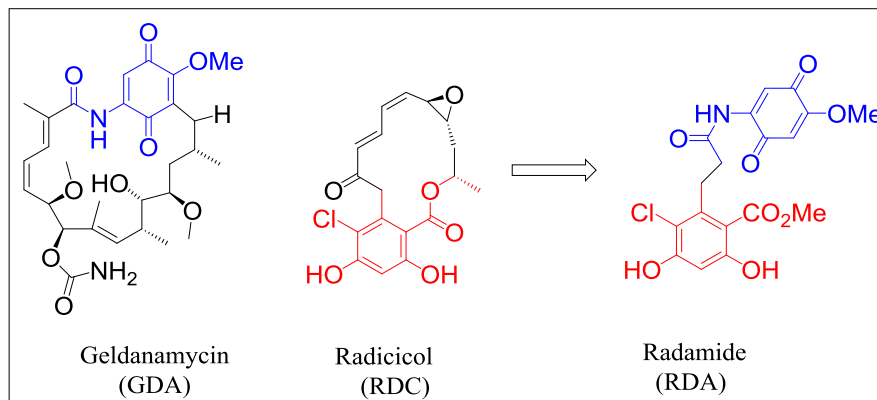


Figure 2.1 Structures of natural product Hsp90 inhibitors GDA and RDC, and chimeric inhibitor RDA.

isosteres of the *cis* amide bond, which ultimately led to the development of BnIm, the first Grp94 selective inhibitor identified.³⁷ Modifications to the benzyl ring of the BnIm were also sought to explore the unique hydrophobic pocket found in Grp94. Therefore, the goal of this project was to establish structure-activity relationships for RDA as well as BnIm, as Grp94 inhibitors.

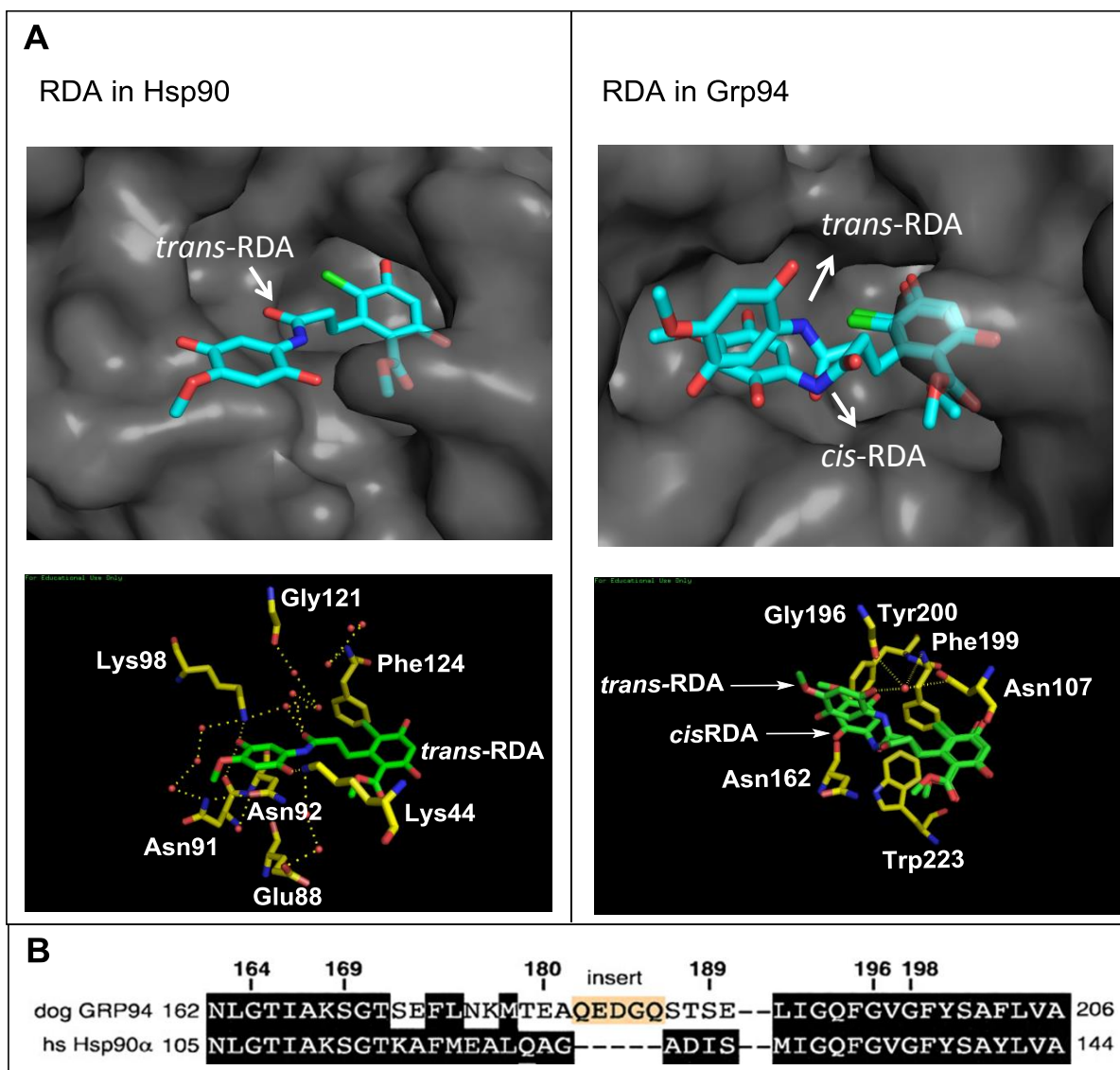
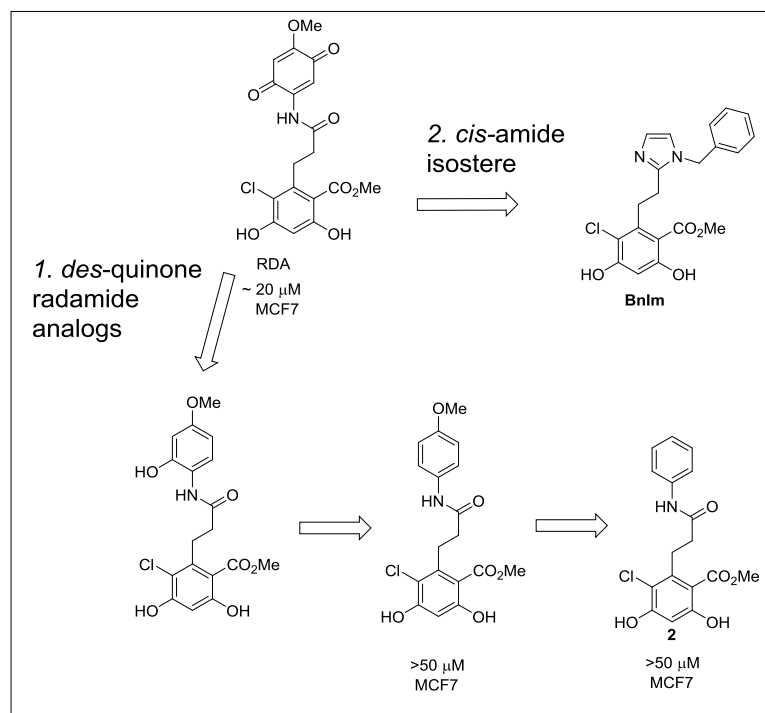


Figure 2.2 (A) Co-crystal structures of RDA bound to Hsp90 (PDB: 2FXS) and Grp94 (PDB: 2GFD) (B) primary amino acid sequence alignment of Grp94 and Hsp90 illustrates the insertion of five amino acids (QEDGQ) in Grp94 but not in Hsp90.³⁶

2. Structure Activity Relationship (SAR) studies on RDA and BnIm Analogs



Scheme 2.1 Proposed approaches for design of Grp94 selective inhibitors

2.1 *des*-quinone approach (RDA analogs)

Previous studies in our lab demonstrated that removal of the quinone moiety in RDA results in the loss of anti-proliferative activity in MCF7 cells,⁴³ which translates to a loss in Hsp90 affinity for the *des*-quinone molecules. Additionally, the phenyl ring provides opportunities for modifications that can access the hydrophobic pocket of Grp94. Molecular modeling studies suggested that additional methylene linker between amide nitrogen and aromatic ring would be detrimental for efficacy, which was further validated via the synthesis and evaluation of the compounds containing extended linkers (Figure 2.3). In the event, acid **1**⁴⁴ (figure2.4) was coupled with the corresponding amines, utilizing 1-ethyl-3-(3-dimethylaminopropyl)carbodiimide (EDCI) and 4-(Dimethyl)aminopyriine (DMAP) in

dichloromethane to generate the respective amides. The amides were subsequently subjected to tetrabutylammonium fluoride (TBAF) for deprotection and to provide phenols **2-4** in good yield. These compounds were then screened for binding affinity against Grp94 via a fluorescence polarization assay with FITC-GDA as the tracer.^{45, 46} It was found that the binding affinity decreased with increased linker length, mirroring the results obtained from the modeling studies. Therefore, phenyl amide (compound **2** figure 2.3) was used for further modifications on the phenyl ring.

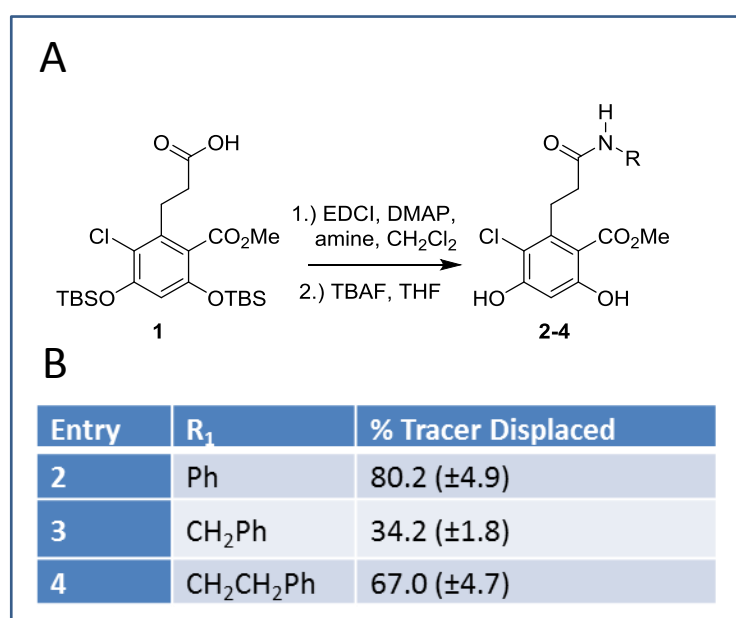


Figure 2.3 A) Synthetic scheme and B) Biological evaluation of the linker RDA analogs using fluorescence polarization assay.

Functionalization of phenyl amide **2** was pursued to explore the spatial and electronic requirements of the hydrophobic pocket by the inclusion of electron donating/withdrawing groups. As can be seen in the crystal structure, there exist two subpockets surrounding the phenyl ring of the RDA in Grp94, labeled as pockets **A** and **B** (figure 2.4). Molecular docking studies predicted that pocket **A** would be responsible for the accommodation of functional groups at the 2-position of the phenyl ring, whereas the 3- and 4-positions would project towards pocket **B**.

Substitutions at these positions could also provide potential π -stacking interactions with Phe199 and Tyr200 (figure 2.2) as well as hydrogen bonding interactions.

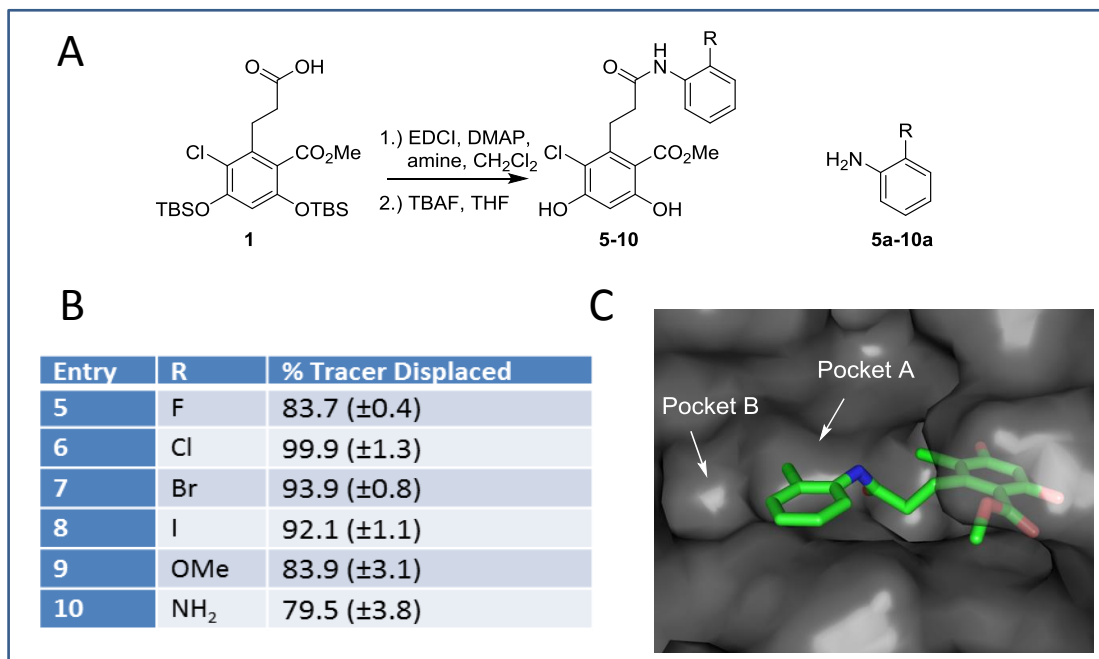


Figure 2.4 A) Synthetic scheme for compounds **5-10** B) biological evaluation of the 2-substituted RDA analogs using fluorescence polarization assay C) Compounds **6** docked in the Grp94 (PDB code 2GFD), arrows indicating the subpockets **A** and **B**.

Functionalization of **2** at the 2-position of the phenyl ring was performed in order to explore pocket **A** and/or change the electronic nature of the phenyl ring to access π - π interactions with aromatic residues within the binding pocket. EDCI-DMAP was used for activation of acid **1** for coupling with the corresponding anilines, **5a-10a**, followed by deprotection of the phenols, to generate amides **5-10** in good yields. Compounds **5-10** were then evaluated using the fluorescence polarization (FP) assay, establishing that 2-position substitutions with hydrophobic groups such as halogens provide compounds with significantly higher binding affinity ($\geq 80\%$ tracer displaced).

These compounds demonstrated that both electronic and steric effects influence the ability of these amides to bind Grp94 with the 2-chlorine exhibiting the highest affinity (**6**, 99.9% tracer displaced). It was observed that substituents larger than chlorine (for example, 2-bromine and 2-Iodine, compounds **7** and **8**, respectively) exhibit a size-dependent decline in binding affinity. The 2-fluorine derivative, **5**, also exhibits a low binding affinity when compared to **6**, which may be the result of the fluorine not occupying pocket **A** sufficiently. In addition, this could be perceived a consequence of the electronic effects manifested by fluorine on the amide

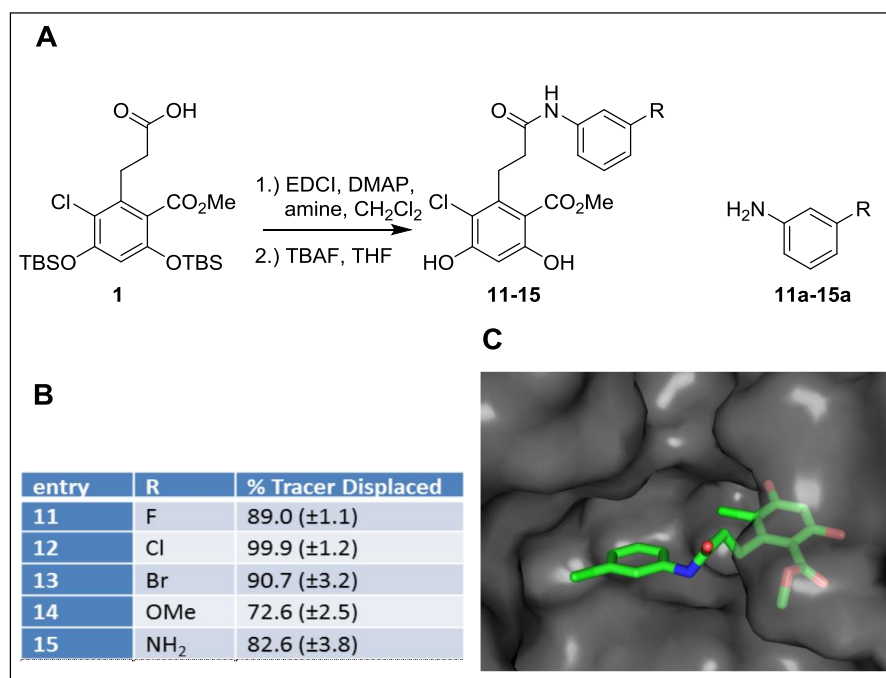


Figure 2.5 A) Synthetic scheme for compounds **11-15** B) Biological evaluation of the 3-substituted RDA analogs using fluorescence polarization assay C) Compounds **12** docked in the Grp94 (PDB code: 2GFD).

bond geometry, which is likely to disfavor the *cis*-conformation of the amide bond.⁴⁷ Substitutions with polar groups such as NH₂ and methoxy group resulted in a decrease in binding

affinity for Grp94. Finally, it was concluded that a chlorine atom at the 2-position (compound **6**) is optimal.

Additional structure-activity relationships studies were performed by the incorporation of the substituents at the 3-position of the phenyl ring of compound **2**. As can be seen in figure 2.4C, the 3-position of the phenyl ring projects into surface between pocket A and B and the amide bond may rotate to allow the 3-substitutions to enter either pocket A or B. A series of modeling studies suggested that Pocket B would best accommodate substitutions at the 3-position when compared to pocket A (figure 2.5 C). Similar to compounds **5-10**, substitutions at the 3-position

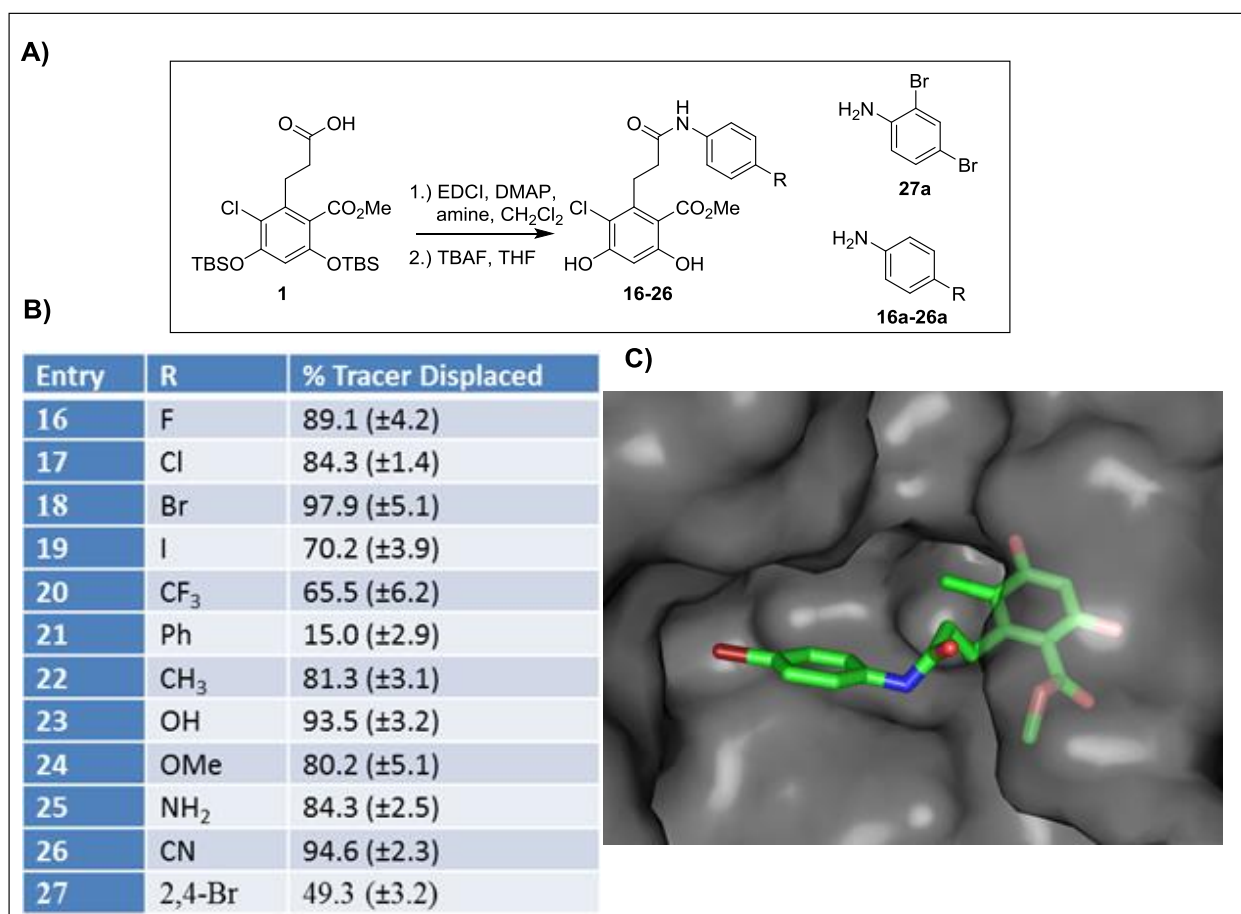


Figure 2.6 A) Synthetic scheme for compounds **16-27** B) Biological evaluation of the 4-

substituted RDA analogs using fluorescence polarization assay C) Compounds **18** docked in the Grp94 protein.

also contributed towards understanding the spatial and electronic requirements of the Grp94 hydrophobic pocket. Synthesis of 3-substituted amides was conducted via an EDCI-DMAP mediated coupling of acid **1** with the corresponding anilines, **11a-15a**, followed by silyl-deprotection to obtain the desired amides, **11-15**, in good yield. As seen in Figure 2.5, these substitutions followed a similar trend as observed for the 2-position analogs, wherein the 3-chlorine manifested the highest affinity for Grp94. In comparison, larger (compound **13**) and smaller (compound **11**) substituents resulted in diminished binding. Amino and methoxy substitutions at the 3-position manifested decreased binding affinity, establishing that a hydrogen bond donor/acceptor group at 3-position is not beneficial. Ultimately, compound **12** proved to exhibit highest affinity for Grp94 amongst the 3-substituted derivatives.

The 4-position of the phenyl ring was also substituted with electron donating and withdrawing groups. As seen in figure 2.6 C, the 4-position substitutions are oriented towards pocket **B**, as visualized by molecular docking studies. Substitutions with polar groups were sought to gain hydrogen bond interactions with Gly196. In addition, the 4-position was also investigated for steric constraints within pocket **B**, as well to alter the electronic nature of the phenyl ring to increase π - π interactions with Phe199 and Tyr200. Compounds **16-27** were synthesized with similar conditions that involved an EDCI-mediated coupling of **1** with the corresponding anilines, **16a-27a**, followed by silyl-deprotection to give amides **16-27** in good yields. When evaluated for their ability to bind Grp94, the 4-position followed an SAR trend with particular sensitivity to sterics (as shown in Figure 5). The 4-position proved to accommodate larger groups as compared to the 2-and 3-positions, which is exemplified by compound **18** as can be seen in

figure 2.6 C, wherein the bromine atom occupies pocket **B** and results in a greater affinity for compound **18**. Furthermore, compounds with smaller groups (compound **16** and **17**) and larger than bromine (compounds **19** and **20**) displayed a loss in affinity towards Grp94.

Compound	K_d in Grp94 (μM)	K_d in Hsp90(μM)
Radamide (RDA)	7.53 ± 0.31	7.56 ± 0.16
6	1.85 ± 0.22	8.22 ± 0.14
7	2.317 ± 0.15	7.62 ± 0.36
12	6.41 ± 0.11	14.6 ± 0.33
18	1.50 ± 0.18	10.45 ± 0.41
26	4.38 ± 0.33	13.08 ± 0.61

Table 2.2: K_d values determined using fluorescence polarization assay for listed compounds using Grp94 and Hsp90.

Following the trends observed for the 2- and 3-positions, electron withdrawing groups at the 4-position also exhibited a higher binding affinity than electron donating groups. Interestingly, the hydroxyl containing compound, **23**, showed higher affinity than aniline compound **25**, but less than compound **18**. Hydrogen bond acceptors such as a methoxy in compound **24** resulted in a loss of binding affinity, potentially because of the bulk arising from the methoxy group. Compound **26** containing a nitrile substitution also showed better binding affinity, bolstering the hypothesis that pocket **B** is larger than pocket **A**. Additionally, the nitrile may be acting as a hydrogen bond acceptor (potential interaction with TYR 200) and could affect the π -stacking nature of the phenyl ring.

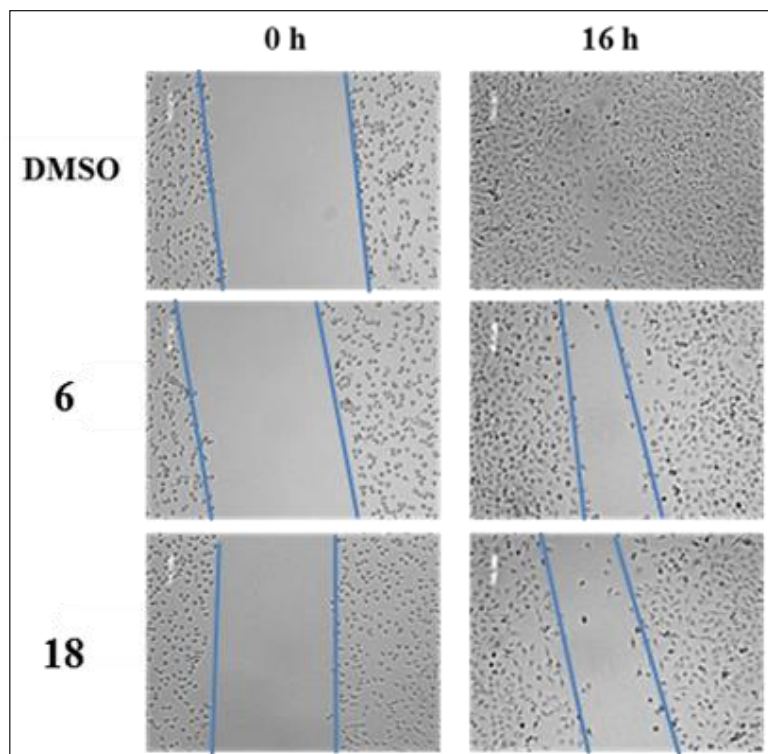


Figure 2.7 Inhibition of MDA-MB-231 cell migration by compounds **6** and **18**. MDA-MB-231 cells were cultivated for 24 h prior to treatment with compounds. Cells were incubated for 16 h at 37°C with the respective compounds indicated above (2.5 μ M).

These observations were in line with the results obtained via molecular modeling that predicted compounds **18**, **23** and **26** to bind with increased binding affinity. K_d values of the selected compounds were determined using the fluorescence polarization assay for both Grp94 as well as Hsp90. Compound **6** displayed ~4 fold selectivity and compound **18** exhibited ~7 fold selectivity, which is due to binding to pocket **B**, which is found only in Grp94. Surprisingly, compound **12** was not as effective in binding to Grp94 as compounds **6** and **18**, displaying only a moderate increase in potency and selectivity for Grp94. Compound **27** was synthesized to investigate the combined steric requirements of both the 2 and 4-positions. Unfortunately, 2-4 disubstitution led to decreased binding affinity, concluding that substitutions about the 2-and 4-

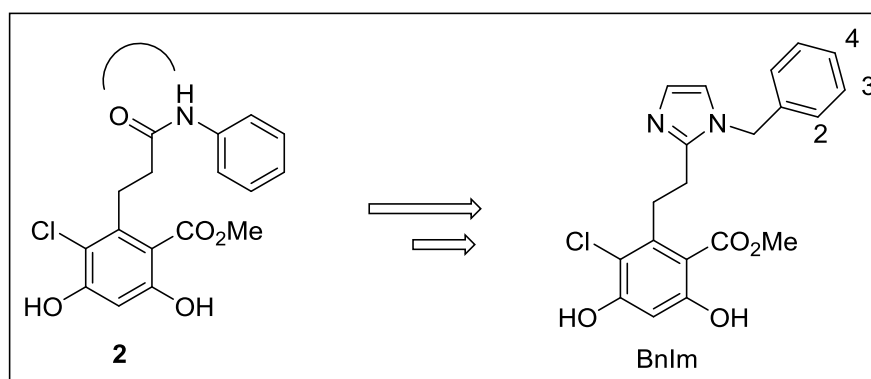
position are mutually exclusive. To determine the cellular efficacy of these compounds, a wound healing scratch assay was performed utilizing MDA-MB-231 cells, a highly metastatic breast cancer cell line that has been previously used to establish that Grp94 knockdown diminishes the ability of these cells to migrate²⁹. Hence, supporting the hypothesis that Grp94 inhibition is a potential strategy for development of anti-metastatic agents. In this assay, Compounds **6** and **18** inhibited migration of MD-MB-231 cells, which mirrored the binding affinity trend observed in fluorescence polarization assays. Furthermore, an MTS assay was performed utilizing the MDA-MB-231 cells to determine that the anti-migratory activity of these compounds did not result from their anti-proliferative activity. In the event, MDA-MB-231 cells were treated with the same concentration as in the wound healing assay (2.5 μ M) and it was found that compounds exhibited a negligible effect on the proliferation of these cells.

Compounds	% viability at 2.5 μ M compound
6	> 95
18	> 95

Table 2.3 Percent viability of MDA-MB-231 cells determined using MTS assay with DMSO serving as a positive control.

2.2 *cis*-amide isostere approach: Since the *cis*-amide conformation of RDA was observed to be responsible for selective binding to Grp94, it was hypothesized that putting a constraint onto would lock it into a predisposed *cis* conformation, which would lead to potent and selective Grp94 inhibitors. After a series of molecular modeling studies, it was determined that an imidazole ring could serve as a *cis* amide surrogate to project the phenyl ring of radamide into the unique hydrophobic pocket of Grp94. After screening the linker length between the amide

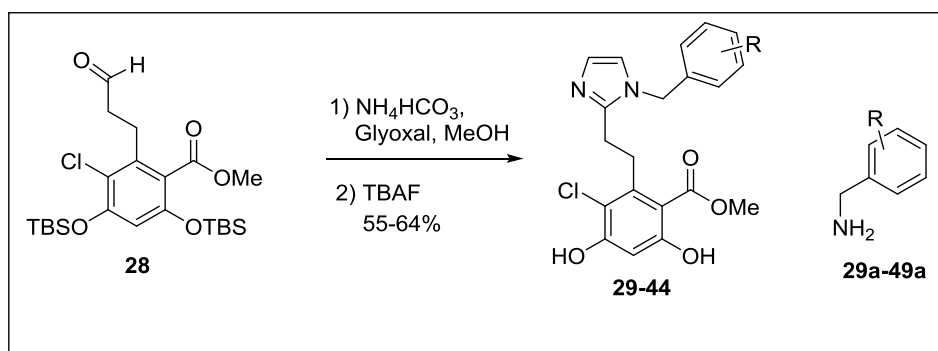
nitrogen and the phenyl ring, it was determined that the one carbon linker compound (BnIm) selectively binds to Grp94 with the highest binding affinity.³⁷ Since, the linker length was different than that optimized for RDA, binding mode of BnIm was believed to be slightly different than that of RDA. Therefore, a SAR study was needed for the BnIm scaffold to distinguish its binding mode from RDA.



Scheme 2.2 *cis*-amide constraint employed on the RDA scaffold

BnIm analogs **30-44** were synthesized using a one pot cyclization method, employing aldehyde **28** (a precursor to acid **1**)³⁷ and the corresponding substituted benzylamines, followed by deprotection to give the free phenols. The 2-position of the phenyl ring was explored via substitutions that could modify the electronic nature of the ring, potentially providing increased π -interactions with aromatic residues TYR 200 and PHE 199. In addition, substitutions were also sought to extend into the hydrophobic pocket and increase hydrophobic interactions. Among the halogen substitutions, the fluorine containing compound **30** displayed the greatest binding affinity, however it was comparable with the unsubstituted analog i.e. compound **29** (BnIm). This observation suggested that the fluorine does not affect the binding significantly, possibly because the 2-position faces the solvent in the case of the radamide crystal structure (figure **2.4**). When the size of the halogen was increased from fluorine to chlorine to bromine, such as in compounds **31** and **32**, a decrease in binding affinity was observed. The methoxy analog was prepared to

explore the binding pocket for potential hydrogen bonding interactions, and to help establish spatial requirements at the 2-position. Unfortunately, compound **33** did not show any improvement in binding affinity, and in fact, the binding affinity was diminished, suggesting that the methoxy group is not well tolerated at the 2-position.



Scheme 2.3 Synthesis of the *cis*-amide isostere analogs

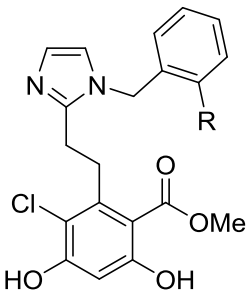
	Entry	R	% Tracer Displaced
		29 (BnIm)	H
	30	F	91.947 (±2.3)
	31	Cl	73.792 (±1.9)
	32	Br	57.8 (±2.5)
	33	OMe	19.67 (±3.6)

Table 2.4 Determination of binding affinity of compounds **29-33** (25 μ M) towards Grp94 by fluorescence polarization assay using 1 % DMSO as positive control (tracer displaced 0%).

Similarly, the 3-position of BnIm was modified with halogens to explore the hydrophobic pocket. Although it had been established with RDA analogs that the 3-position of the RDA phenyl does not allow substitution as favorably as the 4 and 2-position of the RDA phenyl ring, it was still worth pursuing with the BnIm scaffold, as it utilizes a carbon linker that may provide additional flexibility for projecting the substitutions into the Grp94 hydrophobic pocket.

Unfortunately, modifications to the 3-position led to decreased binding affinities as compared to the parent compound (**29**). The fluorine containing compound was the least active at the 3-position, followed by bromine substituted compound **36**. Interestingly, the chlorine containing compound (**35**) was the most active compound as compared to other substitutions, potentially due to the combined effects of both sterics and electronic changes to the phenyl ring. However, it did not exhibit an improvement in Grp94 binding affinity as compared to compound **29**.

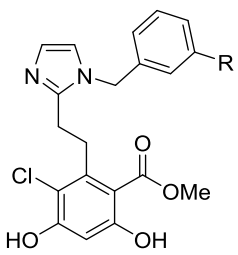
	Entry	R	% Tracer Displaced
	34	F	81.25 (±4.9)
	35	Cl	91.89 (±2.3)
	36	Br	84.78 (±3.1)
	37	OMe	0 (±4.3)

Table 2.5 Determination of binding affinity of the compounds **34-37** (25 μ M) towards Grp94 by fluorescence polarization assay using 1 % DMSO as positive control (tracer displaced 0%).

Similarly, substitutions at the 4-position were also pursued, in particular, to explore pocket B interactions (Figure **2.4**) as found in the RDA crystal structure. The hydrophobic nature of the pocket B was investigated by the incorporation of halogen and alkyl substitutions. As hypothesized, larger substituents exhibited improved binding affinity with bromine substituted compound **40** manifesting best activity amongst all the halogens. This could be due to the ability of the bromide to occupy pocket B better than other halogens (figure **2.8C**). Loss in activity for the fluorine and chlorine containing compound (**38** and **39**) could be due to the unfavorable changes within electronics of the aromatic ring. Whereas, iodine containing compound **41** appeared too bulky for the pocket **B**

A methyl group was also found beneficial for binding, however, potency was lost with increasing size, such as the incorporation of an ethyl group (**43**). Since the bromide group exhibited the highest potency amongst all substitutions, a trifluoromethyl group was utilized in compound **44** as an isostere of the bromine atom, however, it did not maintain the potency observed for compound **40**. Dissociation constants were determined for BnIm and compound **40** for binding to Hsp90 and Grp94 and compound **40** was found to bind Grp94 more tightly than BnIm. It was also found to exhibit increased selectivity of ~12 fold towards Grp94 (Table 2.6). Compound **40** has been evaluated for cellular efficacy in the mutant myocilin assay, wherein mutant myocilin (Grp94 client) degradation is monitored as a result of Grp94 inhibition. It was

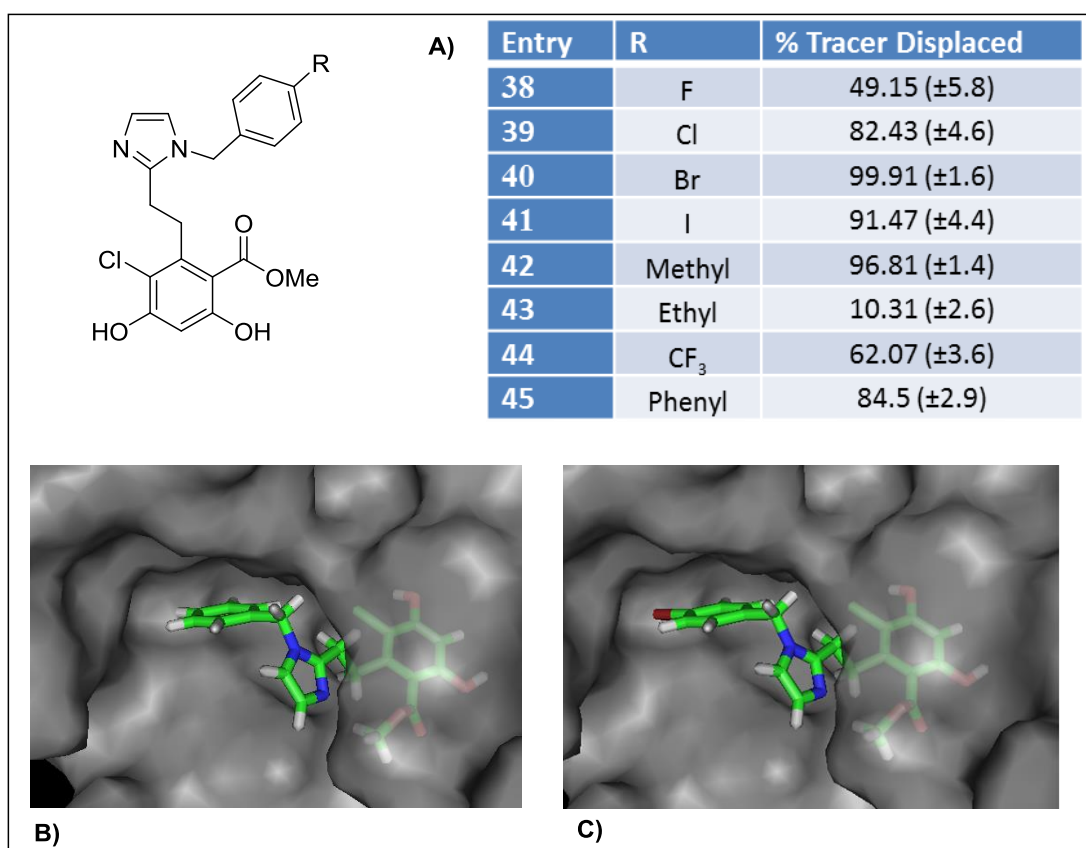


Figure 2.8 A) Determination of the binding affinity of the compounds **38-45** (25 μ M) towards Grp94 by fluorescence polarization assay using 1 % DMSO as positive control (tracer displaced

0%). **B**) Docked pose of BnIm in Grp94 (crystal structure of RDA bound to Grp94). **C**) Compound **40** docked into Grp94.

found that Compound **40** is 15 fold more potent at degrading mutant myocilin than BnIm.⁴⁸

To further explore the available space and to probe for increased π - π interactions around pocket **B**, phenyl substitutions were included at the 4-position, but these compounds manifested a loss in activity, thus concluding that a phenyl is not well tolerated in pocket **B**.

Compound	Grp94	Hsp90	Selectivity for Grp94
BnIm	1.15 (\pm 0.17)	8.32 (\pm 0.02)	\sim 7x
40	0.96 (\pm 0.25)	11.22 (\pm 0.02)	\sim 12x

Table 2.6 K_d Values for BnIm and Compound **40** determined using fluorescence polarization assay towards Grp94 and Hsp90.

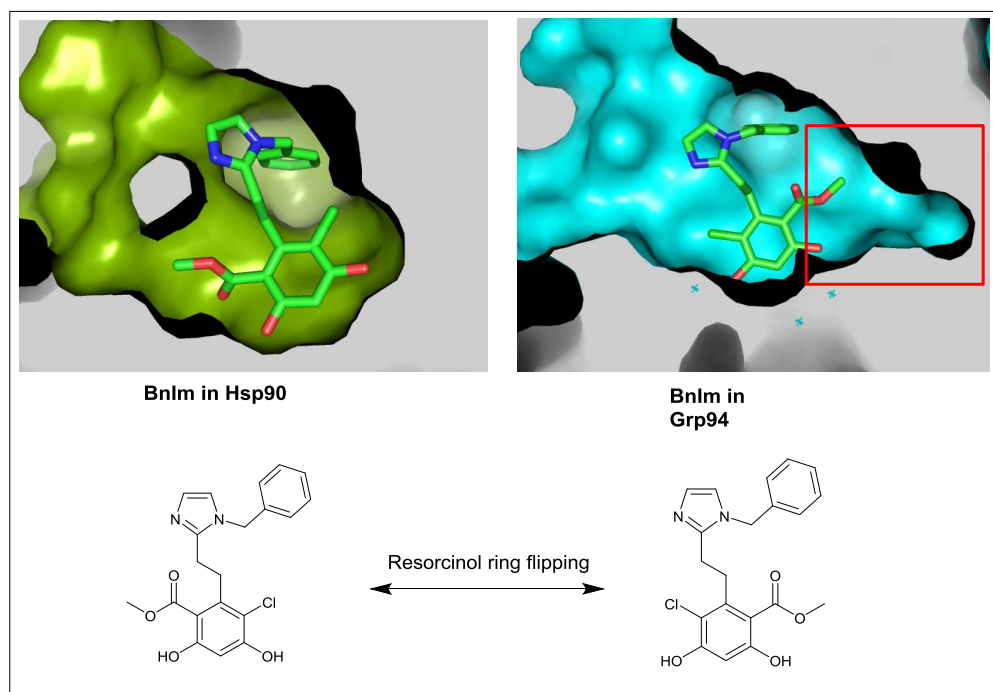


Figure 2.9 Crystal structure of BnIm bound to Hsp90(green) and Grp94(cyan). The binding pocket difference has been highlighted with a red box.

In the meantime, the crystal structures of BnIm bound to Grp94 and Hsp90 were solved in collaboration with Gewirth laboratory. Surprisingly, the binding mode of BnIm in Grp94 and Hsp90 were found to differ significantly. In particular, the resorcinol ring was found to be flipped in the Grp94 and to project the ester into the binding site, unlike the radamide crystal structure, wherein the resorcinol ester faces the open solvent (Figure 2.9). This was in stark contrast to the RDA bound structure of Hsp90 and Grp94. Immediate efforts were made to explore the new subpocket that was observed exclusively (Figure 2.9 outlined with box) in Grp94. For this purpose, the methyl ester in BnIm was replaced with bulkier alkyl substitutions. Compounds **46-48** were evaluated against Grp94 and it was determined that there was loss in potency that correlated with an increase in the size of the alkyl group.

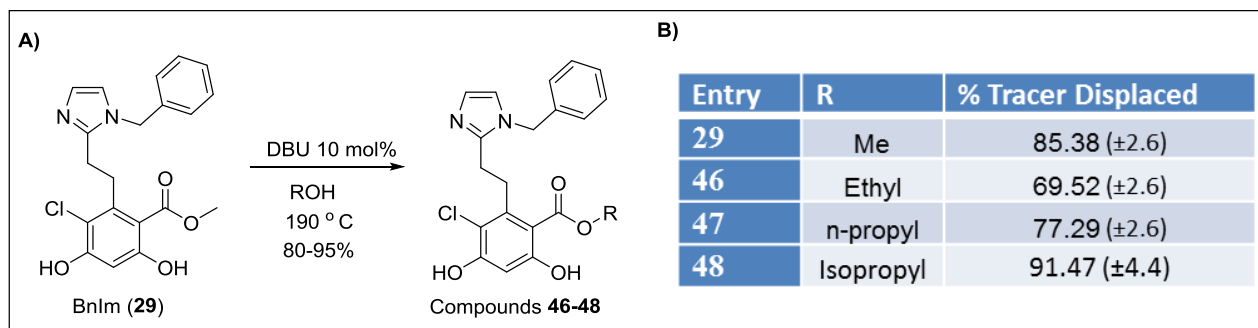


Figure 2.10 A) Synthetic scheme for the ester analogs of BnIm B) Determination of binding affinity of the compounds **29, 46-48** (3 μ M) towards Grp94 by fluorescence polarization assay using 1 % DMSO as positive control (tracer displaced 0%).

3. Conclusions and Future Directions

In summary, preliminary structure-activity relationship study has been performed on radamide and the *cis*-amide isostere containing compounds to probe for Grp94 selective inhibition. With radamide analogs, a selectivity of ~7 fold was achieved with compound **18** that also exhibited ~7 fold increase in binding affinity for Grp94 compared to RDA. In the case of the *cis*-amide isostere analogs, compound **40** manifested ~12 fold selectivity for Grp94 as compared to ~7 fold for the parent compound BnIm. These compounds also display efficacy in cellular assays, such as the wound healing scratch assay and the mutant myocilin degradation assay.

The two carbon linker appears to represent a source of entropic penalties for both scaffolds and future modifications will focus on the same. Multiple *cis*-amide isosteres need to be explored for the BnIm analogs to determine whether enhanced π - π interactions can be achieved. Furthermore, the newly identified pocket in case of BnIm bound to Grp94 will also be explored.

4. General Experimental Methods.

Fluorescence Polarization. Assay buffer (25 μ L, 20 mM HEPES pH 7.3, 50 mM KCl, 5 mM MgCl₂, 1 mM DTT, 20 mM Na₂MoO₄, 0.01% NP-40, and 0.5 mg/mL BGG) was added to 96-well plate (black well, black bottom) followed by the desired compound at the indicated final concentrations in DMSO (1% DMSO final concentration).³² Recombinant cGrp94 (10nM for compounds 2-27, 30 nM for compounds 28-48) and FITC-GDA were then added (6 nM). Plates were incubated with rocking for 24 h at 4°C. Fluorescence was determined using excitation and emission filters of 485 and 528 nm, respectively. Percent FITC-GDA bound was determined by using the DMSO millipolarization unit (mP) as the 100% bound value and the 0% for FITC-GDA. K_d values were calculated from separate experiments performed in triplicate using GraphPad Prism.

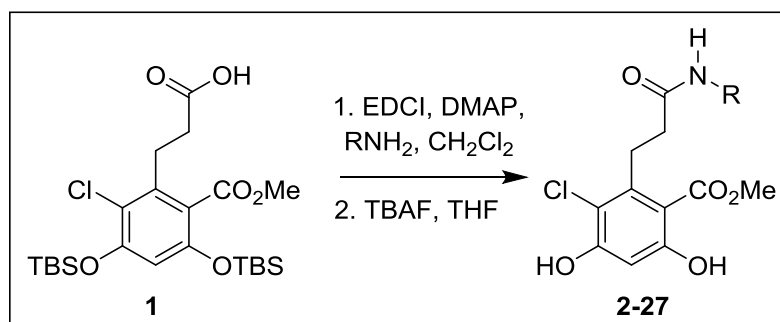
Anti-proliferation Assays. MDA-MB-231 cells were maintained in DMEM (Cellgro) media, supplemented with nonessential amino acids, L-glutamine (2 mM), streptomycin (500 μ g/mL), penicillin (100 units/mL) and 10% FBS. Cells were grown to confluence in a humidified atmosphere (37°C, 5% CO₂), seeded (2000/well, 100 μ L) in 96-well plates, and allowed to attach overnight. Compounds with varying concentrations in DMSO (1% DMSO final concentration) were added, and cells were returned to the incubator for 72 h. After 72 h, the cell viability was determined using an MTS/PMS cell proliferation kit (Promega) per the manufacturer's instructions. Absorption value from 1% DMSO wells were used as 100% proliferation, and values were adjusted accordingly.

Wound-Healing Scratch Assay. MDA-MB-231 cells were grown to confluence in a humidified atmosphere (37°C, 5% CO₂), seeded (200000/well, 1 mL) in 12-well plates, and allowed to grow to a confluent monolayer (24 h) at 37°C and 5% CO₂. Each well was then scratched with a 200 µL sterile pipet tip, and then imaged with an Olympus IX-71 microscope (60x objective, time=0 h), the respective compound solutions (2.5 µL, final DMSO concentration is 0.25%) were added, and the plates were returned to the incubator. Cell migration was recorded after 16 h of incubation. All experiments were run in quadruplicate on two different days.

Molecular Modeling. Surflex-Docking module in Sybyl v8.0 was used for molecular modeling and docking studies. The co-crystal structure of RDA bound to Grp94 and γ Hsp82 was utilized for all docking experiments.³⁰ The docked molecules were locked in a *cis*-amide conformation and rotation of the bonds was unrestricted. Pymol was used for further visualization and figure preparation.

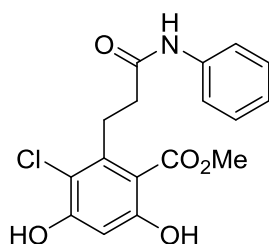
Chemistry

General procedure A: Amide coupling

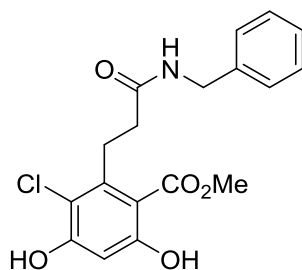


General Amide Formation for Compounds 2-27. To a solution of acid **1** (0.05 mmol), EDCI·HCl (0.12 mmol), and DMAP (0.13 mmol) in CH₂Cl₂ (1 mL) was added the corresponding aniline (0.1 mmol) and stirred at room temperature under Argon overnight. Upon

completion of reaction as monitored by TLC, the solvent was removed in vacuo and redissolved in THF (1 mL). The reaction mixture was then treated with TBAF (0.2 mmol) and stirred for 30 min, and upon completion saturated aqueous NH₄Cl was added and extracted 3x with EtOAc. The combined organic layers were then dried over Na₂SO₄, filtered, and concentrated *in vacuo*. The residue was purified via chromatography (SiO₂, 49:1, CH₂Cl₂:MeOH) to afford the desired amide.

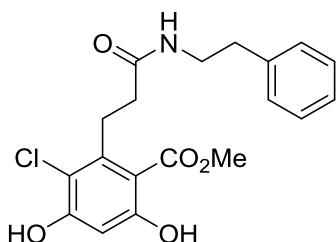


Ethyl 3-chloro-4,6-dihydroxy-2-(3-oxo-3-(phenylamino)propyl)benzoate (2). 15 mg, 86% yield, white solid. ¹H NMR (400 MHz, CDCl₃): δ 11.23 (s, 1 H), 7.53 (d, *J* = 7.91 Hz, 2 H), 7.34 (t, *J* = 7.66 Hz, 2 H), 7.12 (t, *J* = 7.36 Hz, 1 H), 6.59 (s, 1 H), 6.33 (s, 1 H), 3.97 (s, 3 H), 3.50 (dd, *J* = 5.76, 10.15 Hz, 2 H), 2.66-2.59 (m, 2 H). ¹³C NMR (125 MHz, CDCl₃): δ = 170.43, 169.99, 162.91, 156.28, 141.66, 137.73, 129.10 (2 C), 124.40, 119.72 (2 C), 113.92, 106.81, 102.94, 52.75, 36.73, 28.81. HRMS (ESI) *m/z* [M+Na⁺] for C₁₇H₁₆ClNO₅Na: 372.0609, found: 372.0609.

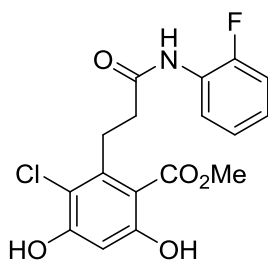


Methyl 2-(3-(benzylamino)-3-oxopropyl)-3-chloro-4,6-dihydroxybenzoate (3). 30 mg, 83% yield, white solid. ¹H NMR (500 MHz, CDCl₃): δ 7.32 – 7.21 (m, 5H), 6.44 (s, 1H), 4.40 (d, *J* =

4.7 Hz, 2H), 3.86 (s, 3H), 3.44 – 3.29 (m, 2H), 2.50 – 2.33 (m, 2H). ^{13}C NMR (125 MHz, CDCl_3) δ 171.98, 170.68, 162.51, 157.03, 141.87, 138.12, 127.81, 127.60, 114.22, 106.34, 102.63, 52.53, 49.78, 43.73, 35.65, 28.92. HRMS (ESI) m/z $[\text{M}+\text{Na}^+]$ for $\text{C}_{18}\text{H}_{18}\text{ClNO}_5\text{Na}$: 386.0874; found: 386.0877.

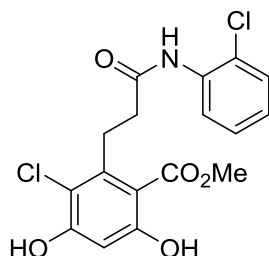


Methyl 3-chloro-4,6-dihydroxy-2-(3-oxo-3-(phenethylamino)propyl)benzoate (4). 17 mg, 90% yield, white solid. ^1H NMR (400 MHz, CDCl_3): δ 11.29 (s, 1H), 7.32 (dd, $J = 6.63, 8.10$ Hz, 2H), 7.26-7.23 (m, 1H), 7.22-7.17 (m, 2H), 6.57 (s, 1H), 5.48 (t, $J = 5.95$ Hz, 2H), 3.91 (s, 3H), 3.56 (q, $J = 6.58$ Hz, 2H), 3.40-3.34 (m, 2H), 2.84 (t, $J = 6.84$ Hz, 2H), 2.41-2.35 (m, 2H). ^{13}C NMR (125 MHz, CDCl_3): δ 171.92, 170.64, 162.90, 156.43, 141.74, 138.72, 128.77, 128.71, 126.63, 113.90, 106.64, 102.80, 52.58, 40.63, 35.81, 35.61, 29.05. HRMS (ESI) m/z $[\text{M}+\text{Na}^+]$ for $\text{C}_{19}\text{H}_{20}\text{ClNO}_5\text{Na}$: 400.0922, found: 400.0931.

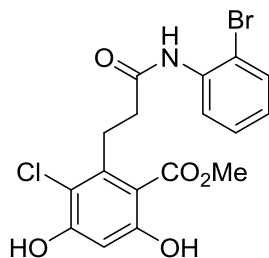


Methyl 3-fluoro-2-(3-((2-chlorophenyl)amino)-3-oxopropyl)-4,6-dihydroxybenzoate (5). 15 mg, 81% yield, white solid. ^1H NMR (500 MHz, CDCl_3) δ 11.19 (s, 1H), 8.49 – 8.00 (m, 1H), 7.34 (s, 1H), 7.12 – 6.97 (m, 3H), 6.53 (s, 1H), 6.05 (s, 1H), 3.91 (s, 3H), 3.49 – 3.37 (m, 2H),

2.67 – 2.57 (m, 2H). ¹³C NMR (125 MHz, CDCl₃) δ 170.45, 169.98, 163.02, 156.23, 141.37, 124.71, 124.68, 124.37, 121.60, 114.87, 114.72, 113.86, 106.81, 102.99, 52.73, 36.80, 28.83. HRMS (ESI) *m/z* [M+Na⁺] for C₁₇H₁₅ClFNO₅Na: 390.0521; found: 390.0547.

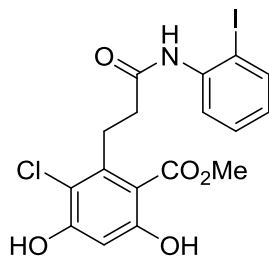


Methyl 3-chloro-2-(3-((2-chlorophenyl)amino)-3-oxopropyl)-4,6-dihydroxybenzoate (6). 14 mg, 73% yield, white solid. ¹H NMR (500 MHz, CDCl₃) δ 11.22 (s, 1H), 8.36 (d, *J* = 8.3 Hz, 1H), 7.61 (s, 1H), 7.31 (dd, *J* = 8.0, 1.5 Hz, 1H), 7.26 – 7.21 (m, 1H), 7.02 – 6.97 (m, 1H), 6.53 (s, 1H), 3.91 (s, 4H), 3.54 – 3.32 (m, 2H), 2.76 – 2.47 (m, 3H). ¹³C NMR (126 MHz, CDCl₃) δ 170.49, 169.99, 163.08, 156.23, 141.30, 134.49, 129.04, 127.85, 124.68, 122.45, 121.47, 113.86, 106.83, 103.00, 52.75, 37.03, 28.90. HRMS (ESI) *m/z* [M+Na⁺] for C₁₇H₁₅Cl₂NO₅Na: 406.0225; found: 406.0246.

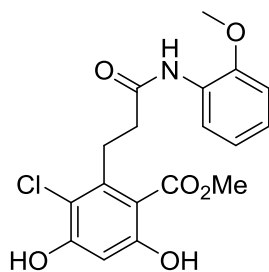


Methyl 2-(3-((2-bromophenyl)amino)-3-oxopropyl)-3-chloro-4,6-dihydroxybenzoate (7). 16.3 mg, 76% yield, pale yellow solid. ¹H NMR (500 MHz, Chloroform-d) δ 11.31 (s, 1H), 8.38 (s, 1H), 7.67 (s, 1H), 7.55 (dd, *J* = 8.1, 1.5 Hz, 1H), 7.34 (m, 1H), 7.00 (m, 1H), 6.59 (s, 1H), 6.20 (s, 1H), 3.98 (s, 3H), 3.59 – 3.42 (m, 2H), 2.71 (t, *J* = 8.3 Hz, 2H). ¹³C NMR (125 MHz, CDCl₃) δ 170.54, 170.04, 163.07, 156.29, 141.26, 135.54, 132.27, 128.50, 125.26, 121.80,

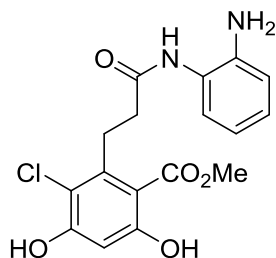
113.89, 113.18, 106.80, 103.01, 52.79, 37.05, 27.08. HRMS (ESI) m/z $[M+Na^+]$ for $C_{17}H_{15}BrClNO_5Na$: 449.9720; found: 449.9767.



Methyl 3-chloro-4,6-dihydroxy-2-(3-((2-iodophenyl)amino)-3-oxopropyl)benzoate (8). 18.2 mg, 77% yield, pale yellow solid. 1H NMR (500 MHz, $CDCl_3$) δ 11.27 (s, 1H), 8.21 (d, $J = 8.2$ Hz, 1H), 7.77 – 7.23 (m, 3H), 6.82 – 6.78 (m, 1H), 6.53 (s, 1H), 6.03 (s, 1H), 3.92 (s, 3H), 3.51 – 3.37 (m, 2H), 2.72 – 2.52 (m, 2H). ^{13}C NMR (126 MHz, $CDCl_3$) δ 170.58, 169.99, 163.13, 156.24, 141.26, 138.84, 138.04, 129.38, 126.07, 122.95, 121.88, 113.88, 106.85, 103.01, 52.84, 37.05, 28.97. HRMS (ESI) m/z $[M+Na^+]$ for $C_{17}H_{15}ClINO_5Na$: 497.9581; found: 497.9593.

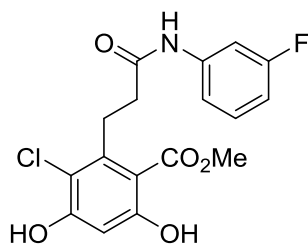


Methyl 3-chloro-4,6-dihydroxy-2-(3-((2-methoxyphenyl)amino)-3-oxopropyl)benzoate (9). 14.5 mg, 77% yield, white solid. 1H NMR (500 MHz, $CDCl_3$) δ 11.40 (s, 1H), 8.41 (dd, $J = 7.9$, 1.7 Hz, 1H), 7.77 (s, 1H), 7.10 – 6.85 (m, 3H), 6.59 (s, 1H), 3.96 (s, 3H), 3.87 (s, 3H), 3.56 – 3.46 (m, 2H), 2.71 – 2.62 (m, 2H). ^{13}C NMR (125 MHz, CD_3OD) δ 173.39, 171.67, 161.61, 158.99, 151.43, 142.28, 128.21, 126.10, 123.37, 121.46, 114.98, 111.74, 109.46, 103.16, 56.19, 52.83, 37.23, 29.40. HRMS (ESI) m/z $[M+H]$ for $C_{18}H_{18}ClNO_6$: 380.0901; found: 380.0920.



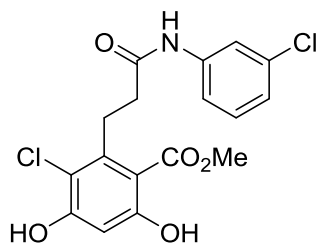
Methyl 2-(3-((2-aminophenyl)amino)-3-oxopropyl)-3-chloro-4,6-dihydroxybenzoate (10).

7.5 mg, 41% yield, pale yellow solid. ^1H NMR (400 MHz, CD_3OD) δ 7.07 – 6.90 (m, 2H), 6.81 – 6.60 (m, 2H), 6.32 (d, $J = 4.7$ Hz, 1H), 3.84 (d, $J = 5.2$ Hz, 3H), 3.33 – 3.23 (m, 2H), 2.68 – 2.58 (m, 2H). ^{13}C NMR (125 MHz, CD_3OD) δ 173.77, 171.72, 161.58, 159.34, 143.21, 142.29, 128.24, 127.13, 125.21, 119.62, 118.61, 115.21, 109.28, 103.28, 52.91, 36.45, 29.33. HRMS (ESI) m/z [$\text{M} + \text{Na}^+$] for $\text{C}_{17}\text{H}_{17}\text{ClN}_2\text{O}_5\text{Na}$: 387.0724; found: 387.0744.

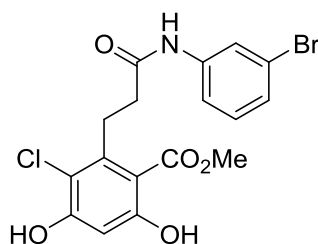


Methyl 3-chloro-2-(3-((3-fluorophenyl)amino)-3-oxopropyl)-4,6-dihydroxybenzoate (11).

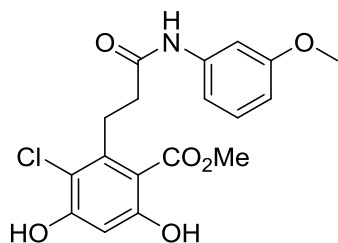
27 mg, 74% yield, white amorphous solid: ^1H NMR (500 MHz, $(\text{CD}_3)_2\text{CO}$) δ 9.38 (br s, 1H), 7.86 – 7.64 (m, 1H), 7.37 – 7.22 (m, 2H), 6.81 (m, 1H), 6.51 (s, 1H), 3.95 (s, 3H), 3.57 – 3.20 (m, 2H), 2.84 – 2.52 (m, 2H); ^{13}C NMR (125 MHz, $(\text{CD}_3)_2\text{CO}$): δ 171.37, 164.74, 162.86, 162.33, 158.65, 143.04, 142.17, 131.08, 130.96, 115.53, 110.44, 108.24, 106.93, 103.28, 52.99, 36.87, 28.86; HRMS (ESI) m/z [$\text{M} + \text{H}^+$] for $\text{C}_{17}\text{H}_{15}\text{ClFNO}_5$: 368.0701; found: 368.0701.



Methyl 3-chloro-2-(3-((3-chlorophenyl)amino)-3-oxopropyl)-4,6-dihydroxybenzoate (12). 30 mg, 78% yield, white amorphous solid: ^1H NMR (500 MHz, $(\text{CD}_3)_2\text{CO}$) δ 9.33 (s, 1H), 8.06 – 7.85 (m, 1H), 7.49 (m, 1H), 7.31 (t, $J = 8.1$ Hz, 1H), 7.08 (m, 1H), 6.51 (s, 1H), 3.95 (s, 3H), 3.69 – 3.33 (m, 2H), 2.85 – 2.53 (m, 2H); ^{13}C NMR(125MHz. $(\text{CD}_3)_2\text{CO}$): δ 171.31, 171.34, 162.37, 158.65, 143.04, 141.89, 134.73, 131.07, 123.82, 119.80, 118.17, 114.82, 108.23, 103.25, 52.97, 36.84, 28.85; HRMS (ESI) m/z $[\text{M} - \text{H}]$ for $\text{C}_{17}\text{H}_{14}\text{Cl}_2\text{NO}_5$: 382.0249; found: 382.0237.

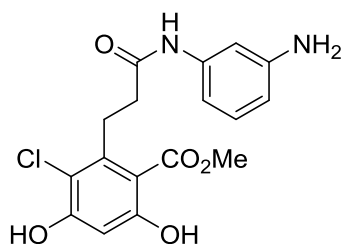


Methyl 2-(3-((3-bromophenyl)amino)-3-oxopropyl)-3-chloro-4,6-dihydroxybenzoate (13). 27 mg, 74% yield, white amorphous solid: ^1H NMR (500 MHz, $(\text{CD}_3)_2\text{CO}$) δ 9.32 (s, 1H), 8.10 (q, $J = 1.6$ Hz, 1H), 7.66 – 7.46 (m, 1H), 7.38 – 7.15 (m, 2H), 6.51 (s, 1H), 3.95 (s, 3H), 3.60 – 3.33 (m, 2H), 2.73 – 2.61 (m, 2H). ^{13}C NMR (125 MHz, $(\text{CD}_3)_2\text{CO}$) δ 171.32, 171.26, 158.63, 142.99, 131.31, 126.77, 122.77, 122.70, 122.62, 118.63, 118.54, 114.81, 108.21, 103.18, 52.93, 36.81, 28.84; HRMS (ESI) m/z $[\text{M} + \text{Na}^+]$ for $\text{C}_{17}\text{H}_{15}\text{ClBrNO}_5\text{Na}$: 449.9720; found: 449.9720.



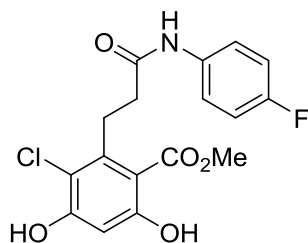
Methyl 3-chloro-4,6-dihydroxy-2-(3-((3-methoxyphenyl)amino)-3-oxopropyl)benzoate (14).

14.6 mg, 76% yield, white solid. ^1H NMR (500 MHz, CDCl_3) δ 11.15 (s, 1H), 7.30 – 7.11 (m, 3H), 6.92 – 6.58 (m, 2H), 6.52 (s, 1H), 6.25 (s, 1H), 3.90 (s, 3H), 3.75 (s, 3H), 3.46 – 3.37 (m, 2H), 2.58 – 2.51 (m, 2H). ^{13}C NMR (126 MHz, CDCl_3) δ 170.82, 170.71, 162.10, 160.03, 157.67, 142.01, 139.24, 129.61, 114.59, 111.83, 109.92, 106.09, 105.39, 102.47, 55.27, 52.54, 36.41, 28.58. HRMS (ESI) m/z [$\text{M}+\text{Na}^+$] for $\text{C}_{18}\text{H}_{18}\text{ClNO}_6$: 402.0720; found: 402.0722.



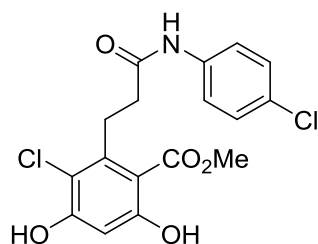
Methyl 2-(3-((3-aminophenyl)amino)-3-oxopropyl)-3-chloro-4,6-dihydroxybenzoate (15).

9 mg, 49% yield, pale yellow solid. ^1H NMR (400 MHz, CDCl_3) δ 7.12 – 7.05 (m, 1H), 7.01 (t, J = 8.0 Hz, 1H), 6.68 (dd, J = 7.8, 2.1 Hz, 1H), 6.44 – 6.26 (m, 2H), 3.87 (s, 3H), 3.38 (t, J = 8.4 Hz, 2H), 2.61 – 2.47 (m, 2H). ^{13}C NMR (125 MHz, CDCl_3) δ 170.50, 162.27, 157.40, 146.36, 141.98, 139.20, 129.72, 114.46, 111.35, 110.11, 106.84, 106.20, 102.55, 52.57, 36.57, 29.69, 28.69. HRMS (ESI) m/z [$\text{M}+\text{Na}^+$] for $\text{C}_{17}\text{H}_{17}\text{ClN}_2\text{O}_5\text{Na}$: 387.0724; found: 387.0736.



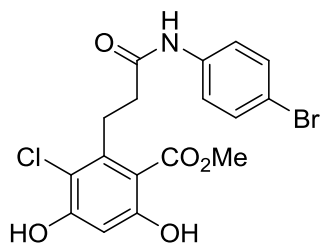
Methyl 3-chloro-2-(3-((4-fluorophenyl)amino)-3-oxopropyl)-4,6-dihydroxybenzoate (16).

14.5 mg, 80% yield, white solid. ^1H NMR (500 MHz, CDCl_3) δ 11.28 (s, 1H), 7.89 (s, 1H), 7.50 (m, 2H), 7.02 (t, $J = 8.7$ Hz, 2H), 6.50 (s, 1H), 3.96 (s, 3H), 3.52 – 3.44 (m, 2H), 2.65 – 2.56 (m, 2H). ^{13}C NMR (125 MHz, CDCl_3) δ 170.34, 169.85, 162.91, 160.34, 156.21, 141.58, 121.57, 121.50, 115.82, 115.64, 113.88, 106.86, 102.98, 52.73, 36.57, 28.79. HRMS (ESI) m/z $[\text{M}+\text{Na}^+]$ for $\text{C}_{17}\text{H}_{15}\text{ClFNO}_5\text{Na}$: 390.0521; found: 390.0553.



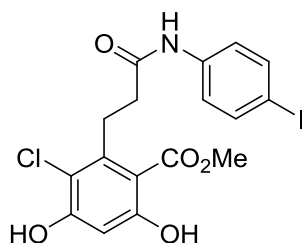
Methyl 3-chloro-2-(3-((4-chlorophenyl)amino)-3-oxopropyl)-4,6-dihydroxybenzoate (17).

13.8 mg, 72% yield, white solid. ^1H NMR (500 MHz, CDCl_3) δ 11.16 (s, 1H), 7.52 – 7.45 (m, 2H), 7.32 – 7.28 (m, 2H), 6.60 (s, 1H), 6.14 (s, 1H), 3.97 (s, 3H), 3.55 – 3.45 (m, 2H), 2.65 – 2.59 (m, 2H). ^{13}C NMR (125 MHz, CDCl_3) δ 170.45, 170.35, 162.39, 157.07, 141.80, 136.48, 129.09, 128.99, 120.84, 114.29, 106.38, 102.70, 52.62, 36.48, 28.64. HRMS (ESI) m/z $[\text{M}+\text{Na}^+]$ for $\text{C}_{17}\text{H}_{15}\text{Cl}_2\text{NO}_5\text{Na}$: 406.0225; found: 406.0234.



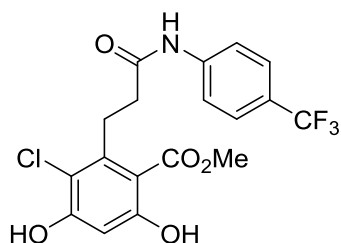
Methyl 2-(3-((4-bromophenyl)amino)-3-oxopropyl)-3-chloro-4,6-dihydroxybenzoate (18).

15 mg, 70% yield, white solid. ^1H NMR (500 MHz, CDCl_3) δ 7.38 (s, 4H), 6.49 (s, 1H), 3.90 (s, 3H), 3.45 – 3.39 (m, 2H), 2.58 – 2.52 (m, 2H). ^{13}C NMR (125 MHz, CDCl_3) δ 170.27, 169.88, 162.91, 156.18, 141.50, 136.83, 132.05, 121.18, 116.89, 113.864, 106.87, 103.01, 52.74, 36.71, 28.71. HRMS (ESI) m/z [$\text{M}+\text{Na}^+$] for $\text{C}_{17}\text{H}_{15}\text{BrClINO}_5\text{Na}$: 449.9720; found: 449.9740.

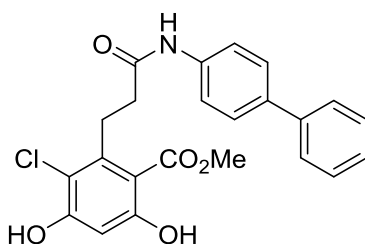


methyl 3-chloro-4,6-dihydroxy-2-(3-((4-iodophenyl)amino)-3-oxopropyl)benzoate (19).

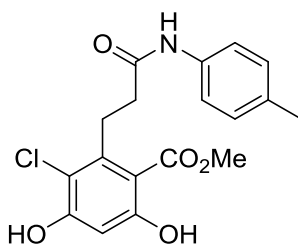
22 mg, 76% yield, white solid. ^1H NMR (500 MHz, CDCl_3 and CD_3OD) δ 7.55 (dd, 2H), 7.28 (dd, 2H), 6.43 (s, 1H), 3.89 (s, 3H), 3.41 – 3.39 (m, 2H), 2.56 – 2.53 (m, 2H). ^{13}C NMR (126 MHz, CDCl_3) δ 169.93, 162.88, 156.22, 149.99, 141.51, 137.99, 129.72, 128.84, 126.65, 126.34, 121.46, 103.01, 52.74, 36.74, 28.69. HRMS (ESI) m/z [$\text{M}+\text{Na}^+$] for $\text{C}_{17}\text{H}_{15}\text{ClINO}_5\text{Na}$: 497.9683; found: 497.9656.



Methyl 3-chloro-4,6-dihydroxy-2-(3-oxo-3-((4-trifluoromethyl)phenyl)amino)propyl)benzoate (20). 31 mg, 74% yield, white amorphous solid: ^1H NMR (500 MHz, $(\text{CD}_3)_2\text{CO}$) δ 8.13 – 7.78 (m, 2H), 7.65 (dd, $J = 8.8, 2.5$ Hz, 2H), 6.51 (t, $J = 1.7$ Hz, 1H), 3.95 (t, $J = 1.8$ Hz, 3H), 3.44 (m, 2H), 2.72 (m, 2H); ^{13}C NMR (125 MHz, $(\text{CD}_3)_2\text{CO}$) δ 171.51, 171.47, 171.30, 162.25, 158.67, 142.94, 126.95, 126.82, 119.82, 119.81, 114.83, 108.27, 103.22, 52.98, 36.82, 28.87. HRMS (ESI) m/z [$\text{M} + \text{H}^+$] for $\text{C}_{18}\text{H}_{16}\text{ClF}_3\text{NO}_5$: 418.0669; found: 418.0669.

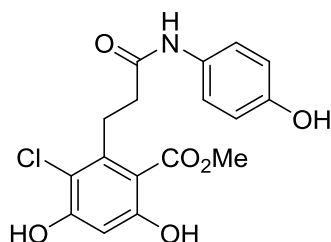


Methyl 2-(3-([1,1'-biphenyl]-4-ylamino)-3-oxopropyl)-3-chloro-4,6-dihydroxybenzoate (21). 12.5 mg, 60% yield, white solid. ^1H NMR (400 MHz, CDCl_3) δ 11.24 (s, 1H), 7.65 – 7.56 (m, 6H), 7.48 – 7.31 (m, 3H), 7.23 (d, $J = 5.6$ Hz, 1H), 6.61 (s, 1H), 6.10 (s, 1H), 4.00 (s, 3H), 3.57 – 3.49 (m, 2H), 2.70 – 2.63 (m, 2H). ^{13}C NMR (125 MHz, CDCl_3) δ 170.41, 169.88, 162.96, 156.19, 141.64, 140.41, 137.25, 137.03, 128.81, 127.70, 127.17, 126.84, 119.96, 113.88, 106.87, 102.96, 52.75, 36.75, 28.82. HRMS (ESI) m/z [$\text{M} + \text{Na}^+$] for $\text{C}_{23}\text{H}_{20}\text{ClNO}_5\text{Na}$: 448.0928; found: 448.0946.



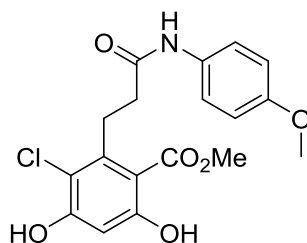
Methyl 3-chloro-4,6-dihydroxy-2-(3-oxo-3-(p-tolylamino)propyl)benzoate (22). 14 mg, 76% yield, white solid. ^1H NMR (500 MHz, CD_3OD) δ 7.32 (dd, $J = 8.5, 2.0$ Hz, 2H), 7.08 – 7.02 (m,

2H), 6.47 (s, 1H), 3.88 (s, 3H), 3.45 – 3.37 (m, 2H), 2.56 – 2.49 (m, 2H), 2.24 (s, 3H). ^{13}C NMR (126 MHz, CD_3OD) δ 168.00, 167.60, 167.51, 154.20, 139.34, 132.64, 131.44, 127.00, 117.21, 111.59, 104.03, 100.23, 50.14, 34.05, 26.29, 18.34. HRMS (ESI) m/z $[\text{M}+\text{Na}^+]$ for $\text{C}_{18}\text{H}_{18}\text{ClNO}_5\text{Na}$: 386.0771 ; found: 386.1007.



Methyl 3-chloro-4,6-dihydroxy-2-(3-((4-hydroxyphenyl)amino)-3-oxopropyl)benzoate (23).

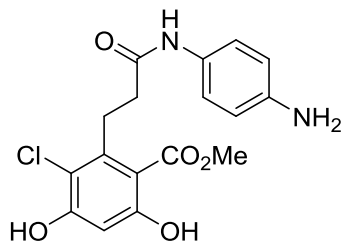
8.8 mg, 48% yield, white solid. ^1H NMR (500 MHz, CD_3OD) δ 7.36 – 7.27 (m, 2H), 6.74 – 6.63 (m, 2H), 6.38 (s, 1H), 3.88 (s, 3H), 3.30-3.28 (m, 2H), 2.64 – 2.55 (m, 2H). ^{13}C NMR (125 MHz, CD_3OD) δ 172.98, 171.64, 161.37, 158.85, 155.34, 142.31, 131.72, 123.38, 116.18, 114.89, 109.69, 103.11, 52.84, 36.88, 29.19. HRMS (ESI) m/z $[\text{M}+\text{Na}^+]$ for $\text{C}_{17}\text{H}_{16}\text{ClNO}_6\text{Na}$: 388.0564 ; found: 388.0556.



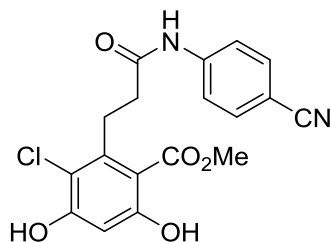
Methyl 3-chloro-4,6-dihydroxy-2-(3-((4-methoxyphenyl)amino)-3-oxopropyl)benzoate (24).

32 mg, 73% yield, white powder. ^1H NMR (500 MHz, CD_3OD): δ 7.42-7.37 (m, 2 H), 6.84-6.79 (m, 2 H), 6.41 (s, 1 H), 3.90 (s, 3 H), 3.75 (s, 3 H), 3.45-3.39 (m, 2 H), 2.58-2.52 (m, 2 H). ^{13}C NMR (125 MHz, CD_3OD): δ 170.74, 170.72, 161.9, 157.8, 156.1, 142.0, 131.1, 121.6, 114.6,

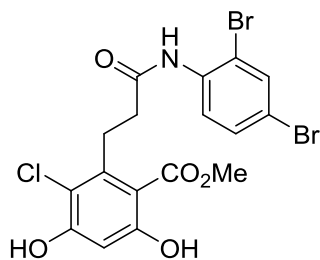
114.0, 106.0, 102.3, 55.4, 52.4, 36.1, 28.6. HRMS (ESI) m/z $[M+Na^+]$ for $C_{18}H_{18}ClNO_6Na$: 402.0720; found: 402.0725.



Methyl 2-(3-((4-aminophenyl)amino)-3-oxopropyl)-3-chloro-4,6-dihydroxybenzoate (25). 8 mg, 33% yield, dark brown solid. 1H NMR (400 MHz, CD_3OD) δ 7.45 – 7.27 (m, 2H), 6.90 – 6.74 (m, 2H), 6.50 (s, 1H), 4.00 (s, 3H), 3.38 (t, $J = 8.4$ Hz, 2H), 2.77 – 2.65 (m, 2H). ^{13}C NMR (125 MHz, $CDCl_3$ and CD_3OD) δ 170.59, 169.91, 162.49, 156.88, 143.10, 141.99, 129.23, 121.91, 115.51, 106.47, 102.65, 52.63, 49.80, 36.43, 28.90. HRMS (ESI) m/z $[M+Na^+]$ for $C_{17}H_{17}ClN_2O_5Na$: 387.0826; found: 387.0836.

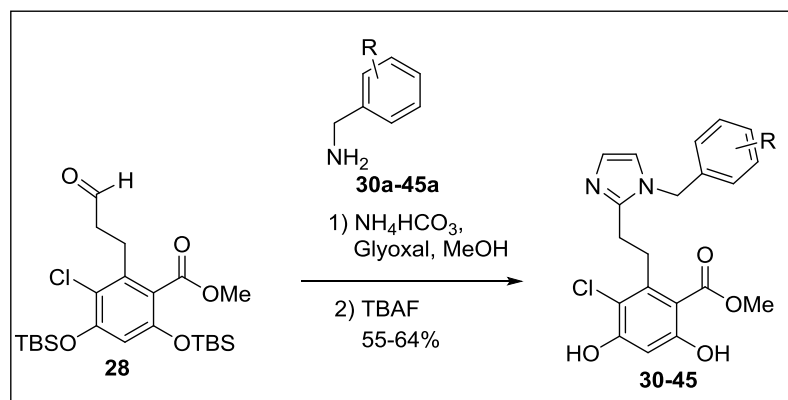


Methyl 3-chloro-2-(3-((4-cyanophenyl)amino)-3-oxopropyl)-4,6-dihydroxybenzoate (26). 13.6 mg, 72% yield, white solid. 1H NMR (500 MHz, $CDCl_3$ and CD_3OD) δ 7.71 – 7.60 (m, 4H), 6.56 (s, 1H), 3.98 (s, 3H), 3.53–3.46 (m, 2H), 2.70–2.64 (m, 2H). ^{13}C NMR (125 MHz, $CDCl_3$) δ 170.97, 170.41, 162.19, 157.38, 142.28, 141.72, 133.26, 119.32, 118.94, 114.44, 106.70, 106.26, 102.66, 52.59, 36.46, 28.41. HRMS (ESI) m/z $[M+H]$ for $C_{18}H_{15}ClN_2O_5$: 375.0748; found: 375.2276.



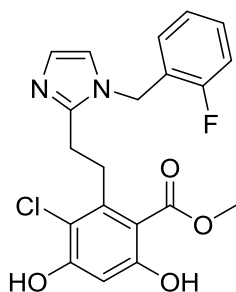
Methyl 3-chloro-2-(3-((2,4-dibromophenyl)amino)-3-oxopropyl)-4,6-dihydroxybenzoate (27). 21 mg, 83%, white solid. ^1H NMR (500 MHz, CDCl_3 and CD_3OD) δ 8.22 (d, $J = 8.9$ Hz, 1H), 7.63 (dd, $J = 2.2, 1.2$ Hz, 1H), 7.49 – 7.33 (m, 1H), 6.44 (d, $J = 1.0$ Hz, 1H), 3.90 (d, $J = 1.2$ Hz, 3H), 3.47 – 3.39 (m, 2H), 2.72 – 2.54 (m, 2H). ^{13}C NMR (126 MHz, CD_3OD) δ 170.52, 170.39, 162.40, 157.48, 141.32, 134.74, 134.42, 131.43, 122.78, 116.73, 114.47, 113.56, 106.14, 102.72, 52.64, 36.99, 28.77. HRMS (ESI) m/z $[\text{M}+\text{Na}^+]$ for $\text{C}_{17}\text{H}_{14}\text{Br}_2\text{ClNO}_5\text{Na}$: 527.8927, found: 527.8935.

General procedure for cis-amide isostere compounds (30-45):

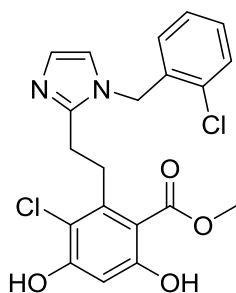


Intermediate **28** (0.1 mmol) was dissolved in MeOH followed by addition of amine (**30a-45a**) (0.1 mmol) dropwise to the reaction flask. Ammonium bicarbonate (NH_3HCO_3), Glyoxal (40 % aqueous solution) (0.1 mmol) are then added to this stirring mixture at 25°C . The reaction was then allowed to stir at 25°C for 8 h. Upon complete consumption of the aldehyde, TBAF was

added dropwise *via* syringe and the reaction was allowed to stir at 25 °C for ~30 min. The reaction was quenched with sat. aq. NH₄Cl and extracted with EtOAc (thrice). The organic layers were combined, dried on Na₂SO₄, and concentrated *in vacuo*. Purification was then carried out *via* chromatography utilizing 95:5 (DCM:MeOH) as the eluent.

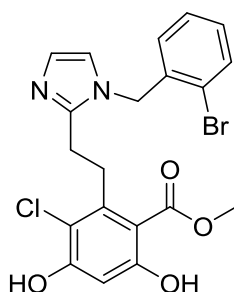


Methyl 3-chloro-2-(2-(1-(2-fluorobenzyl)-1H-imidazol-2-yl)ethyl)-4,6-dihydroxybenzoate (30). 23 mg, 55%, white solid. ¹H NMR (500 MHz, CDCl₃) δ 7.23 (s, 3H), 7.05 – 6.99 (m, 2H), 6.94 (d, *J* = 1.4 Hz, 1H), 6.81 – 6.75 (m, 2H), 6.40 (s, 1H), 5.05 (s, 2H), 3.82 (s, 3H), 3.49 – 3.37 (m, 2H), 2.95 – 2.79 (m, 2H). ¹³C NMR (126 MHz, CDCl₃) δ 170.80, 162.21, 161.09, 159.13, 157.79, 147.67, 141.77, 130.04, 128.42, 127.27, 124.63, 119.93, 115.69, 114.66, 106.02, 102.55, 52.51, 43.46, 30.83, 26.04. HRMS (ESI) *m/z* [M+H] for C₂₀H₁₈ClFN₂O₄: 405.1029, found 405.1017.

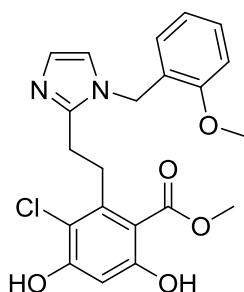


Methyl 2-(2-(1-(2-chlorobenzyl)-1H-imidazol-2-yl)ethyl)-3-chloro-4,6-dihydroxybenzoate (31) 23 mg, 57%, white solid. ¹H NMR (500 MHz, CDCl₃) δ 7.35 (dd, *J* = 8.1, 1.3 Hz, 1H), 7.25

– 7.12 (m, 3H), 7.06 (d, $J = 1.5$ Hz, 1H), 6.79 (d, $J = 1.5$ Hz, 1H), 6.64 – 6.57 (m, 1H), 6.43 (s, 1H), 5.08 (s, 2H), 3.85 (s, 3H), 3.47 – 3.41 (m, 2H), 2.97 – 2.87 (m, 2H). ^{13}C NMR (126 MHz, CDCl_3) δ 170.58, 157.43, 147.63, 141.17, 133.48, 132.58, 129.83, 129.62, 127.72, 127.52, 126.23, 126.18, 120.16, 114.51, 106.20, 102.85, 52.73, 47.48, 30.89, 25.78. HRMS (ESI) m/z [M+H] for $\text{C}_{20}\text{H}_{19}\text{Cl}_2\text{N}_2\text{O}_4$: 421.0722, found: 421.0721.

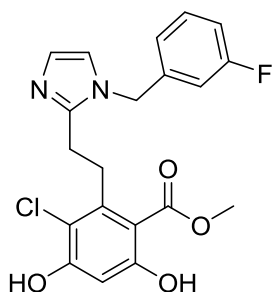


methyl 2-(2-(1-(2-bromobenzyl)-1H-imidazol-2-yl)ethyl)-3-chloro-4,6-dihydroxybenzoate (32) 26 mg, 61%, white solid. ^1H NMR (500 MHz, CDCl_3) δ 7.54 (dd, $J = 8.0, 1.3$ Hz, 1H), 7.24 – 7.20 (m, 1H), 7.15 (td, $J = 7.7, 1.7$ Hz, 1H), 7.10 (d, $J = 1.6$ Hz, 1H), 6.78 (d, $J = 1.6$ Hz, 1H), 6.67 – 6.57 (m, 1H), 6.48 (s, 1H), 5.06 (s, 2H), 3.85 (s, 3H), 3.48–3.33 (m, 2H), 3.06–2.89 (m, 2H). ^{13}C NMR (126 MHz, CDCl_3) δ 170.47, 162.64, 157.77, 147.55, 140.60, 134.53, 133.23, 130.08, 128.23, 128.05, 125.07, 122.57, 120.27, 114.71, 105.94, 103.08, 52.85, 50.15, 30.78, 25.58. HRMS (ESI) m/z [M+H] for $\text{C}_{20}\text{H}_{19}\text{BrClN}_2\text{O}_4$: 465.0217, found : 465.0231.



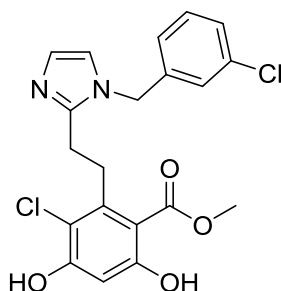
Methyl 3-chloro-4,6-dihydroxy-2-(2-(1-(2-methoxybenzyl)-1H-imidazol-2-yl)ethyl)benzoate

(**33**) 24 mg, 58%, white solid. ^1H NMR (500 MHz, CDCl_3) δ 7.23 (dd, $J = 7.9, 1.7$ Hz, 1H), 6.95 (d, $J = 1.5$ Hz, 1H), 6.85 – 6.80 (m, 2H), 6.78 (d, $J = 1.5$ Hz, 1H), 6.71 (dd, $J = 7.4, 1.7$ Hz, 1H), 6.41 (s, 1H), 5.00 (s, 2H), 3.78 (s, 3H), 3.76 (s, 3H), 3.48 – 3.39 (m, 2H), 3.01 – 2.84 (m, 2H). ^{13}C NMR (126 MHz, CDCl_3) δ 170.94, 162.59, 158.62, 156.68, 147.68, 141.40, 129.56, 127.91, 125.74, 124.26, 120.78, 120.20, 115.10, 110.38, 105.43, 102.67, 55.32, 52.54, 45.12, 30.76, 25.84. HRMS (ESI) m/z [M+H] for $\text{C}_{21}\text{H}_{22}\text{ClN}_2\text{O}_5$: 417.1217, found: 417.1216.



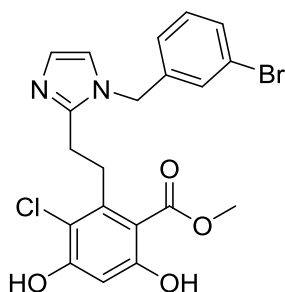
Methyl 3-chloro-2-(2-(1-(3-fluorobenzyl)-1H-imidazol-2-yl)ethyl)-4,6-dihydroxybenzoate

(**34**) 26 mg, 59% pale yellow solid. ^1H NMR (500 MHz, CDCl_3) δ 7.29 – 7.20 (m, 1H), 7.01 (d, $J = 1.4$ Hz, 1H), 6.92 (m, 1H), 6.82 (d, $J = 1.4$ Hz, 1H), 6.75 (m, 1H), 6.70 – 6.58 (m, 1H), 6.46 (s, 1H), 5.01 (s, 2H), 3.80 (s, 3H), 3.52 – 3.40 (m, 2H), 2.88 – 2.74 (m, 2H). ^{13}C NMR (126 MHz, CDCl_3) δ 156.91, 147.47, 141.64, 130.71, 127.65, 121.98, 120.09, 115.15, 114.98, 114.24, 113.55, 113.38, 106.52, 102.84, 99.96, 53.44, 52.63, 48.82, 30.86, 26.12. HRMS (ESI) m/z [M+H] for $\text{C}_{20}\text{H}_{19}\text{ClFN}_2\text{O}_4$: 405.1017, found: 405.1009.



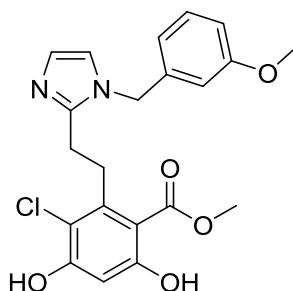
Methyl 3-chloro-2-(2-(1-(3-chlorobenzyl)-1H-imidazol-2-yl)ethyl)-4,6-dihydroxybenzoate

(35) 27 mg, 62%, white solid. ^1H NMR (500 MHz, CDCl_3) δ 7.27 (s, 1H), 7.24 – 7.16 (m, 2H), 7.01 (d, $J = 1.6$ Hz, 1H), 6.94 (dd, $J = 1.9, 1.0$ Hz, 1H), 6.84 (m, 2H), 6.38 (s, 1H), 4.98 (s, 2H), 3.80 (s, 3H), 3.45 – 3.35 (m, 2H), 2.94 – 2.85 (m, 2H). ^{13}C NMR (126 MHz, CDCl_3) δ 174.40, 165.70, 162.00, 151.36, 144.93, 141.56, 138.94, 134.29, 132.38, 130.62, 129.70, 128.71, 124.29, 118.63, 110.07, 106.57, 56.46, 34.48, 33.56, 29.64. HRMS (ESI) m/z [M+H] for $\text{C}_{20}\text{H}_{19}\text{Cl}_2\text{N}_2\text{O}_4$: 421.0722, found: 421.0714.



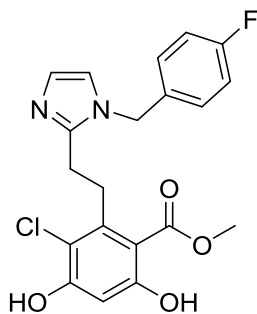
Methyl 2-(2-(1-(3-bromobenzyl)-1H-imidazol-2-yl)ethyl)-3-chloro-4,6-dihydroxybenzoate

(36) 23 mg, 55%, white solid. ^1H NMR (500 MHz, MeOD) δ 7.38 (m, 1H), 7.19 – 7.09 (m, 2H), 6.99 (d, $J = 1.5$ Hz, 1H), 6.91 (m, 1H), 6.84 (d, $J = 1.5$ Hz, 1H), 6.40 (s, 1H), 5.00 (s, 2H), 3.83 (s, 3H), 3.46–3.38 (m, 2H), 2.92 – 2.79 (m, 2H). ^{13}C NMR (126 MHz, MeOD) δ 168.02, 159.25, 155.49, 145.00, 138.77, 135.70, 128.71, 128.01, 126.95, 124.05, 122.60, 120.52, 117.64, 112.15, 103.58, 100.01, 49.95, 46.22, 28.09, 23.35. HRMS (ESI) m/z [M+H] for $\text{C}_{20}\text{H}_{19}\text{BrClN}_2\text{O}_4$: 465.0217, found: 465.0225.



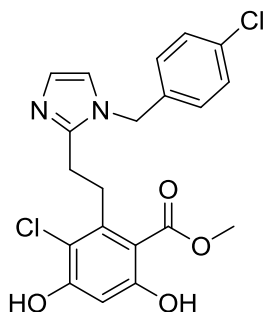
Methyl 2-(2-(1-(3-methoxybenzyl)-1H-imidazol-2-yl)ethyl)-3-chloro-4,6-dihydroxybenzoate

(**37**) 21 mg, 55%, white solid. ^1H NMR (500 MHz, CDCl_3) δ 7.24 (s, 1H), 6.89 (t, $J = 1.6$ Hz, 1H), 6.84 (m, 2H), 6.61 – 6.57 (m, 1H), 6.57 – 6.50 (m, 2H), 6.49 (d, $J = 2.8$ Hz, 1H), 4.95 – 4.91 (m, 2H), 3.92 (d, $J = 4.7$ Hz, 3H), 3.75 (d, $J = 4.2$ Hz, 3H), 3.55 (q, $J = 6.7$ Hz, 2H), 3.19 (q, $J = 17.3, 12.3$ Hz, 2H). ^{13}C NMR (126MHz, CDCl_3) δ 164.53, 162.14, 160.13, 157.93, 141.34, 135.60, 130.52, 120.69, 119.27, 114.43, 113.87, 113.10, 106.17, 68.50, 55.23, 52.84, 31.81, 30.10, 24.35, 22.14, 13.62. HRMS (ESI) m/z [M+H] for $\text{C}_{21}\text{H}_{22}\text{ClN}_2\text{O}_5$: 417.1217, found: 417.1221.

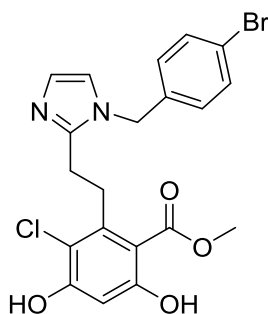


Methyl 3-chloro-2-(2-(1-(4-fluorobenzyl)-1H-imidazol-2-yl)ethyl)-4,6-dihydroxybenzoate

(**38**) 22 mg, 55%, white solid. ^1H NMR (500 MHz, MeOD) δ 7.07–6.94 (m, 5H), 6.86 (d, $J = 1.4$ Hz, 1H), 6.29 (s, 1H), 5.00 (s, 2H), 3.69 (s, 3H), 3.22–3.19 (m, 2H), 2.84 (m, 2H). ^{13}C NMR (126 MHz, MeOD) δ 171.22, 164.76, 162.81, 160.69, 158.81, 148.82, 141.37, 134.18, 127.28, 121.71, 116.58, 114.85, 110.41, 103.34, 52.85, 49.61, 31.45, 27.26. HRMS (ESI) m/z [M+H] for $\text{C}_{20}\text{H}_{19}\text{ClFN}_2\text{O}_4$: 405.1017, found: 405.1009.

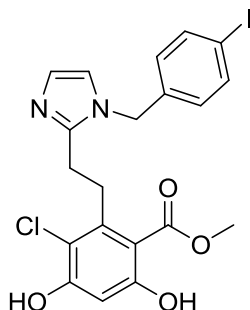


Methyl 3-chloro-2-(2-(1-(4-chlorobenzyl)-1H-imidazol-2-yl)ethyl)-4,6-dihydroxybenzoate (39) 28 mg, 63%, white solid. ^1H NMR (500 MHz, CDCl_3) δ 7.24 (d, $J = 8.4$ Hz, 2H), 6.98 (d, $J = 1.4$ Hz, 1H), 6.90 (d, $J = 8.4$ Hz, 2H), 6.78 (d, $J = 1.4$ Hz, 1H), 6.40 (s, 1H), 4.97 (s, 2H), 3.81 (s, 3H), 3.46–3.40 (m, 2H), 2.89–2.80 (m, 2H). ^{13}C NMR (126 MHz, CDCl_3) δ 170.63, 162.30, 157.66, 147.57, 141.56, 134.60, 134.02, 129.19, 127.92, 127.05, 120.00, 114.57, 106.08, 102.68, 52.59, 48.83, 30.87, 26.04. HRMS (FAB) m/z $[\text{M}+\text{H}]$ for $\text{C}_{20}\text{H}_{19}\text{Cl}_2\text{N}_2\text{O}_4$: 421.0722, found: 421.0714.



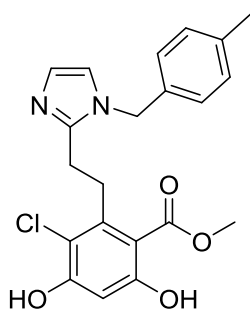
Methyl 2-(2-(1-(4-bromobenzyl)-1H-imidazol-2-yl)ethyl)-3-chloro-4,6-dihydroxybenzoate (40) 26 mg, 58%, white solid. ^1H NMR (500 MHz, $\text{CDCl}_3/\text{MeOD}$) δ 7.43 – 7.33 (m, 2H), 6.95 (d, $J = 1.3$ Hz, 1H), 6.87 – 6.79 (m, 2H), 6.77 (d, $J = 1.3$ Hz, 1H), 6.44 – 6.28 (m, 1H), 4.95 (s, 2H), 3.82 (d, $J = 1.1$ Hz, 3H), 3.46 – 3.38 (m, 2H), 2.86 – 2.75 (m, 2H). ^{13}C NMR (500 MHz, $\text{CDCl}_3/\text{MeOD}$) 171.9, 163.5, 159.3, 148.8, 142.6, 136.1, 133.5, 129.6, 127.6, 123.5, 121.4,

116.0, 107.3, 104.07, 54.0, 50.4, 32.1, 27.2. HRMS (ESI) m/z [M+H] for $C_{20}H_{19}BrClN_2O_4$: 465.0217, found: 465.0237.



Methyl 3-chloro-4,6-dihydroxy-2-(2-(1-(4-iodobenzyl)-1H-imidazol-2-yl)ethyl)benzoate (41)

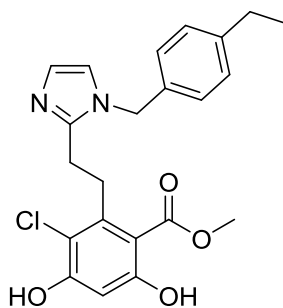
22mg, 55%, white solid. 1H NMR (500 MHz, $CDCl_3$) δ 7.59 (d, $J = 8.3$ Hz, 2H), 6.98 (d, $J = 1.3$ Hz, 1H), 6.80 – 6.75 (m, 1H), 6.71 (d, $J = 7.9$ Hz, 2H), 6.41 (s, 1H), 4.96 (s, 2H), 3.80 (s, 3H), 3.47 – 3.38 (m, 2H), 2.87 – 2.79 (m, 2H). ^{13}C NMR (126 MHz, $CDCl_3$) δ 170.60, 162.43, 157.62, 147.61, 141.52, 138.10, 135.88, 128.41, 127.20, 120.02, 114.57, 106.06, 102.72, 93.56, 52.61, 48.96, 30.90, 26.07. HRMS (ESI) m/z [M+H] for $C_{20}H_{19}ClIN_2O_4$: 513.0078, found: 513.0079.



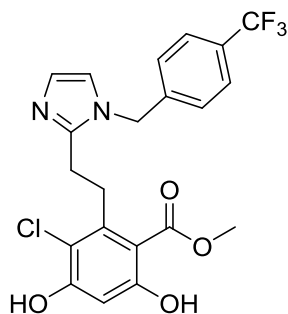
Methyl 3-chloro-4,6-dihydroxy-2-(2-(1-(4-methylbenzyl)-1H-imidazol-2-yl)ethyl)benzoate

(42) 28 mg, 62%, white solid. 1H NMR (500 MHz, MeOD) δ 7.05 (d, $J = 7.9$ Hz, 2H), 6.93 (d, $J = 1.5$ Hz, 1H), 6.88 (d, $J = 8.1$ Hz, 2H), 6.84 (s, 1H), 6.29 (s, 1H), 4.95 (s, 2H), 3.67 (s, 3H), 3.22 (d, $J = 4.0$ Hz, 2H), 2.87 – 2.78 (m, 2H), 2.21 (s, 3H). ^{13}C NMR (126 MHz, MeOD) δ 171.32,

160.89, 159.03, 148.82, 141.51, 138.89, 135.09, 130.52, 127.95, 127.08, 121.76, 114.99, 110.11, 103.34, 52.82, 50.15, 31.47, 27.30, 21.10. HRMS (ESI) m/z [M+H] for C₂₁H₂₂ClN₂O₄: 401.1268, found: 401.1285.

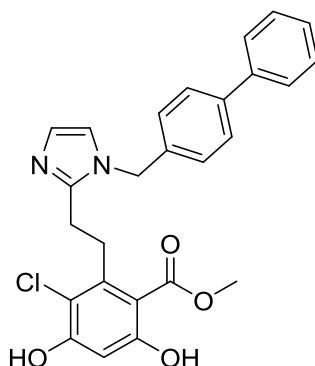


Methyl 3-chloro-2-(2-(1-(4-ethylbenzyl)-1H-imidazol-2-yl)ethyl)-4,6-dihydroxybenzoate (43) 25 mg, 59%, white solid. ¹H NMR (500 MHz, CDCl₃) δ 7.11 (d, J = 8.1 Hz, 2H), 7.07 (d, J = 1.7 Hz, 1H), 6.92 – 6.88 (m, 2H), 6.82 (d, J = 1.5 Hz, 1H), 6.41 (s, 1H), 4.93 (s, 2H), 3.82 (s, 3H), 3.46 (dd, J = 9.0, 6.7 Hz, 2H), 3.00 (d, J = 7.7 Hz, 2H), 2.57 – 2.53 (m, 2H), 1.17 – 1.11 (m, 3H). ¹³C NMR (126 MHz, CDCl₃) δ 169.54, 161.04, 157.10, 146.05, 143.86, 139.75, 130.97, 127.68, 126.08, 123.07, 119.47, 113.81, 105.12, 101.88, 51.74, 48.87, 29.55, 27.47, 24.47, 14.46. HRMS (ESI) m/z [M+H] for C₂₂H₂₃ClN₂O₄: 415.1346, found: 415.1354.



Methyl 3-chloro-4,6-dihydroxy-2-(2-(1-(4-(trifluoromethyl)benzyl)-1H-imidazol-2-yl)ethyl)benzoate (44) 24 mg, 58%, white solid. ¹H NMR (500 MHz, CDCl₃) δ 7.56 (d, J = 8.1 Hz, 2H), 7.15 (d, J = 1.7 Hz, 1H), 7.09 (d, J = 8.1 Hz, 2H), 6.86 (d, J = 1.7 Hz, 1H), 6.44 (s, 1H),

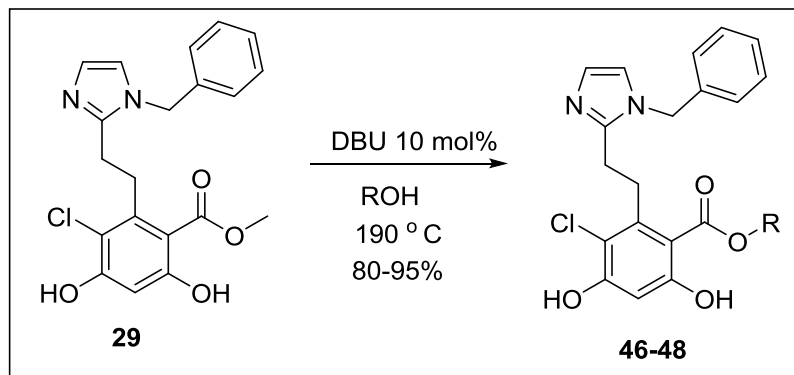
5.06 (s, 2H), 3.85 (s, 3H), 3.45 (dd, $J = 8.8, 6.8$ Hz, 2H), 3.02 (t, $J = 7.9$ Hz, 2H). ^{13}C NMR (126 MHz, CDCl_3) δ 170.22, 162.13, 157.84, 147.28, 140.34, 138.67, 131.08, 130.82, 127.12, 126.25, 126.23, 120.50, 114.62, 106.11, 103.08, 52.86, 49.53, 30.58, 25.29. HRMS (ESI) m/z $[\text{M}+\text{H}]$ for $\text{C}_{21}\text{H}_{19}\text{ClF}_3\text{N}_2\text{O}_4$: 455.0985, found: 455.1011.



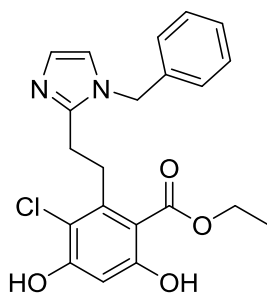
Methyl-2-(2-(1-([1,1'-biphenyl]-4-ylmethyl)-1H-imidazol-2-yl)ethyl)-3-chloro-4,6-

dihydroxybenzoate (45) 27 mg, 57%, white solid. ^1H NMR (400 MHz, $\text{CDCl}_3+\text{MeOD}$) δ 7.61 – 7.56 (m, 4H), 7.46 (t, $J = 7.5$ Hz, 2H), 7.40 – 7.35 (m, 1H), 7.15 (d, $J = 8.1$ Hz, 2H), 7.10 (d, $J = 1.4$ Hz, 1H), 6.93 (d, $J = 1.4$ Hz, 1H), 6.52 (s, 1H), 5.17 (s, 2H), 3.86 (s, 3H), 3.57 (dd, $J = 14.8, 6.5$ Hz, 2H), 3.06–2.95 (m, 2H). ^{13}C NMR (126 MHz, $\text{CDCl}_3+\text{MeOD}$) δ 170.68, 161.64, 158.06, 147.67, 141.53, 141.51, 140.97, 140.24, 135.18, 128.75, 127.56, 127.46, 127.03, 126.92, 126.80, 120.19, 114.65, 106.32, 102.41, 52.32, 30.70, 26.14. HRMS (ESI) m/z $[\text{M}+\text{H}]$ for $\text{C}_{26}\text{H}_{23}\text{ClN}_2\text{O}_4$: 463.1346, found: 463.1349.

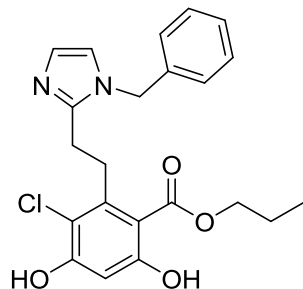
General procedure for synthesis of compounds 46-48



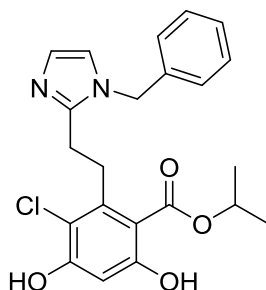
In a reaction vessel, Compound **29** (BnIm) (10 mg, 0.025 mmol) was suspended into the corresponding alcohol (2ml), 1,8-Diazabicyclo[5.4.0]undec-7-ene (DBU) (0.0025 mmol) was added, then the reaction vessel is sealed and heated to 190° C overnight . The alcohol is evaporated in vacuo and the remaining residue is loaded onto a preparative TLC plate and 5% MeOH in DCM is used as the solvent system for purification of product.



Ethyl 2-(2-(1-benzyl-1H-imidazol-2-yl)ethyl)-3-chloro-4,6-dihydroxybenzoate (46) 9.5 mg, 88%, white solid. ^1H NMR (500 MHz, CDCl_3) δ 7.29 – 7.22 (m, 3H), 6.97 (m, 3H), 6.81 (d, J = 1.5 Hz, 1H), 6.44 (s, 1H), 4.98 (s, 2H), 4.26 (q, J = 7.1 Hz, 2H), 3.55–3.43 (m, 2H), 2.92 – 2.79 (m, 2H), 1.14 (t, J = 7.1 Hz, 3H). ^{13}C NMR (126 MHz, CDCl_3) δ 169.19, 161.52, 156.36, 146.34, 140.68, 134.98, 127.98, 127.07, 125.72, 125.63, 119.09, 113.53, 105.28, 101.65, 60.98, 48.44, 29.31, 25.08, 12.90. HRMS (ESI) m/z $[\text{M}+\text{H}]$ for $\text{C}_{21}\text{H}_{21}\text{ClN}_2\text{O}_4$: 401.1268, found: 401.1269.



Propyl 2-(2-(1-benzyl-1H-imidazol-2-yl)ethyl)-3-chloro-4,6-dihydroxybenzoate (47) 10 mg, 96%, white solid. ^1H NMR (500 MHz, CDCl_3) δ 7.29 – 7.21 (m, 3H), 7.01 – 6.92 (m, 3H), 6.80 (d, $J = 1.4$ Hz, 1H), 6.46 (s, 1H), 4.98 (s, 2H), 4.15 (t, $J = 7.0$ Hz, 2H), 3.58 – 3.49 (m, 2H), 2.87 (dd, $J = 9.0, 7.1$ Hz, 2H), 1.55 (q, $J = 7.2$ Hz, 2H), 0.79 (t, $J = 7.4$ Hz, 3H). ^{13}C NMR (126 MHz, CDCl_3) δ 169.24, 161.74, 156.40, 146.23, 140.61, 134.94, 127.97, 127.08, 126.14, 125.66, 119.07, 113.58, 105.31, 101.77, 66.61, 48.45, 29.30, 25.15, 20.64, 9.34. HRMS (ESI) m/z [M+H] for $\text{C}_{22}\text{H}_{24}\text{ClN}_2\text{O}_4$: 415.1425, found: 415.1418.



Isopropyl 2-(2-(1-benzyl-1H-imidazol-2-yl)ethyl)-3-chloro-4,6-dihydroxybenzoate (48) 9.5 mg, 85%, white solid. ^1H NMR (500 MHz, CDCl_3) δ 7.28 – 7.21 (m, 3H), 7.04 – 6.91 (m, 3H), 6.82 (d, $J = 1.4$ Hz, 1H), 6.47 (s, 1H), 5.16 (p, $J = 6.3$ Hz, 1H), 4.96 (s, 2H), 3.60 – 3.49 (m, 2H), 2.88 – 2.79 (m, 2H), 1.16 (d, $J = 6.3$ Hz, 6H). ^{13}C NMR (126 MHz, CDCl_3) δ 168.71, 161.84, 156.11, 146.14, 140.70, 134.88, 127.99, 127.08, 125.69, 119.13, 113.46, 105.65, 101.76, 69.23, 48.45, 29.05, 25.19, 20.57. HRMS (ESI) m/z [M+H] for $\text{C}_{22}\text{H}_{24}\text{ClN}_2\text{O}_4$: 415.1425, found: 415.1435.

5. References

1. Hartl, F. U. Molecular chaperones in cellular protein folding. *Nature* **1996**, *381*, 571-579.
2. Hartl, F.U. Molecular chaperones in protein folding and proteostasis. *Nature* **2011**, *475*, 324-332.
3. Pearl, L.H.; Prodromou, C. Structure and in vivo function of Hsp90. *Curr. Opin. Struct. Biol.* **2000**, *10*, 46-51.
4. Prodromou, C., Pearl, L.H. Structure and functional relationships of Hsp90. *Curr. Cancer Drug Targets* **2003**, *3*, 301-323.
5. Pearl, L.H.; Prodromou, C. Structure, function, and mechanism of the Hsp90 molecular chaperone. *Adv. Protein Chem.* **2001**, *59*, 157-186.
6. Meyer, P.; Prodromou, C.; Hu, B.; Vaughan, C.; Roe, S. M.; Panaretou, B.; Piper, P.W.; Pearl, L.H. Structural and functional analysis of the middle segment of Hsp90: implications for ATP hydrolysis and client protein and cochaperone interactions. *Mol. Cell* **2003**, *11*, 647-658.
7. Panaretou, B.; Siligardi, G.; Meyer, P.; Maloney, A.; Sullivan, J.K.; Singh, S.; Millson, S.H.; Clarke, P.A.; Naaby-Hansen, S.; Stein, R.; Cramer, R.; Mollapour, M.; Workman, P.; Piper, P.W.; Pearl, L.H.; Prodromou, C. Activation of the ATPase activity of Hsp90 by the stress-regulated cochaperone *aha1*. *Mol. Cell* **2002**, *10*, 1307-1318.
8. Marcu, M.G.; Chadli, A.; Bouhouche, I.; Catelli, M.; Neckers, L.M. The heat shock protein 90 antagonist novobiocin interacts with a previously unrecognized ATP-binding domain in the carboxyl terminus of the chaperone. *J. Biol. Chem.* **2000**, *275*, 37181-37186.
9. Soti, C.; Racz, A.; Csermely, P. A nucleotide-dependent molecular switch controls ATP binding at the C-terminal domain of Hsp90, N-terminal nucleotide binding unmasks a C-terminal binding pocket. *J. Biol. Chem.* **2002**, *277*, 7066-7075.
10. Whitesell, L.; Bagatell, R.; Falsey, R. The stress response: implications for the clinical development of Hsp90 inhibitors. *Curr. Cancer Drug Targets* **2003**, *3*, 349-358.
11. Whitesell, L.; Lindquist, S. L. Hsp90 and the chaperoning of cancer. *Nat. Rev. Cancer* **2005**, *5*, 761-772.
12. Zhang, H.; Burrows, F. Targeting multiple signal transduction pathways through inhibition of Hsp90. *J. Mol. Med.* **2004**, *82*, 488-499.
13. Yu, X.M.; Shen, G.; Neckers, L.; Blake, H.; Holzbeierlein, J.; Cronk, B.; Blagg, B.S.J. Hsp90 inhibitors identified from a library of novobiocin analogues. *J. Am. Chem. Soc.* **2005**, *127*, 12778-12779.
14. Burlison, J.A.; Blagg, B.S.J. Synthesis and evaluation of coumermycin A1 analogues that inhibit the Hsp90 protein folding machinery. *Org. Lett.* **2006**, *8*, 4855-4858.
15. Burlison, J.A.; Neckers, L.; Smith, A.B.; Maxwell, A.; Blagg, B.S.J. Novobiocin: redesigning a DNA gyrase inhibitor for selective inhibition of Hsp90. *J. Am. Chem. Soc.* **2006**, *128*, 15529-15536.
16. Burlison, J.A.; Avila, C.; Vielhauer, G.; Lubbers, D.J.; Holzbeierlein, J.; Blagg, B.S.J. Development of novobiocin analogues that manifest anti-proliferative activity against several cancer cell lines. *J. Org. Chem.* **2008**, *73*, 2130-2137.
17. Donnelly, A.C.; Mays, J.R.; Burlison, J.A.; Nelson, J.T.; Vielhauer, G.; Holzbeierlein, J.; Blagg, B.S.J. The design, synthesis, and evaluation of coumarin ring derivatives of the novobiocin scaffold that exhibit antiproliferative activity. *J. Org. Chem.*, **2008**, *73*, 8901-8920.
18. Zhao, H.; Kusuma, B.R.; Blagg, B.S.J. Synthesis and evaluation of noviose replacements on novobiocin that manifest antiproliferative activity. *ACS Med. Chem. Lett.*, **2010**, *1*, 311-315.

19. Matts, R.L.; Dixit, A.; Peterson, L.B.; Sun, L.; Voruganti, S.; Kalyanaraman, P.; Hartson, S.D.; Verkhivker, G.M.; Blagg, B.S.J. Elucidation of the Hsp90 C-terminal binding site. *ACS Chem. Biol.*, **2011**, *6*, 800-807.
20. Zhao, H., Donnelly, A.C.; Kusuma, B.R.; Brandt, G.E.L.; Brown, D.; Rajewski, R.A.; Vielhauer, G.; Holzbeierlein, J.; Cohen, M.S.; Blagg, B.S.J. Engineering an antibiotic to fight cancer: Optimization of the novobiocin scaffold to produce anti-proliferative agents. *J. Med. Chem.*, **2011**, *54*, 3839-3853.
21. Kusuma, B.R.; Zhang, L.; Sundstrom, T.; Peterson, L.B.; Dobrowsky, R.T.; Blagg, B.S.J. Synthesis and evaluation of novologues as C-terminal Hsp90 inhibitors with cytoprotective activity against sensory neuron glucotoxicity. *J. Med. Chem.*, **2012**, *55*, 5797-5812.
22. Khandelwal, A.; Hall, J.A.; Blagg, B.S.J. Synthesis and structure-activity relationships of EGCG analogues, a recently identified Hsp90 inhibitor. *J. Org. Chem.*, **2013**, *78*, 7859-7884.
23. Kim, Y. S.; Alarcon, S. V.; Lee, S.; Lee, M. J.; Giaccone, G.; Neckers, L.; Trepel, J. B. Update on Hsp90 inhibitors in clinical trial. *Curr. Top. Med. Chem.* **2009**, *9*, 1479-1492.
24. Biamonte, M. A.; Van de Water, R.; Arndt, J. W.; Scannevin, R. H.; Perret, D.; Lee, W. Heat shock protein 90: inhibitors in clinical trials. *J. Med. Chem.* **2010**, *53*, 3-17.
25. Peterson, L.B.; Esker, J.D.; Vielhauer, G.A.; Blagg, B.S. The hERG channel is dependent upon the Hsp90 α isoform for maturation and trafficking. *Mol. Pharm.*, **2012**, *9*, 1841-1846.
26. Sreedhar, A.S.; Kalmar, E.; Csermely, P.; Shen, Y.F. Hsp90 isoforms: functions, expression and clinical importance. *FEBS Lett.*, **2004**, *562*, 11-15.
27. McLaughlin, M.; Vandenbroeck, K. The endoplasmic reticulum protein folding factory and its chaperones: new targets for drug discovery? *Br. J. Pharmacol.*, **2011**, *162*, 328-345.
28. Goodman, S.L.; Picard, M. Integrins as therapeutic targets. *Trends Pharmacol. Sci.*, **2012**, *33*, 405-412.
29. Dejeans, N.; Glorieux, C.; Guenin, S.; Beck, R.; Sid, B.; Rousseau, R.; Bisig, B.; Delvenne, P.; Buc Calderon, P.; Verrax, J. Overexpression of Grp94 in breast cancer cells resistant to oxidative stress promotes high levels of cancer cell proliferation and migration: implications for tumor recurrence. *Free Radic. Biol. Med.*, **2012**, *52*, 993-1002.
30. Suntharalingam, A.; Abisambra, J.F.; O'Leary, J.C. III; Koren, J. III; Zhang, B.; Joe, M.K.; Blair, L.J.; Hill, S.E.; Jinwal, U.K.; Cockman, M.; Duerfeldt, A.S.; Tomarev, S.; Blagg, B.S.; Lieberman, R.L.; Dickey, C.A. Glucose-regulated protein 94 triage of mutant myocilin through endoplasmic reticulum-associated degradation subverts a more efficient autophagic clearance mechanism. *J. Biol. Chem.*, **2012**, *287*, 40661-40669.
31. Gullo, C.A.; Teoh, G. Heat shock protein: to present or not, that is the question. *Immunol. Lett.*, **2004**, *94*, 1-10.
32. Obeng, E.A.; Carlson, L.M.; Gutman, D.M.; Harrington, W.J.; Lee, K.P.; Boise, L.H. Proteasome inhibitors induce a terminal unfolded protein response in myeloma cells. *Blood*, **2006**, *107*, 4907-4916.
33. Davenport, E.L.; Moore, H.E.; Dunlop, A.S.; Sharp, S.Y.; Workman, P.; Morgan, G.J.; Davies, F.E. Heat shock protein inhibition is associated with activation of the unfolded protein response pathway in myeloma plasma cells. *Blood*, **2007**, *110*, 2641-2649.
34. Hua, Y.; White-Gilbertson, S.; Kellner, J.; Rachidi, S.; Usmani, S.Z.; Chiosis, G.; DePinho, R.; Li, Z.; Liu, B. Molecular chaperone gp96 is a novel therapeutic target for multiple myeloma. *Clin. Cancer Res.*, **2013**, *19*, 6242-6251.
35. Braakman, I.; Bulleid, N. Protein folding and modification in the mammalian endoplasmic reticulum. *Annu. Rev. Biochem.* **2011**, *80*, 71-99.

36. Soldano, K.L.; Jivan, A.; Nicchitta, C.V.; Gewirth, D.T. Structure of the N-terminal domain of Grp94. Basis for ligand specificity and regulation. *J. Biol. Chem.*, **2003**, *278*, 48330-48338.
37. Duerfeldt, A.S.; Peterson, L.B.; Maynard, J.C.; Ng, C.L.; Eletto, D.; Ostrovsky, O.; Shinogle, H.E.; Moore, D.S.; Argon, Y.; Nicchitta, C.V.; Blagg, B.S.J. Development of a Grp94 inhibitor. *JACS*, **2012**, *134*, 9796-9804.
38. Immormino, R.M.; Metzger, L.E.; Reardon, P.N.; Dollins, D.E.; Blagg, B.S.; Gewirth, D.T. Different poses for ligand and chaperone in inhibitor-bound Hsp90 and Grp94: implications for paralog-specific drug design. *J. Mol. Biol.*, **2009**, *388*, 1033-1042.
39. Hadden, K.M.; Blagg, B.S.J. Synthesis and evaluation of radamide analogues, a chimera of radicicol and geldanamycin. *J. Org. Chem.*, **2009**, *74*, 4697-4704.
40. Duerfeldt, A.S.; Brandt, G.E.L.; Blagg, B.S.J. Design, synthesis and biological evaluation of conformationally constrained *cis*-amide Hsp90 inhibitors. *Org. Lett.*, **2009**, *11*, 2353-2356.
41. Shen, G.; Wang, M.; Welch, T.R.; Blagg, B.S.J. Design, synthesis and structure activity relationships for chimeric inhibitors of Hsp90. *J. Org. Chem.*, **2006**, *71*, 7618-7631.
42. Shen, G.; Blagg, B.S.J. Radester, a novel inhibitor of the Hsp90 protein folding machinery. *Org. Lett.*, **2005**, *7*, 2157-2160.
43. Duerfeldt, A. A New Generation of Hsp90 Inhibitors: Addressing Isoform Selectivity and Heat Shock Induction, The University of Kansas, **2011**.
44. Clevenger, R. C.; Blagg, B. S. J. Design, synthesis, and evaluation of a radicicol and geldanamycin chimera, radamide. *Org. Lett.*, **2004**, *6*, 4459-4462.
45. Kim, J.; Felts, S.; Llauger, L.; He, H.; Huezos, H.; Rosen, N.; Chiosis, G. Development of a fluorescence polarization assay for the molecular chaperone Hsp90. *J. Biomol. Screen*, **2004**, *9*, 375-381.
46. Taldone, T.; Patel, P.D.; Patel, M.; Patel, H.J.; Evans, C.E.; Rodina, A.; Ochiana, S.; Shah, S.K.; Uddin, M.; Gewirth, D.; Chiosis, G. Experimental and structural testing module to analyze paralog-specificity and affinity in the Hsp90 inhibitors series. *J. Med. Chem.*, **2013**, *56*, 6803-6818.
47. Hunter, L. The C-F bond as a conformational tool in organic and biological chemistry. *Beilstein J. Org. Chem.*, **2010**, *6*, 38.
48. Stothert, A.; Suntharalingam, A.; Huard, D.; Fontaine, S.; Crowley, V.; Mishra, S.; Blagg, B.; Lieberman, R.; Dickey, C. Exploiting the interaction between Grp94 and aggregated myocilin to treat glaucoma. *Hum. Mol. Gen.* **2014**, *23*, 6470-80.

**Discovery of ACO, A Novel Scaffold for Grp94-
Selective Inhibition**

Chapter 3

1. Introduction

Conformational maturation of polypeptides into biologically active proteins is performed via assistance from a class of proteins called chaperones.¹ The heat shock proteins of 90 KDa (Hsp90), belong to a family of chaperones that are associated with folding, maturation and refolding of around 200 client proteins in the cell.² Hsp90 serves to maintain homeostasis in a normal cell, however, cellular stress induces increased levels of Hsps, thereby facilitating rescue of the denatured proteins.^{3,4} Similarly, Hsp90 is upregulated in cancerous cells, wherein they are required to provide client proteins that are essential for the proliferation of cancer.³⁻¹² As a consequence, Hsp90 contributes significantly towards the growth of cancer cells. Thus, Hsp90 has emerged as a promising therapeutic target for the development of novel anti-cancer therapeutics.^{13, 14} Hsp90 exists as four isoforms; cytosolic Hsp90 α and β , the endoplasmic reticulum-localized isoform, glucose regulated protein Grp94, and the mitochondrial chaperone, Trap1.¹⁵ Structurally, Hsp90 is a homodimer protein with each monomer comprising a C-terminus, N-terminus and Middle domain. The N-terminus contains a ATP binding site, which is responsible for ATP hydrolysis and providing the energy required for client protein folding.^{16,17} Natural products such as geldanamycin (GDA) and radicicol (RDC) were the first Hsp90 inhibitors identified and have since served as probes to advance Hsp90 research, helping establish Hsp90 as a druggable target for the treatment of cancer.¹⁸⁻²⁰ There are 17 Hsp90 inhibitors being evaluated in clinical trials for their efficacy, all of which exhibit pan inhibition of all four Hsp90 isoforms.^{21,22} Additionally, the side effects observed with all these inhibitors are hypothesized to be linked to pan-inhibition of Hsp90 isoforms.²³ Therefore, it is important to

establish a causal relationship between the inhibition of individual Hsp90 isoforms and the observed biological effects.

Glucose regulated protein 94KDa (Grp94) is the endoplasmic reticulum (ER) residing Hsp90 isoform and is less studied in comparison to cytosolic Hsp90s.²⁴ Grp94 is the most abundant protein present in the ER lumen, where it is involved in the folding of secretory proteins that find application in immunity, cellular communication and cellular adhesion. Grp94 expression can be induced by the accumulation of misfolded proteins to initiate the unfolded protein response (UPR), a proteostatic mechanism in the secretory pathway.^{25,26} Grp94 clients such as the integrins regulate cellular metastasis, making Grp94 a potential target for the development of anti-metastatic agents.²⁷ A recent study has further supported this claim by determining that Grp94 knockdown leads to inhibition of cell proliferation, migration and metastasis in highly metastatic breast cancer cell lines (MDA-MB-231 cells) and reactive oxygen species (ROS) resistant MCF-7 cells.²⁸ Myocilin is another Grp94 client, which upon aggregation leads to primary open angle glaucoma (POAG), thus making Grp94 inhibition a potential therapeutic strategy for the treatment of glaucoma.²⁹ Grp94 also mediates the maturation of Wnt co-receptor LRP6, which is overexpressed in multiple myelomas.³⁰⁻³¹ Grp94 knockdown/inhibition results in the reduced proliferation of multiple myeloma cells.³² In light of all these findings, it is apparent that a Grp94 selective inhibitor may provide a treatment for various cancers and glaucoma, while avoiding the side effects resulting from pan-Hsp90 inhibition.

2. Rationale for Design

As discussed in the previous chapter, the first Grp94 selective compound, BnIm, that contains a resorcinolic scaffold was co-crystallized with Grp94 and Hsp90. This led to identification of key structural changes that occur Grp94 versus Hsp90 (figure 2.1).

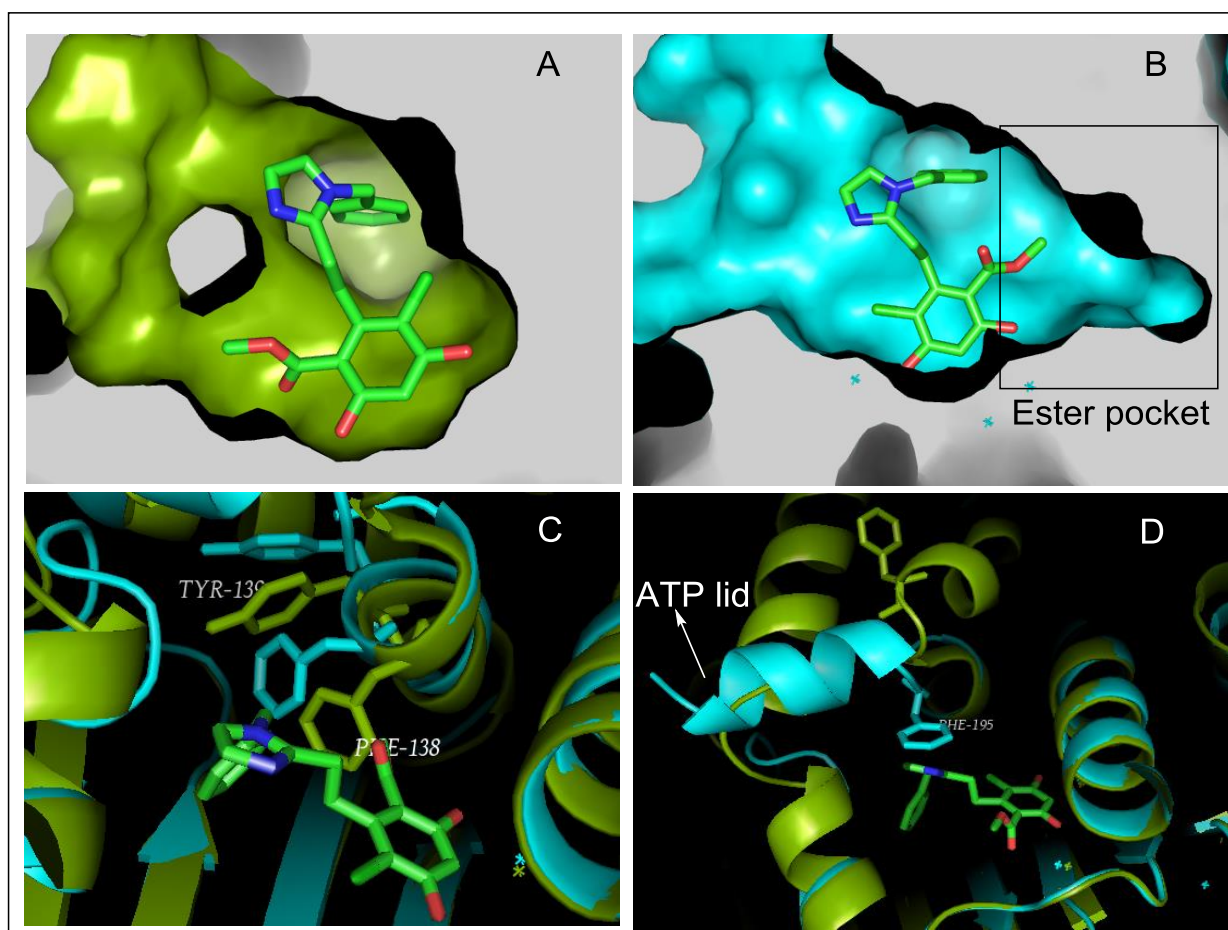
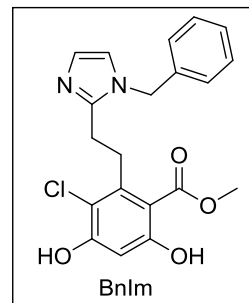


Figure 3.1 A) BnIm bound to Hsp94 (green) B) BnIm bound to Grp94 (cyan) with the resorcinol ring flipped into an extended pocket. C) Overlay of the Hsp94 and Grp94 crystal structures, showing the movement of the PHE 138 and TYR 139. D) ATP lid movement in Grp94 and Hsp94 bound to BnIm.

Two structural differences stand out upon comparison of the co-crystal structures between Grp94 and Hsp94 bound to BnIm. First, the presence of an extended pocket in Grp94

(figure **2.1 B**) causes the resorcinol ring to flip and the ester to project into this new pocket (named the ester pocket), which is not observed in Hsp90. Creation of this new pocket results from the movement of backbone helix residues PHE138 and TYR 139 of Grp94 (figure **2.1C**), which in turn, results from an insertion of five amino acids into the primary sequence of Grp94. The second structural difference observed is movement of the ATP lid, which is closed in Grp94 but is open in Hsp90 (figure **2.1 D**). These two changes in Grp94 upon binding to BnIm, led to a new induced conformation of the Grp94. Attempts to explore the ester pocket were made by extending the ester group of BnIm, unfortunately, the binding potencies were found to decrease with an increase in size (discussed in previous chapter) of the ester. In order to develop compounds with high selectivity for Grp94, it was essential to probe the Grp94 ester pocket. Investigation of the resorcinolic scaffold revealed that modifications to BnIm may not occupy the ester pocket sufficiently. Furthermore, the presence of rotatable carbons in BnIm were postulated to be a source of entropic penalty, leading to a loss in binding energy. Therefore, scaffold screening was performed by overlaying the BnIm crystal structure with scaffolds that are currently being investigated in clinical trials. It was desired that the design of a new compound should not elicit high entropy, and therefore should incorporate minimal number of rotatable bonds. This screening led to the observation that benzamide containing compound, SNX-2112, could be modified to occupy the ester pocket of Grp94. SNX 2112, an indazolone containing compound identified in 2007 as pan Hsp90 inhibitor,^{33, 34} and is based upon a privileged scaffold, unlike the natural products such as geldanamycin and radicicol. The selection of this scaffold was favored by the synthetic feasibility for modifying and exploring the different pockets of Grp94. Figure **2.2** illustrates the overlay of SNX-2112 with BnIm when co-crystallized with Grp94, and it can be observed that the benzamide group serves as a hydrogen bond donor-acceptor motif similar to the phenols on the resorcinol ring. The benzamide ring also

covers the distance of the linker carbons of BnIm (figure 2.2 A), which could help design more rigid compounds.

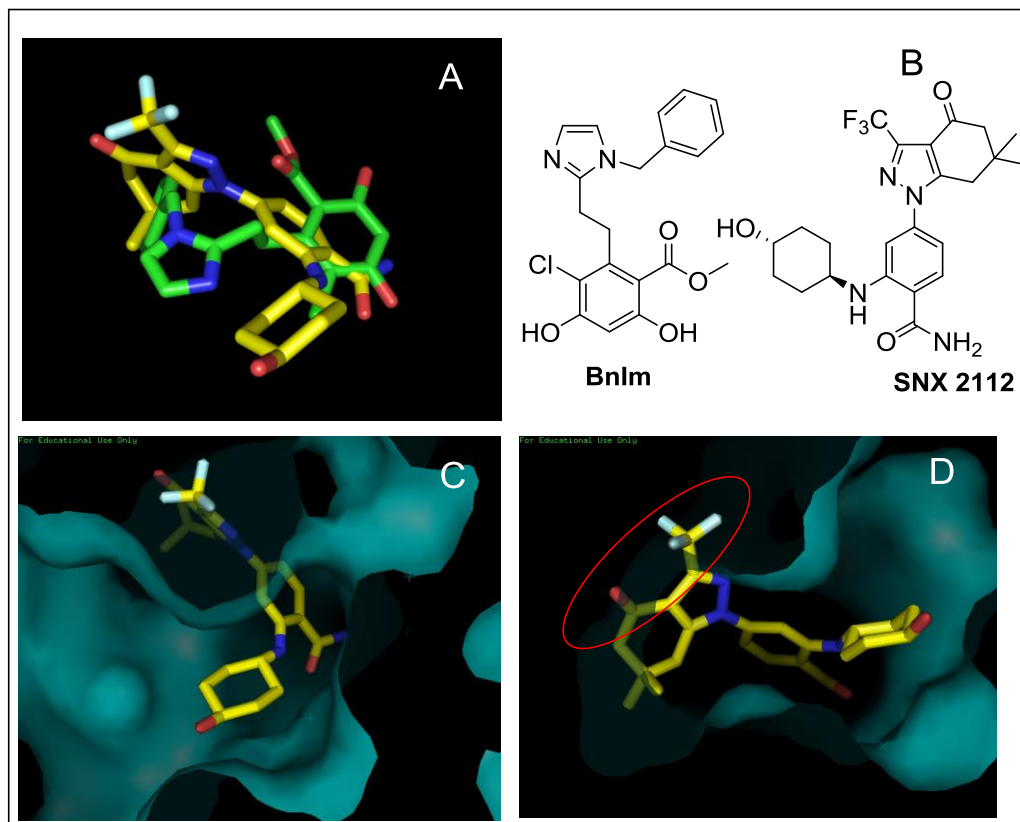


Figure 3.2 A) Overlay of BnIm bound to Grp94 and SNX 2112 bound to Hsp90 (PDB code: 4NH7) B) structures of BnIm and SNX 2112. C) Overlay of SNX 2112 with BnIm (not displayed) in Grp94 (cyan surface) D) the steric clash between SNX 2112 and induced conformation (BnIm bound) of Grp94 circled with red.

The aminocyclohexanol ring projects into the solvent exposed region and does not exhibit steric clash with the Grp94 induced conformation. Therefore, the benzamide along with the aminocyclohexanol ring could be used for the design of new Grp94-selective compounds without significant steric clash (figure 2.2 C). However, the trifluoromethyl and the ketone group of the tetrahydroindazolone ring found in SNX 2112 exhibit a steric clash with the induced conformation of Grp94 (figure 2.2 D). Therefore, the new design omitted the

tetrahydroindazolone ring, instead the pyrrole was hypothesized to occupy the Grp94 ester pocket upon substitution. In particular, the 2-position of pyrrole ring when substituted with a phenyl ring should bind the induced conformation of Grp94 preferentially over Hsp90.

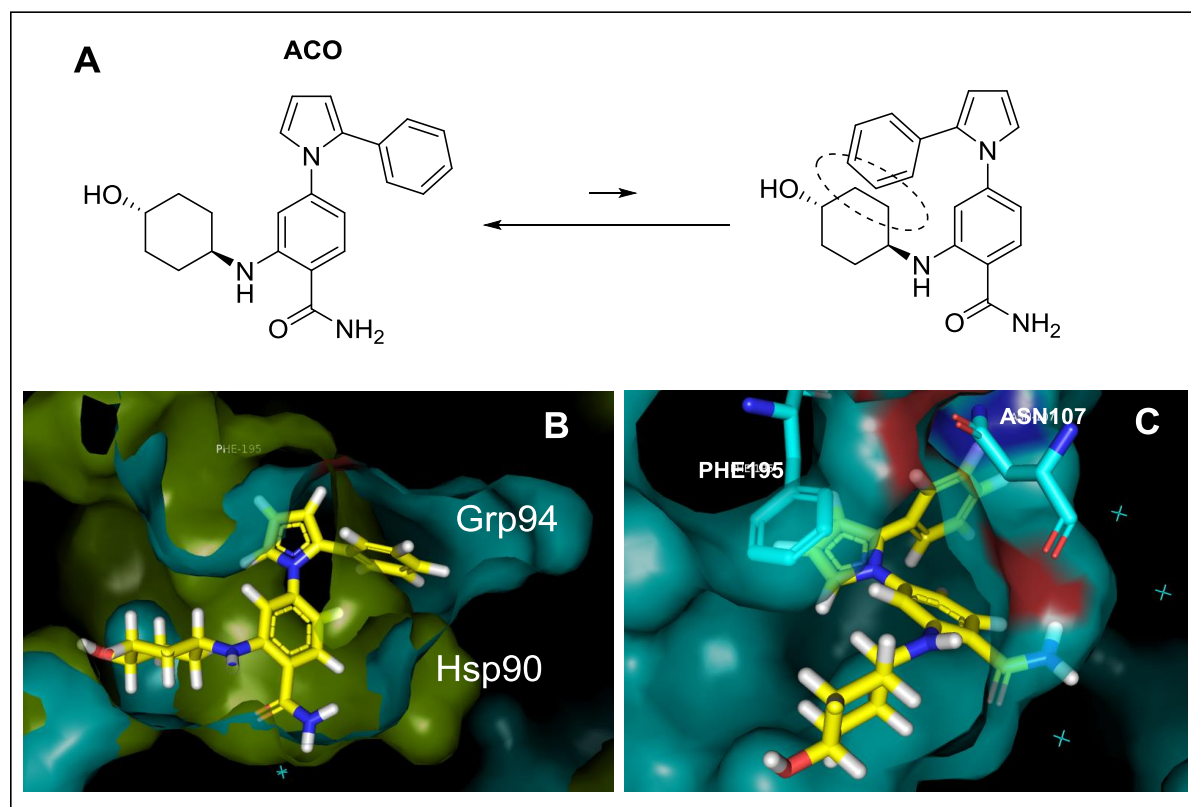


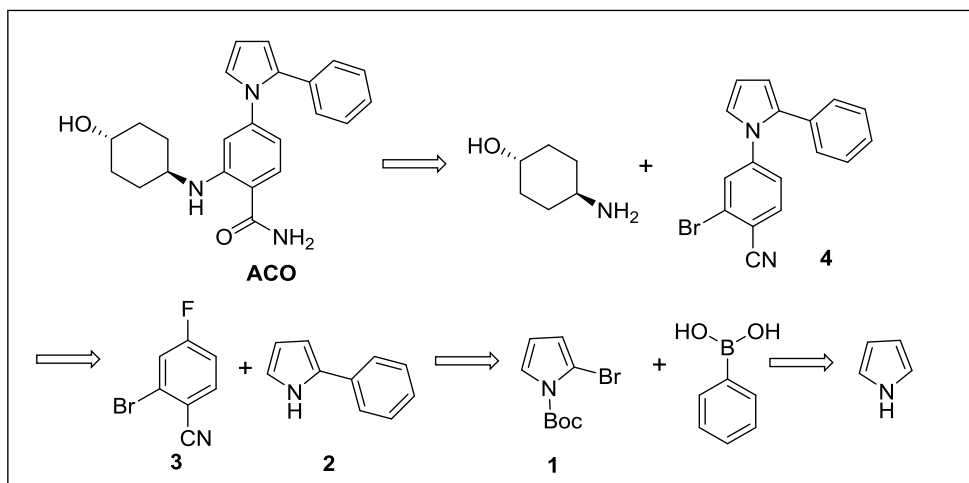
Figure 3.3 A) Proposed compound for Grp94 selective inhibition. B) Overlay of Grp94 (cyan) and Hsp90 (green) along with the docked ACO compound. C) Grp94 binding site residues illustrated.

SNX 2112 binding affinity for Hsp90 α/β is 4/6 nM, whereas, it binds to Grp94 with a K_i 484nM.³⁵ This difference in binding affinity could result from the change in the Grp94 conformation, which leads to steric clash with the tetrahydroindazolone ring. In the proposed aminocyclohexanol containing compound ACO (scheme 2.1), the pyrrole was expected to manifest π - π interaction with PHE195, which is responsible for interactions with the imidazole moiety in BnIm (Fig 2.3 C). Additionally, the ASN107 on top could be targeted with

substitutions on the phenyl ring. Incorporation of these two interactions would then increase the potency of the compounds for Grp94, but diminish affinity for Hsp90. The Desired conformation for ACO binding is shown in figure **2.3 B**, wherein the phenyl ring at the 2-position projects into the ester pocket. Molecular modeling studies suggested that ACO would favor the conformation shown in Figure **2.3 B**, due to a clash between the cyclohexylamine and phenyl ring as depicted in Figure **2.3 A**.

3. Synthesis and Evaluation

Synthesis of ACO was envisioned by modifying the previously disclosed synthetic route for SNX 2112. Retrosynthetic analysis of the compound was performed and pyrrole fragment **2** could be accessed via Suzuki coupling of various phenyl boronic acids with N-protected 2-bromopyrrole, **1**.

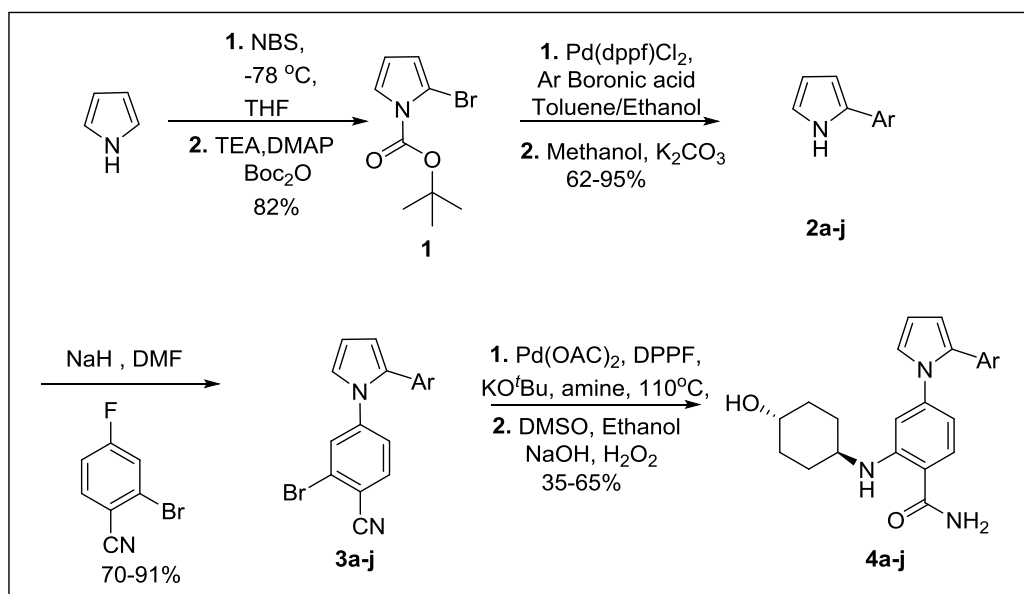


Scheme **3.1**. Retrosynthetic analysis of compound **ACO**

The pyrrole containing fragment could then be coupled via nucleophilic aromatic substitution reaction to the commercially available benzonitrile, **3**. Following this step, Buchwald-Hartwig

amination could be accomplished to couple the cyclohexylamine with the benzonitrile. Subsequent hydrolysis of the nitrile would then furnish the desired compound, **5**.

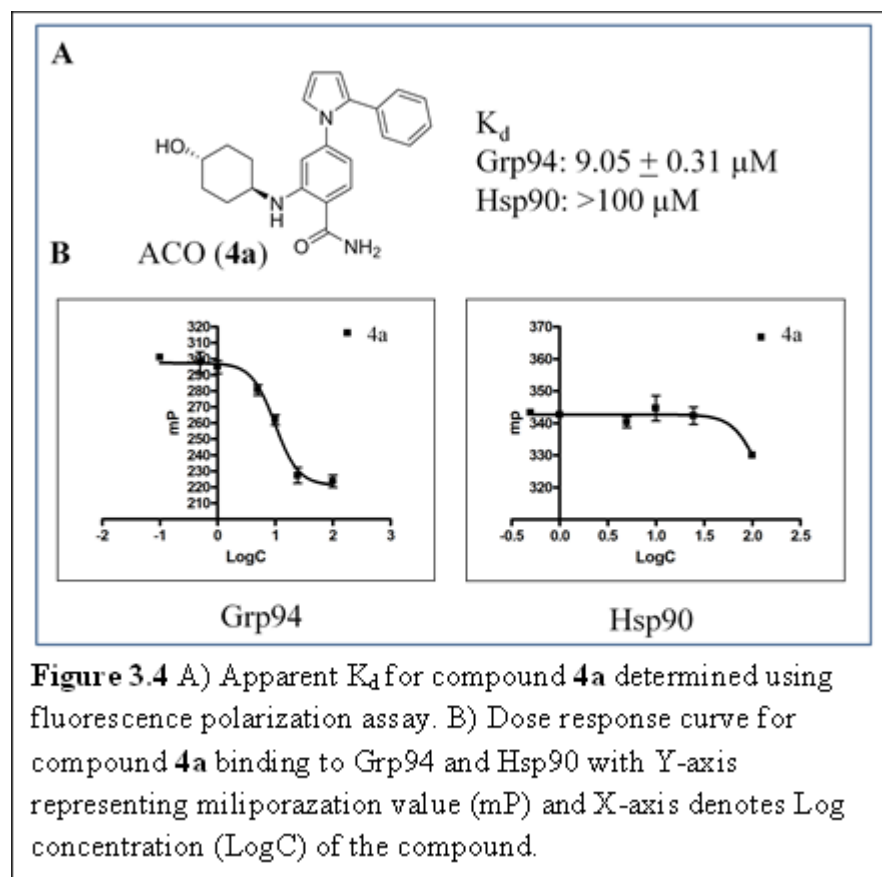
Synthesis of compounds **4a-j** began with bromination of the pyrrole and *in situ* protection of the nitrogen using the butyloxy carbonyl (Boc) group.^{36, 37} The brominated pyrrole was then utilized for the subsequent Suzuki coupling reaction, followed by basic Boc deprotection³⁸ to give



Scheme 3.2 Synthetic scheme for compounds **4a-j**

intermediates **2a-j**. Intermediate **3a-j** were obtained via a nucleophilic substitution reaction between **2a-j** with 4-fluoro-2-bromobenzonitrile. In the final step, amination was carried out using *trans*-aminocyclohexanol, followed by hydrolysis of the nitrile moiety to give the final benzamide products **4a-j**.

Upon synthesis of the parent compound, **4a**, which contains an unsubstituted phenyl ring, it was



evaluated for binding affinity towards Grp94 and Hsp90. It was observed that compound **4a** bound Grp94 with greater affinity than Hsp90 (Figure 2.4).

Thus, supporting the hypothesis that the designed compound, **4a**, binds Grp94 in its induced conformation as depicted

in figure 2.3 B. Following this exciting result, structure activity relationship (SAR) studies were performed on the phenyl ring to explore the spatial and electronic requirements of the Grp94 ester pocket (Figure 2.1 B). Methyl substitutions were made on the phenyl ring to explore the steric demand of the ester pocket, and among the compounds evaluated, the 2- and 3-methyl containing compounds, **4b** and **4c**, were shown to exhibit comparable potency to the parent compound (**4a**), suggesting that there is space around the ester pocket to accommodate methyl substitution while maintaining potency. Interestingly, the 4-methyl containing compound **4d** was found to bind Grp94 more tightly than **4a**, suggesting additional space in the pocket that could be probed further. In addition to the exploration of the steric requirement, chlorine substituted

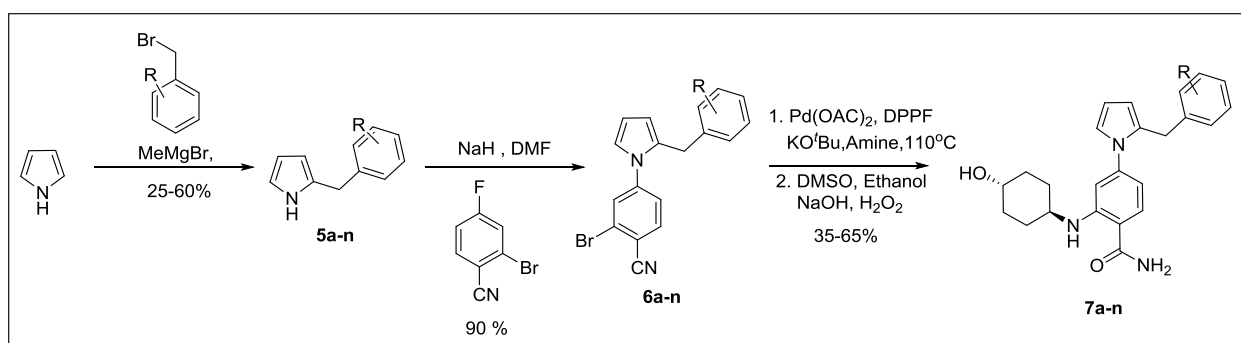
compounds, **4e-g**, were synthesized to study the effect on the electronics.

	Compound	R =	K_d for Grp94 (μM)	K_d for Hsp90 (μM)
	4b	2-Me	9.9 ± 0.54	>100
	4c	3-Me	9.43 ± 0.26	>100
	4d	4-Me	8.35 ± 0.14	>100
	4e	2-Cl	2.94 ± 0.27	>100
	4f	3-Cl	15.8 ± 0.31	>100
	4g	4-Cl	10.62 ± 0.54	>100
	Compound	N-Scan	K_d for Grp94 (μM)	K_d for Hsp90 (μM)
	4h	C ₂ = N	13.98 ± 0.27	>100
	4i	C ₃ = N	5.5 ± 0.15	>100
	4j	C ₄ = N	13.2 ± 0.12	>100

Table 3.1 Determined K_d values for compounds **4b-j** using fluorescence polarization assay.

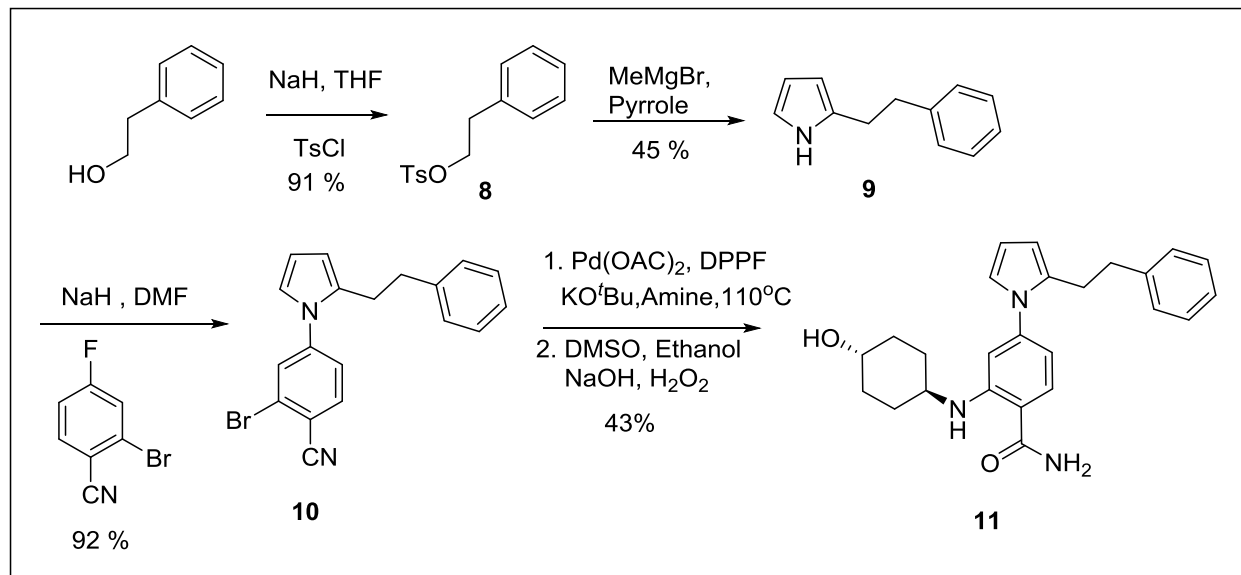
Among these compounds, the 3- and 4-chlorine substituted compounds **4f** and **4g** lost affinity, however, the 2-chlorine substituted compound **4e** was found to exhibit potency of ~3 μM. Analysis of the binding data for 2-methyl and 2-chlorine substituted compounds suggested that the potency manifested by the 2-chlorine compound, **4e**, might not result from steric effects, as the 2-methyl compound was less active. To explore the possibility of gaining a hydrogen bond, potentially with ASN107 (labeled in figure 2.3 C), the phenyl ring was replaced with a pyridine as shown with compounds **4h-j**. Unfortunately, 2- and 4-pyridine analogues manifested decreased binding for Grp94, however, **4i**, which contains a 3-pyridine ring was more active than **4a**. Although **4i** led to an increase in affinity, it was not reflective of strong interactions with Grp94. It was therefore proposed that there could be two factors affecting potency: First, the nitrogen atom

of the pyridine ring does not appear to align properly in the binding site, second, the rigidity of the scaffold may cause an inherent clash between the compounds and the protein, thus resulting in a loss of potency, regardless of the substitution. Molecular modeling studies were then directed to search for the potential clashes in the ester binding pocket with compound **4a**. These studies concluded that the rigidity of the phenyl ring could be detrimental to potency, as it was found that the 3-position of the phenyl ring was in close proximity to the Grp94 surface (figure **2.3B**).



Scheme 3.3 Synthetic scheme for compounds **7a-n**

To incorporate flexibility into compound **4a**, linker carbons were introduced between the pyrrole and phenyl rings. Synthesis of compound **7a** (unsubstituted benzyl) was achieved by constructing the 2-benzyl pyrrole **5a** via a S_N2 reaction involving the pyrrole and corresponding benzyl bromide, using methyl magnesium bromide as a base. Fragment **5a** then underwent the same sequence of reactions as in the case of non-linker based compounds.



Scheme 3.4 Synthetic scheme for compound **11**

The two-carbon linker containing compound (**11**) hypothesized to be unfavorable for binding to either Grp94 or Hsp90, was synthesized and evaluated to validate the proposed model for Grp94 ester pocket. Synthesis of compound **11** was achieved through modification of phenethyl alcohol to make the tosylated compound **8**, which served as a leaving group (LG) in the subsequent SN2 reaction with the pyrrole to furnish fragment **9**. In subsequent steps, fragment **9** was utilized for the construction of compound **11** following similar synthetic scheme as outlined for the non-linker based compound, **4a**.

Evaluation of the linker led to interesting results that determined the unsubstituted benzyl containing compound, **7a**, to manifest a K_d of $\sim 1.3 \mu\text{M}$, which was greater than the non-linker compound, **4a**. Whereas the phenethyl containing compound (**11**) displayed a decrease in affinity, which corroborated the hypothesis that the Grp94 ester pocket cannot accommodate a phenethyl fragment. Excited with the results produced by **7a**, SAR studies were initiated to probe the ester pocket with substitutions on the benzyl ring.

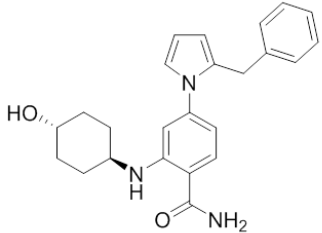
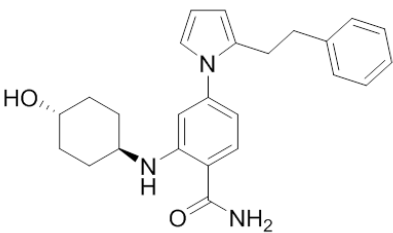
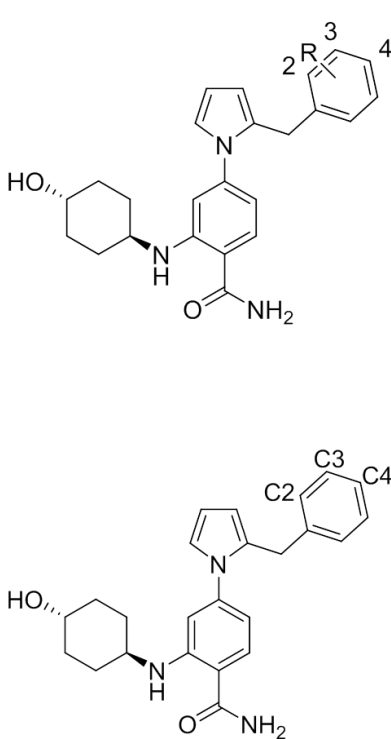
		
Compound 7a	Compound 11	
Compound	K_d in Grp94 (μM)	K_d in Hsp90 (μM)
Benzyl (7a)	1.3 ± 0.13	>100
Phenethyl (11)	> 25	> 100

Table 3.2 K_d values for linker compounds **7a** and **11** using fluorescence polarization assay.

SAR studies were initiated with the chlorine substituted compounds, **7b-d**. The 4-chlorine substituted compound **7d** lost affinity for Grp94, indicating that the 4-position on the benzyl ring did not project into a region of the ester pocket spacious for accommodation of a chlorine atom. The 3-chlorine compound **7b** manifested a slight loss in potency as compared to **7a**. Whereas, the 2-chlorine substituted compound increased potency towards Grp94, while maintaining negligible binding towards Hsp90. To further probe the pocket around the 2-position, compound **7i** was synthesized to contain a 2-methyl substitution. This compound exhibited a loss in potency of ~3 fold, thus explaining that a hydrophobic substitution at 2-position is not tolerated. Therefore, it was concluded that the increase in potency for the 2-chlorine compound, **7b**, was not due to the hydrophobic nature of chlorine substituent. SAR studies continued to explore the pocket with compounds substituted with a fluorine atom, compounds **7e-g**. Increased potency was observed (~724 nM) with the 2-fluorine compound **7e**. Since the ester pocket does not contain aromatic amino acids, the fluorine alters electronics of the benzyl group that may not

have significant effect on potency. However, fluorine could interact with ASN107, and such interactions are known to occur with fluorine acting as hydrogen bond acceptor.³⁹



Compound	R=	K _d for Grp94 (μM)	K _d for Hsp90 (μM)
7b	2-Cl	0.830 ± 0.12	>100
7c	3-Cl	2.45 ± 0.45	>100
7d	4-Cl	> 25	>100
7e	2-F	0.724 ± 0.14	>100
7f	3-F	4.53 ± 0.12	>100
7g	4-F	8.35 ± 0.14	>100
7h	2-Br	12.97 ± 0.11	>100
7i	2-Me	4.2 ± 0.23	>100

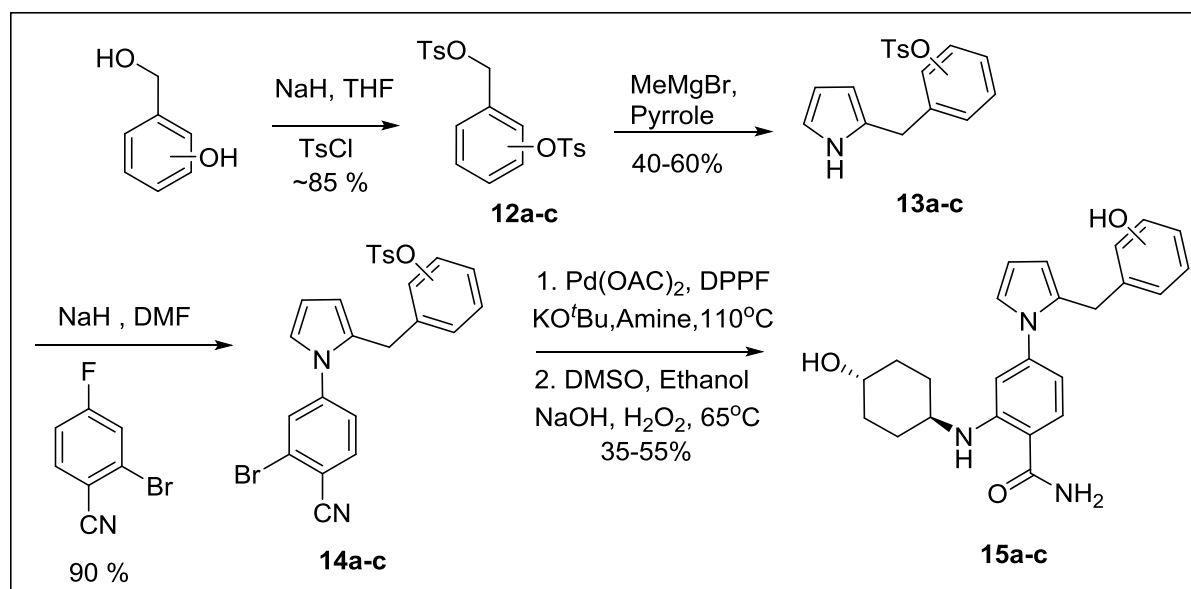
Compound	N-Scan	K _d for Grp94 (μM)	K _d for Hsp90 (μM)
7j	C2 = N	12.3 ± 0.23	>100
7k	C3 = N	> 25	>100
7l	C4 = N	8.09 ± 0.3	>100

Table 3.3 K_d values for linker compounds **7b-i** determined using fluorescence polarization assay.

In the case of the 3-fluorine (**7f**) and 4-fluorine (**7g**) analogs, a loss in potency was observed similar to that of the chlorine derivatives. To further explore the 2-position, Compound **7h** was synthesized to contain bromine which also exhibited less affinity than the chlorine and the fluorine analogs. A trend was observed for halogens determining that fluorine is most active and bromine is least active. Following a trend for the halogen substitution with fluorine being the most and the bromine analog the least active.

SAR studies concluded that the 2-position of the benzyl ring is critical for a gain in affinity and that ASN107 in Grp94 may be involved in hydrogen bonding. Therefore, hydroxyl

containing compounds **15a-c** were synthesized to establish hydrogen bonds with ASN107. The synthesis began with 2-hydroxy benzyl alcohol reacting with two equivalents of tosyl chloride in presence of base to give intermediates **12a-c**. These intermediates were subsequently utilized for the synthesis of compounds **15a-c** via the same synthetic as shown earlier.



Scheme 3.5 Synthetic route for compounds **15a-c**

Upon their preparation, phenol-containing compounds were evaluated for binding affinity. Interestingly, the 2-hydroxyl substituted derivative (**15a**) exhibited K_d value of ~446nM towards Grp94 while maintaining $>100 \mu\text{M}$ K_d for binding Hsp90 (>200 fold selectivity for Grp94 vs Hsp90). Increased potency of compound **15a** could once again be explained via the potential hydrogen bonding interactions with ASN107 through phenol hydroxyl group. Furthermore, 3-phenol substituted compound, **15b**, and the 4-phenol **15c** could only bind Grp94 with high K_d values (Table 2.4). Loss in activity for the 3-and 4-position substitutions (table **2.3**). However, a hydroxyl group could serve as both a hydrogen bond donor and acceptor; therefore, the 2-methoxy containing compound, **7m**, was synthesized to differentiate the role of hydroxyl group in relation to

ASN107.

Compound	R =	K _d for Grp94 (μM)	K _d for Hsp90 (μM)
15a	2-OH	0.446 ± 0.09	>100
15b	3-OH	>25	>100
15c	4-OH	20.55 ± 0.74	>100
7m	2-OMe	1.15 ± 0.02	>100

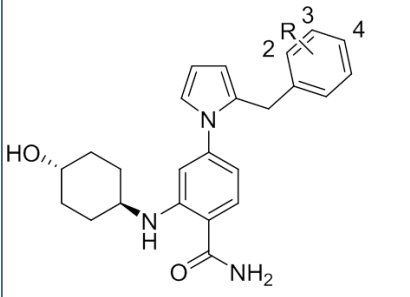


Table 3.4 K_d values for compounds **15a-c** and **7m** using fluorescence polarization assay.

for compound **7m** was determined to be ~1.1 μM, which was slightly better than the parent compound, validating the role of hydroxyl as a hydrogen bond acceptor.

To investigate whether the 2,6-disubstituted compound would lead to an increase in affinity, 2,6-difluoro substituted compound **16a** was synthesized. Upon evaluation of binding affinity, compound **16a** exhibited decreased affinity, leading to the conclusion that the

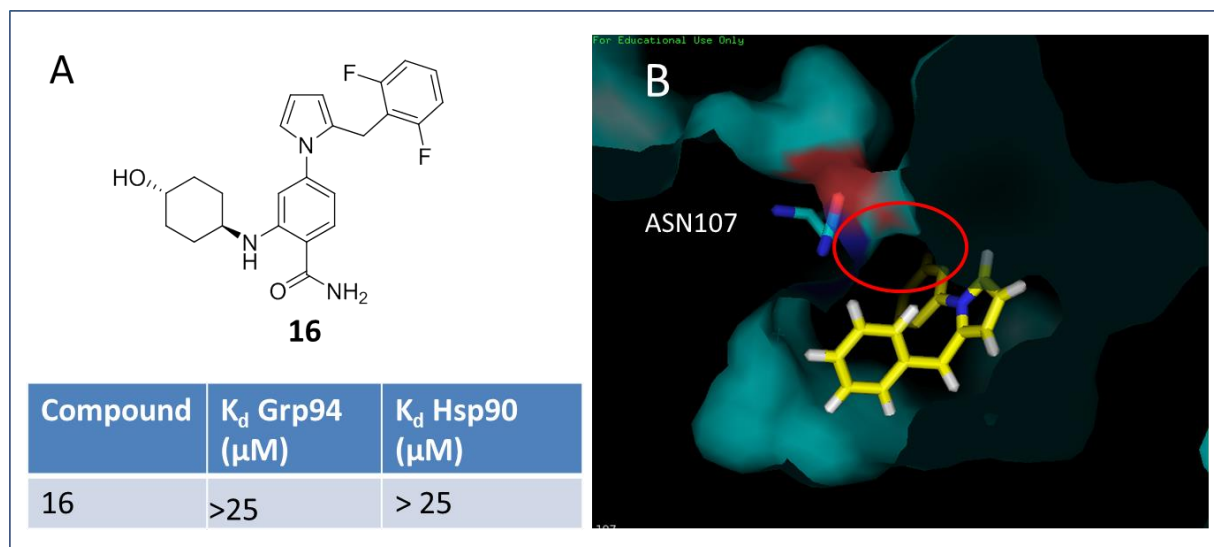


Figure 3.5 A) K_d values for linker compounds **16** using fluorescence polarization assay. B) Docking image compound **4a** in Grp94 depicting the cavity around ASN 107 (circled in red).

occupancy of the binding pocket about the 2-and 6-positions are mutually exclusive. The loss in affinity for the 2,6-disubstituted compounds could be attributed to presence of a channel around ASN107 that can only accommodate one 2-position substitution, while the 6-position is aligned too close to surface of the protein (figure 2.5).

Following the SAR studies with compounds **15a** and **7e**, their cellular efficacy in a wound healing scratch assay investigated with the highly metastatic breast cancer cell line, MDA-MB-231.²⁸

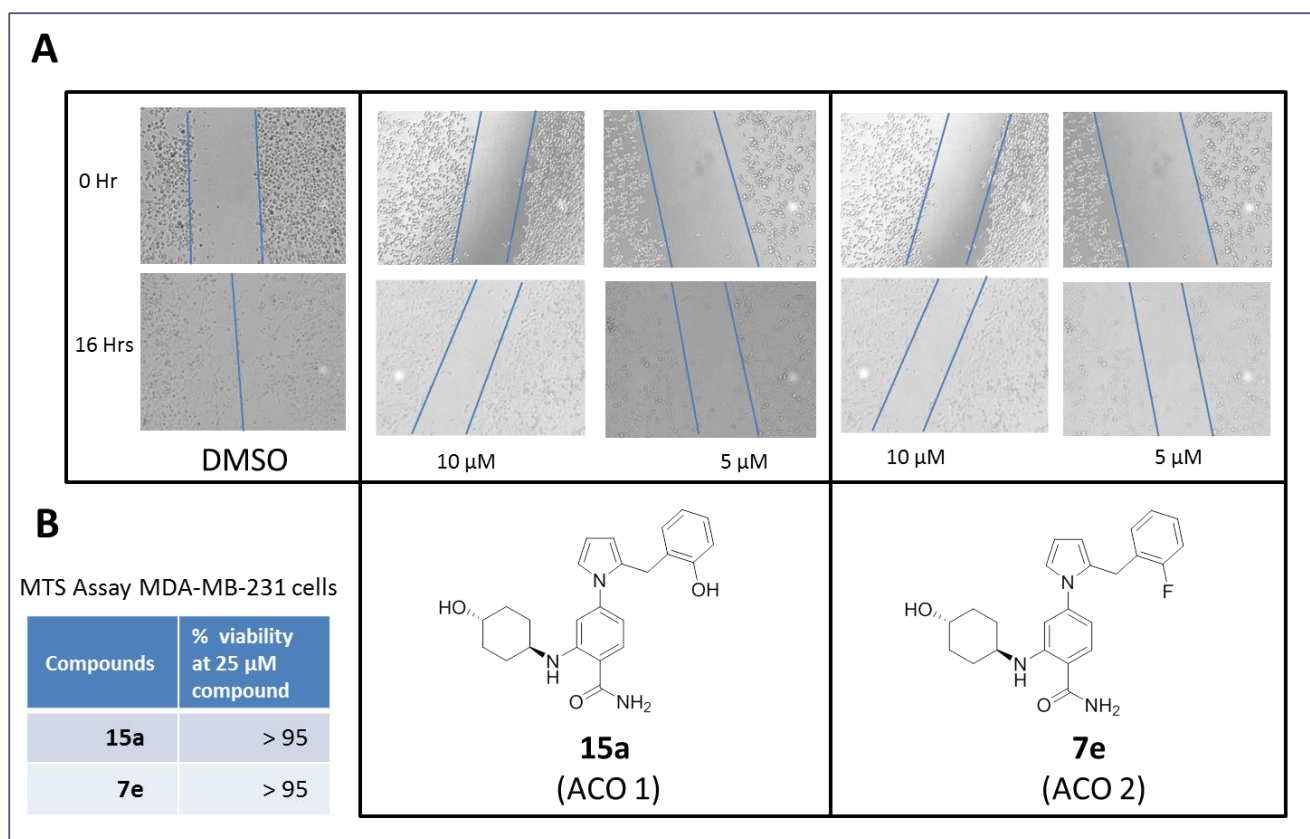


Figure 3.6 A) Inhibition of MDA-MB-231 cell migration by compounds **15a** and **7e** 10 and 5 μ M determined at 0 and 16Hrs.B) percent viability of MDA-MB-231 cells determined using MTS assay.

It can be seen in figure 2.6 A that compound **15a** and **7e** inhibited MDA-MB-231 cell migration at 10 μ M as well as 5 μ M. To confirm that the inhibition of migration was not due to anti-

proliferative activities, an MTS assay was performed to measure cellular viability of MDA-MB-231 at 25 μ M of **15a** and **7e**. In the MTS assay, both compounds did not affect the proliferation of MDA-MB-231 (>95 % viability at 25 μ M **15a** and **7e**), confirming that inhibition of the cell migration was not the result of anti-proliferative activity.

4. Conclusion and Future Directions

In summary, co-crystal structures of the first Grp94 selective compound (BnIm) bound to Grp94 and Hsp90 were examined to reveal the existence of a unique pocket in Grp94, which is not observed in Hsp90. Using a structure-based drug design approach, a new aminocyclohexanol (ACO) based scaffold was developed that selectively binds Grp94 as compared to Hsp90. Further SAR studies led to analogs with a benzyl group that manifested increased potency. Subsequent modifications to the benzyl group led to compounds containing a phenol at the 2-position of the benzyl ring, which displayed the highest affinity. Discovery of the novel Grp94 selective scaffold, ACO, has enabled exploration of the biological consequences of Grp94 perturbation and the development of potential anti-metastatic agents. Future modification to the ACO scaffold will focus on substitutions at the linker carbon and the introduction of various hydrogen bond acceptors on the benzyl group. Additionally, pyrrole replacements will be sought to gain the π - π interaction with PHE195.

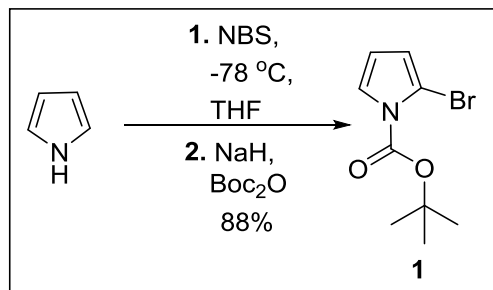
5. General Experimental Methods.

Fluorescence Polarization. Assay buffer (25 μ L, 20 mM HEPES pH 7.3, 50 mM KCl, 5 mM $MgCl_2$, 1 mM DTT, 20 mM Na_2MoO_4 , 0.01% NP-40, and 0.5 mg/mL BGG) was added to 96-well plate (black well, black bottom) followed by the desired compound at the indicated final concentrations in DMSO (1% DMSO final concentration).³² Recombinant cGrp94 (10nM for compounds 2-27, 30 nM for compounds 28-48) and FITC-GDA were then added (6 nM). Plates were incubated with rocking for 5 h at 4°C. Fluorescence was determined using excitation and emission filters of 485 and 528 nm, respectively. Percent FITC-GDA bound was determined by using the DMSO millipolarization unit (mP) as the 100% bound value and the 0% for FITC-GDA. K_d values were calculated from separate experiments performed in triplicate using GraphPad Prism.

Procedure for Anti-proliferation assay, wound healing assay and molecular modeling as described in chapter 2.

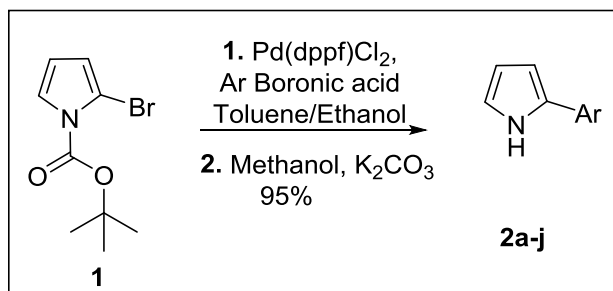
General chemistry

Preparation of tert-butyl 2-bromo-1H-pyrrole-1-carboxylate (1)



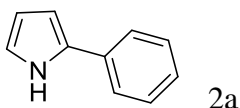
Pyrrole (5 g, 74.6 mmol) was dissolved in 200 mL of dry tetrahydrofuran (THF), the solution is cooled down to -78 C using dry ice-isopropanol bath. To this stirring solution was added N-

bromosuccininmide (NBS) (13.2 g, 74.6 mmol) in portions. The solution was allowed to stir for 5 mins before it was transferred to a freezer (-20° C) for 2 hr during which the solution turns light green. This solution it then filtered into a 500mL flask that was cooled to -78 C via suction. The flask is then flushed with argon and triethylamine (TEA) (3.1g, 29.8 mmol) followed immediately by sequential addition of 4-dimethylaminopyridine (DMAP) (~0.1 g) and di-tert-butyl dicarbonate (22.6 g, 104.2 mmol). This mixture was stirred for 8 hr while it was allowed to warm to room temperature. The solvent was removed *in vacuo*, ethyl acetate 150ml was added to the remaining crude mixture, washed with water (3 X 100 ml) and dried over sodium sulfate and concentrated to give compound **1** as a colorless oil (14.9g, 82%). ¹H NMR (500 MHz, Chloroform-d) δ 7.33 (dd, *J* = 3.6, 1.9 Hz, 1H), 6.32 (dd, *J* = 3.5, 2.0 Hz, 1H), 6.18 (t, *J* = 3.5 Hz, 1H), 1.64 (s, 9H). ¹³C NMR (126 MHz, CDCl₃) δ 148.06, 123.00, 117.23, 111.58, 100.29, 84.83, 27.99. HRMS (ESI) *m/z* [M+Na] for C₉H₁₂BrNO₂Na: 267.9943; found, 267.9949.

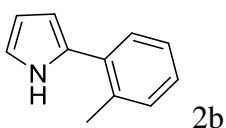


General procedure for preparation of 2a-j: Compound **1** (200 mg, 0.81 mmol) was taken in a 15 mL reaction vessel, aryl boronic acid (0.88 mmol), potassium bicarbonate (331 mg, 2.4 mmol), were then added to the vessel. This was followed by addition of toluene (3 mL), ethanol (0.5 mL) and water (0.5 mL). argon was purged through the solvent for 15 mins and then Pd(dppf)Cl₂ (30 mg, 0.04 mmol) was added the reaction vessel was sealed and heated to 110° C for 12 Hr. Reaction was cooled to room temperature and water (5 mL) and ethyl acetate (5 mL) are added to the reaction mixture, organic fraction is collected and dried *in vacuo*, the remaining

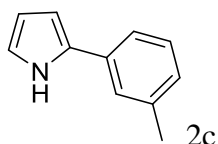
crude mass was dissolved in 3mL methanol and 1mL water mixture. Potassium carbonate (331mg, 2.4 mmol) was then added. The reaction was refluxed until the reaction was complete, as monitored by TLC. The reaction was allowed to cool and the solvent was evaporated under vacuum till 1/4th volume remained. To this 2mL water was added and then extracted thrice with 5mL ethyl acetate. Organic fraction was then collected and dried over sodium sulfate, purification was then performed using column chromatography eluting with 20% ethyl acetate in hexanes to yield the corresponding products.



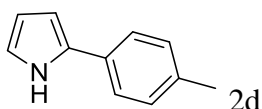
2-phenyl-1H-pyrrole (2a): 77% yield, light orange solid. ¹H NMR (400 MHz, Chloroform-d) δ 8.46 (s, 1H), 7.54 – 7.48 (m, 2H), 7.39 (dd, J = 8.5, 7.0 Hz, 2H), 7.27 – 7.21 (m, 1H), 6.90 (m, J = 2.7, 1.4 Hz, 1H), 6.56 (m, J = 3.8, 2.7, 1.5 Hz, 1H), 6.33 (m, J = 3.4, 2.5 Hz, 1H). HRMS (ESI) m/z [M+H] for C₁₀H₁₀N: 144.0813, found 144.0818.



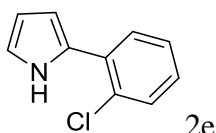
2-(o-tolyl)-1H-pyrrole (2b): 83 % yield, white solid. ¹H NMR (500 MHz, CDCl₃) δ 8.20 (s, 1H), 7.28 (dd, J = 7.5, 1.6 Hz, 1H), 7.20 – 7.17 (m, 2H), 7.16 – 7.10 (m, 2H), 6.81 (m, J = 2.7, 1.5 Hz, 1H), 6.33 – 6.19 (m, 2H), 2.39 (s, 3H). ¹³C NMR (126 MHz, CDCl₃) δ 135.10, 132.85, 131.32, 131.04, 127.91, 126.79, 126.05, 117.92, 109.24, 108.78, 21.27. HRMS (ESI) m/z [M+H] for C₁₁H₁₂N: 158.0970, found 158.0965.



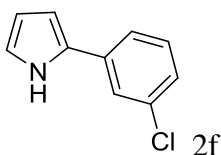
2-(m-tolyl)-1H-pyrrole (2c): 77 % yield, white solid. ^1H NMR (500 MHz, CDCl_3) δ 8.35 (s, 1H), 7.23 (m, 1H), 7.21-7.17 (m, 2H), 6.96 (m, 1H), 6.79 (m, 1H), 6.44 (m, 1H), 6.22 (m, 1H), 2.31 (d, $J = 0.7$ Hz, 3H). ^{13}C NMR (126 MHz, CDCl_3) δ 138.46, 132.70, 132.25, 128.78, 127.03, 124.64, 120.98, 118.63, 110.05, 105.82, 21.55. HRMS (ESI) m/z $[\text{M}+\text{H}]$ for $\text{C}_{11}\text{H}_{12}\text{N}$: 158.0970, found 158.0965.



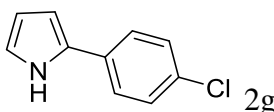
2-(p-tolyl)-1H-pyrrole (2d): 73 % yield, white solid. ^1H NMR (500 MHz, CDCl_3) δ 8.32 (s, 1H), 7.30 (m, 2H), 7.13 – 7.09 (m, 2H), 6.78 (m, 1H), 6.41 (m, 1H), 6.22 (m, 1H), 2.28 (s, 3H). ^{13}C NMR (126 MHz, CDCl_3) δ 135.93, 132.28, 130.04, 129.55, 123.84, 118.38, 109.99, 105.38, 21.13. HRMS (ESI) m/z $[\text{M}+\text{Na}]$ for $\text{C}_{11}\text{H}_{11}\text{NNa}$: 180.0789, found 180.0788.



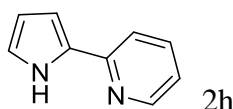
2-(2-chlorophenyl)-1H-pyrrole (2e): 84 % yield, white solid. ^1H NMR (500 MHz, CDCl_3) δ 9.03 (s, 1H), 7.50 (dd, $J = 7.8, 1.8$ Hz, 1H), 7.33 (dd, $J = 8.0, 1.5$ Hz, 1H), 7.23 – 7.19 (m, 1H), 7.14 – 7.04 (m, 1H), 6.90 – 6.85 (m, 1H), 6.54 (m, 1H), 6.25 (m, 1H). ^{13}C NMR (126 MHz, CDCl_3) δ 131.02, 130.74, 129.78, 129.34, 127.31, 127.18, 119.00, 109.39, 109.31. HRMS (ESI) m/z $[\text{M}+\text{H}]$ for $\text{C}_{10}\text{H}_9\text{ClN}$: 178.0424, found 178.0429.



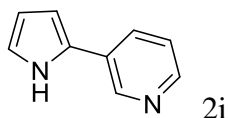
2-(3-chlorophenyl)-1H-pyrrole (2f): 80 % yield, white solid. ^1H NMR (500 MHz, CDCl_3) δ 8.35 (s, 1H), 7.38 (t, $J = 1.9$ Hz, 1H), 7.27 (m, 1H), 7.22 (t, $J = 7.8$ Hz, 1H), 7.10 (m, 1H), 6.82 (m, 1H), 6.47 (m, 1H), 6.24 (m, 1H). ^{13}C NMR (126 MHz, CDCl_3) δ 134.82, 134.48, 130.69, 130.14, 126.05, 123.82, 121.82, 119.50, 110.40, 106.92. HRMS (ESI) m/z $[\text{M}+\text{H}]$ for $\text{C}_{10}\text{H}_9\text{ClN}$: 178.0424, found 178.0429.



2-(4-chlorophenyl)-1H-pyrrole (2g): 78% yield, white solid. ^1H NMR (500 MHz, CDCl_3) δ 8.32 (s, 1H), 7.34 – 7.30 (m, 2H), 7.28 – 7.24 (m, 2H), 6.81 (m, 1H), 6.44 (m, 1H), 6.23 (m, 1H). ^{13}C NMR (126 MHz, CDCl_3) δ 131.74, 131.26, 129.04, 125.00, 119.22, 110.35, 106.42. HRMS (ESI) m/z $[\text{M}+\text{H}]$ for $\text{C}_{10}\text{H}_9\text{ClN}$: 178.0424, found 178.0421.

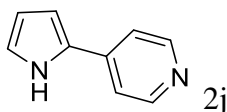


2-(1H-pyrrol-2-yl)pyridine (2h): 65% yield, White solid. ^1H NMR (400 MHz, CDCl_3) δ 9.82 (s, 1H), 8.55 – 8.44 (m, 1H), 7.72 – 7.54 (m, 2H), 7.06 (m, 1H), 6.94 (m, 1H), 6.75 (m, 1H), 6.32 (m, 1H). ^{13}C NMR (126 MHz, CDCl_3) δ 150.31, 148.46, 136.74, 131.18, 120.48, 120.12, 118.24, 110.32, 107.44. HRMS (ESI) m/z $[\text{M}+\text{H}]$ for $\text{C}_9\text{H}_9\text{N}_2$: 145.0766, found 145.0762.

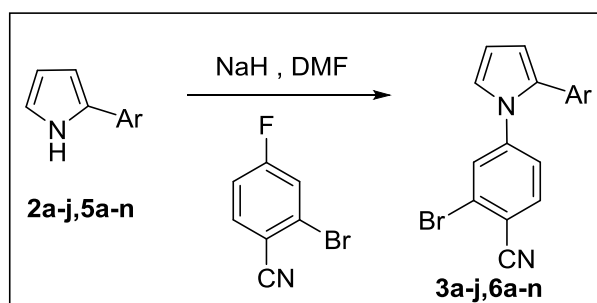


3-(1H-pyrrol-2-yl)pyridine (2i): 74 % yield, white solid. ^1H NMR (500 MHz, CDCl_3) δ 9.02 – 8.86 (m, 1H), 8.72 (dd, $J = 2.4, 0.9$ Hz, 1H), 8.35 (dd, $J = 4.8, 1.6$ Hz, 1H), 7.71 (m, 1H), 7.22

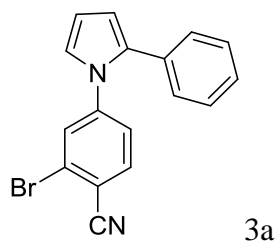
(m, 1H), 6.87 (m, 1H), 6.53 (m, 1H), 6.31 (m, 1H). ^{13}C NMR (126 MHz, CDCl_3) δ 146.90, 145.11, 136.28, 131.11, 128.88, 123.78, 120.12, 110.45, 107.27. HRMS (ESI) m/z $[\text{M}+\text{H}]$ for $\text{C}_9\text{H}_9\text{N}_2$: 145.0766, found 145.0762.



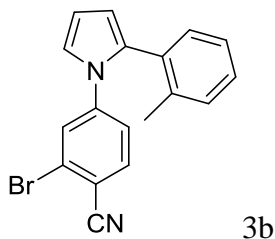
4-(1H-pyrrol-2-yl) pyridine (2j): 73% yield, white solid. ^1H NMR (500 MHz, CDCl_3) δ 8.72 (s, 1H), 8.55 – 8.41 (m, 2H), 7.33 – 7.23 (m, 2H), 6.91 (m, 1H), 6.69 (m, 1H), 6.28 (m, 1H). ^{13}C NMR (126 MHz, CDCl_3) δ 149.92, 139.61, 129.01, 121.24, 117.70, 111.00, 109.21. HRMS (ESI) m/z $[\text{M}+\text{H}]$ for $\text{C}_9\text{H}_9\text{N}_2$: 145.0766, found 145.0768.



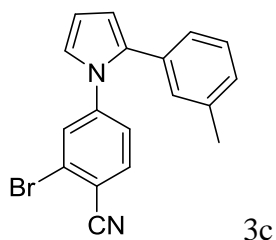
General procedure A (preparation of 3a-j, 6a-n): Pyrrole intermediates **2a-j**, **5a-n** (0.7 mmol) and 2-bromo-4-fluorobenzonitrile (0.7 mmol) are taken in a reaction vial, 0.5 mL dry dimethyl formamide (DMF) is then added to the reaction vial. The mixture is stirred till dissolution of solids, sodium hydride (60% dispersion in oil) (0.7 mmol) is then added to the stirring reaction mixture under argon. Reaction is stirred at room temperature for 4 hrs or until the completion of reaction as monitored by TLC. 10 mL water is then added to the reaction mixture and ethyl acetate (2 x 15 mL) was used for extraction. The organic fraction was dried over sodium sulfate and adsorbed onto silica for column chromatography, which was performed utilizing 20% ethyl acetate in hexanes as the elution solvent system.



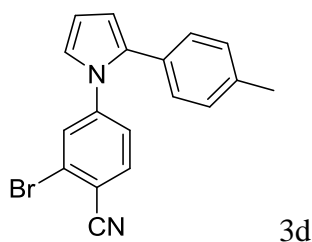
2-bromo-4-(2-phenyl-1H-pyrrol-1-yl) benzonitrile (3a): 84% yield, beige colored solid. ^1H NMR (400 MHz, CDCl_3) δ 7.58 – 7.54 (m, 2H), 7.38 – 7.28 (m, 3H), 7.16 – 7.09 (m, 3H), 6.98 (dd, $J = 3.0, 1.7$ Hz, 1H), 6.48 (dd, $J = 3.5, 1.7$ Hz, 1H), 6.44 (dd, $J = 3.5, 2.9$ Hz, 1H). ^{13}C NMR (126 MHz, CDCl_3) δ 144.64, 134.51, 133.97, 131.93, 129.01, 128.56, 128.50, 127.26, 125.74, 124.31, 123.70, 116.83, 113.04, 112.82, 111.22. HRMS (ESI) m/z [M+H] for $\text{C}_{17}\text{H}_{12}\text{BrN}_2$: 323.0183, found 323.0174.



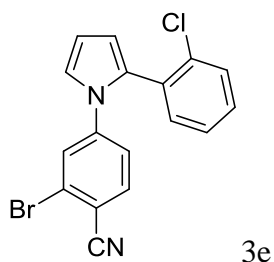
2-bromo-4-(2-(o-tolyl)-1H-pyrrol-1-yl) benzonitrile (3b) : 85% yield, pale yellow solid. ^1H NMR (500 MHz, CDCl_3) δ 7.45 (d, $J = 8.5$ Hz, 1H), 7.42 (d, $J = 2.1$ Hz, 1H), 7.27– 7.23 (m, 1H), 7.20 – 7.15 (m, 3H), 7.01 – 6.95 (m, 2H), 6.44 (t, $J = 3.3$ Hz, 1H), 6.33 (m, 1H), 1.99 (s, 3H). ^{13}C NMR (126 MHz, CDCl_3) δ 144.61, 137.21, 134.46, 132.96, 132.05, 131.05, 130.48, 128.46, 127.79, 125.97, 125.60, 122.71, 121.67, 116.86, 113.21, 112.42, 110.98, 20.14. HRMS (ESI) m/z [M+Na] for $\text{C}_{18}\text{H}_{13}\text{BrN}_2\text{Na}$: 359.0160, found 359.0165.



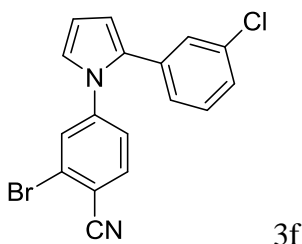
2-bromo-4-(2-(m-tolyl)-1H-pyrrol-1-yl)benzonitrile (3c) : 82 % yield, pale yellow solid. ^1H NMR (500 MHz, CDCl_3) δ 7.55 – 7.52 (m, 2H), 7.15 (t, $J = 7.6$ Hz, 1H), 7.09 – 7.06 (m, 2H), 7.02 (m, 1H), 6.94 (m, 1H), 6.85 – 6.82 (m, 1H), 6.44 (m, 1H), 6.41 (m, H), 2.31 (s, 3H). ^{13}C NMR (126 MHz, CDCl_3) δ 144.71, 138.31, 134.45, 134.44, 131.85, 129.14, 129.14, 128.89, 128.35, 128.06, 125.70, 124.30, 123.54, 116.90, 112.90, 112.72, 111.18, 21.45. HRMS (ESI) m/z $[\text{M}+\text{Na}]$ for $\text{C}_{18}\text{H}_{13}\text{BrN}_2\text{Na}$: 359.0160, found 359.0175.



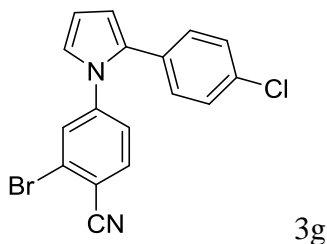
2-bromo-4-(2-(p-tolyl)-1H-pyrrol-1-yl)benzonitrile (3d) : 86 % yield, pale yellow solid. ^1H NMR (500 MHz, Chloroform-d) δ 7.75 – 7.64 (m, 1H), 7.60 – 7.37 (m, 2H), 7.24 (m, 1H), 7.15 – 7.06 (m, 2H), 7.05 – 6.87 (m, 2H), 6.43 (d, $J = 6.5$ Hz, 2H), 2.37 (s, 3H). ^{13}C NMR (126 MHz, CDCl_3) δ 144.82, 137.25, 136.10, 134.51, 129.28, 129.05, 128.95, 128.42, 125.74, 124.43, 123.42, 115.82, 112.93, 112.43, 111.15, 21.11. HRMS (ESI) m/z $[\text{M}+\text{H}]$ for $\text{C}_{18}\text{H}_{14}\text{BrN}_2$: 337.0340, found 337.0334.



2-bromo-4-(2-(2-chlorophenyl)-1H-pyrrol-1-yl)benzonitrile (3e) : 74 % yield, light yellow solid. ^1H NMR (500 MHz, CDCl_3) δ 7.49 (d, $J = 8.4$ Hz, 1H), 7.43 (d, $J = 2.1$ Hz, 1H), 7.36 – 7.27 (m, 4H), 7.05 – 7.01 (m, 2H), 6.47 – 6.43 (m, 2H). ^{13}C NMR (126 MHz, CDCl_3) δ 144.59, 134.53, 134.08, 132.42, 131.49, 130.55, 130.03, 129.68, 128.05, 126.98, 125.63, 122.85, 122.51, 116.84, 114.15, 112.79, 110.98. HRMS (ESI) m/z $[\text{M}+\text{H}]$ for $\text{C}_{17}\text{H}_{11}\text{BrClN}_2$: 356.9794, found 356.9803.



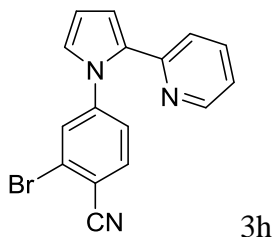
2-bromo-4-(2-(3-chlorophenyl)-1H-pyrrol-1-yl)benzonitrile (3f): 86% yield, pale yellow solid. ^1H NMR (500 MHz, CDCl_3) δ 7.59 – 7.52 (m, 2H), 7.25 – 7.15 (m, 3H), 7.09 (dd, $J = 8.4$, 2.1 Hz, 1H), 6.96 (dd, $J = 3.0$, 1.7 Hz, 1H), 6.89 – 6.86 (m, 1H), 6.48 (dd, $J = 3.6$, 1.7 Hz, 1H), 6.42 (dd, $J = 3.6$, 2.9 Hz, 1H). ^{13}C NMR (126 MHz, CDCl_3) δ 144.27, 134.66, 134.50, 133.69, 132.38, 129.69, 129.01, 128.21, 127.26, 126.51, 125.94, 124.39, 124.33, 116.73, 113.58, 113.42, 111.39. HRMS (ESI) m/z $[\text{M}+\text{Na}]$ for $\text{C}_{17}\text{H}_{11}\text{BrClN}_2$: 378.9614, found 378.9616.



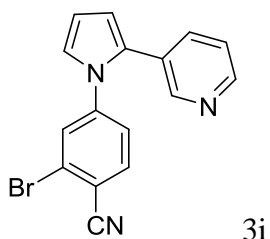
2-bromo-4-(2-(4-chlorophenyl)-1H-pyrrol-1-yl)benzonitrile (3g): 88% yield, pale yellow solid. ^1H NMR (500 MHz, CDCl_3) δ 7.50 (d, $J = 8.4$ Hz, 1H), 7.48 (d, $J = 2.1$ Hz, 1H), 7.34 – 7.24 (m, 1H), 7.20 (d, $J = 1.9$ Hz, 1H), 7.19 (s, 1H), 7.02 – 6.96 (m, 3H), 6.88 (m, 1H), 6.38 (m,

1H), 6.35 (m, 1H). ¹³C NMR (126 MHz, CDCl₃) δ 144.37, 134.65, 130.39, 129.55, 129.03, 128.82, 125.95, 125.00, 124.38, 124.16, 116.69, 113.39, 113.18, 111.34, 110.34.

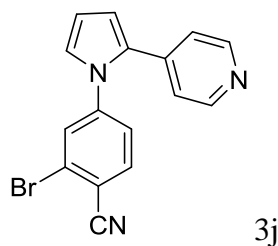
HRMS (ESI) m/z [M+H] for C₁₇H₁₁BrClN₂: 356.9794, found 356.9803.



2-bromo-4-(2-(2-chlorophenyl)-1H-pyrrol-1-yl)benzonitrile (3h): 75% yield, white solid. ¹H NMR (500 MHz, CDCl₃) δ 8.36 – 8.27 (m, 1H), 7.60 (m, 1H), 7.55 – 7.44 (m, 2H), 7.32 (d, *J* = 7.9 Hz, 1H), 7.12 – 7.02 (m, 2H), 6.90 (m, 1H), 6.70 (s, 1H), 6.36 (m, 1H). ¹³C NMR (126 MHz, CDCl₃) δ 150.55, 148.86, 145.31, 136.71, 134.29, 134.04, 129.39, 125.81, 125.48, 124.55, 122.18, 121.39, 116.95, 114.77, 113.18, 111.21. HRMS (ESI) m/z [M+H] for C₁₆H₁₁BrN₃: 324.0136, found 324.0133.

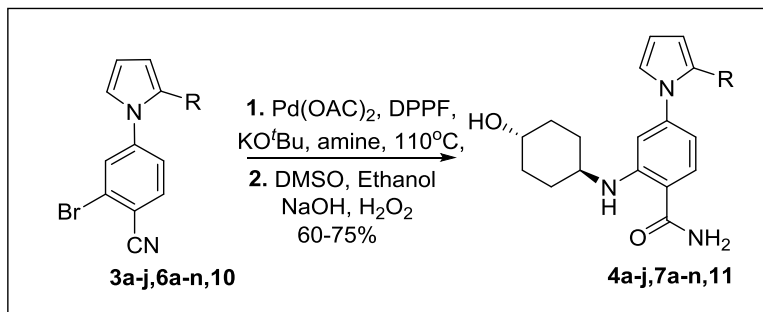


2-bromo-4-(2-(pyridin-3-yl)-1H-pyrrol-1-yl)benzonitrile (3i): 65 % yield, white solid. ¹H NMR (400 MHz, CDCl₃) δ 8.56 – 8.49 (m, 2H), 7.62 (m, 1H), 7.56 (d, *J* = 2.1 Hz, 1H), 7.43 – 7.36 (m, 1H), 7.25 (m, 1H), 7.13 (m, 1H), 7.03 (m, 1H), 6.57 (m, 1H), 6.49 (m, 1H). ¹³C NMR (126 MHz, CDCl₃) δ 148.31, 147.47, 144.00, 135.77, 134.90, 129.90, 129.31, 128.31, 126.23, 125.10, 124.41, 123.43, 116.52, 114.09, 113.93, 111.66. HRMS (ESI) m/z [M+Na] for C₁₆H₁₀BrN₃Na: 345.9956, found 345.9948.



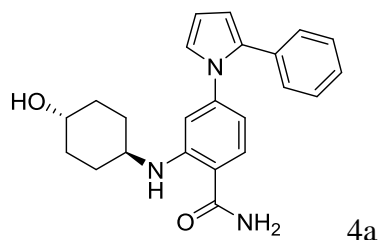
2-bromo-4-(2-(pyridin-4-yl)-1H-pyrrol-1-yl)benzonitrile (3j) : 66% yield, white solid. ^1H NMR (500 MHz, CDCl_3) δ 8.48 – 8.39 (m, 2H), 7.59 – 7.48 (m, 2H), 7.07 (dd, $J = 8.4, 2.1$ Hz, 1H), 6.96 – 6.89 (m, 3H), 6.60 (dd, $J = 3.7, 1.6$ Hz, 1H), 6.39 (dd, $J = 3.7, 2.9$ Hz, 1H). ^{13}C NMR (126 MHz, CDCl_3) δ 149.78, 144.03, 139.35, 134.90, 130.91, 129.25, 126.30, 126.23, 124.52, 122.01, 116.52, 115.22, 114.15, 111.82. HRMS (ESI) m/z $[\text{M}+\text{H}]$ for $\text{C}_{16}\text{H}_{11}\text{BrN}_3$: 324.0136, found 324.0133.

General procedure B: Amination and hydration of Nitrile (for intermediates 4a-j, 7a-n, 11)

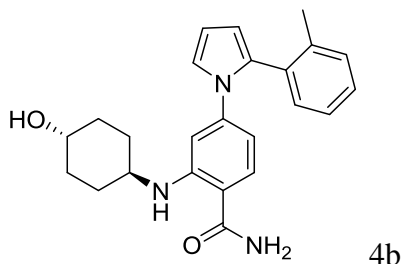


Intermediates **3a-j, 6a-n, 10** (0.07 mmol), *trans*-4-aminocyclohexanol (0.2 mmol), $\text{Pd}(\text{OAc})_2$ (5 mol%), DPPF (10 mol %) and KO^tBu (0.14 mmol) were suspended in toluene (0.4 mL). Argon was purged through the reaction mixture for 15 min. The reaction was then microwaved at 120°C for 20 min, cooled and concentrated. The residue was diluted with water, extracted with 5 mL ethyl acetate thrice. The combined organic fractions were dried over sodium sulfate and concentrated. To this residue was added 5 mL of ethanol and DMSO mixture (4:1), 0.5 mL 1N NaOH solution, 0.5 mL 30% H_2O_2 solution. The reaction was then stirred at room temperature or

at increased temperature (65°C for compounds 15a-c) until the benzonitrile intermediate disappears as observed using TLC. The solvent is evaporated and saturated NH₄Cl solution ~20 ml is added followed by extraction with ethyl acetate (3 x 25 mL). Combined organic layers were washed with brine (2 x 10 mL), dried over sodium sulfate and adsorbed onto silica gel for column chromatography using 50-80% ethyl acetate in hexanes to give the corresponding benzamide product.

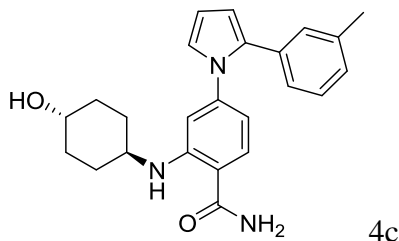


2-(((1r,4r)-4-hydroxycyclohexyl)amino)-4-(2-phenyl-1H-pyrrol-1-yl)benzamide (4a): 51% yield, white solid. ¹H NMR (400 MHz, CDCl₃) δ 7.53 (d, *J* = 8.9 Hz, 1H), 7.32 – 7.21 (m, 1H), 7.19 (m, 2H), 7.01 (m, 1H), 6.68 (d, *J* = 8.2 Hz, 1H), 6.44 (dd, *J* = 4.4, 2.6 Hz, 2H), 6.39 (t, *J* = 3.2 Hz, 1H), 6.12-5.4 (s, 2H) 3.60 (s, 1H), 2.81 (s, 1H), 1.89 (s, 2H), 1.71 (s, 2H), 1.18 (q, *J* = 9.4 Hz, 4H). ¹³C NMR (126 MHz, CDCl₃) δ 169.24, 155.66, 145.77, 144.74, 133.75, 130.22, 128.84, 128.45, 126.99, 123.67, 112.79, 111.11, 99.83, 85.76, 68.99, 33.09, 30.97, 27.88, 14.21. HRMS (ESI) *m/z* [M+Na] for C₂₃H₂₅N₃O₂Na: 398.1844, found 398.1834.

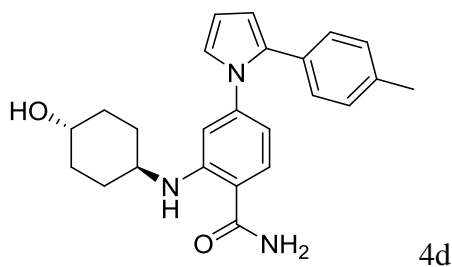


2-(((1r,4r)-4-hydroxycyclohexyl)amino)-4-(2-(o-tolyl)-1H-pyrrol-1-yl)benzamide (4b): 45% yield, white solid. ¹H NMR (400 MHz, CDCl₃) δ 7.35 (d, *J* = 8.5 Hz, 1H), 7.23 – 7.20 (m, 2H), 7.18 – 7.15 (m, 1H), 7.06 (dd, *J* = 2.9, 1.8 Hz, 1H), 6.50 (dd, *J* = 8.5, 2.1 Hz, 1H), 6.40 (m, 1H),

6.31 (dd, $J = 3.5, 1.8$ Hz, 1H), 6.14 (d, $J = 2.0$ Hz, 1H), 5.55 (s, 2H), 3.63 (m, 1H), 2.64 (s, 1H), 2.03 (s, 3H), 1.91 (d, $J = 12.3$ Hz, 2H), 1.66 (d, $J = 12.8$ Hz, 2H), 1.37 – 1.18 (m, 4H). ^{13}C NMR (126 MHz, CDCl_3) δ 171.52, 149.66, 144.66, 137.46, 133.49, 132.76, 130.88, 130.21, 129.54, 127.67, 125.78, 121.83, 112.10, 109.37, 107.82, 69.96, 50.09, 42.69, 33.96, 30.12, 30.08, 20.22. HRMS (ESI) m/z $[\text{M}-\text{H}]$ for $\text{C}_{24}\text{H}_{26}\text{N}_3\text{O}_2$: 388.2025, found 388.2028.

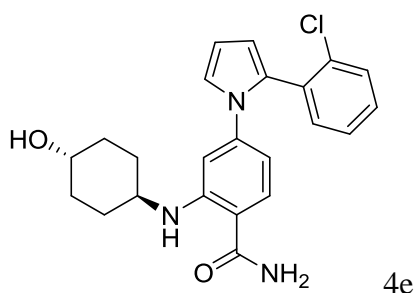


2-(((1r,4r)-4-hydroxycyclohexyl)amino)-4-(2-(m-tolyl)-1H-pyrrol-1-yl)benzamide (4c): 50 % yield, white solid. ^1H NMR (400 MHz, CDCl_3) δ 7.39 (d, $J = 8.5$ Hz, 1H), 7.14 (m, 2H), 7.05 – 6.98 (m, 2H), 6.95 (d, $J = 7.6$ Hz, 1H), 6.52 (d, $J = 8.3$ Hz, 1H), 6.43 (m, 1H), 6.39 (t, $J = 3.2$ Hz, 1H), 6.29 (s, 1H), 5.59 (s, 2H), 3.62 (s, 1H), 2.87 (s, 1H), 2.31 (s, 3H), 1.88 (d, $J = 10.4$ Hz, 2H), 1.71 (d, $J = 10.4$ Hz, 2H), 1.18 (q, $J = 9.9$ Hz, 4H). ^{13}C NMR (126 MHz, CDCl_3) δ 171.59, 149.83, 144.57, 137.85, 133.88, 133.06, 129.51, 129.10, 128.10, 127.27, 125.76, 123.62, 111.38, 110.05, 109.59, 109.43, 69.92, 50.10, 33.84, 30.09, 29.97, 21.51. HRMS (ESI) m/z $[\text{M}+\text{H}]$ for $\text{C}_{24}\text{H}_{28}\text{N}_3\text{O}_2$: 390.2182, found 390.2184.



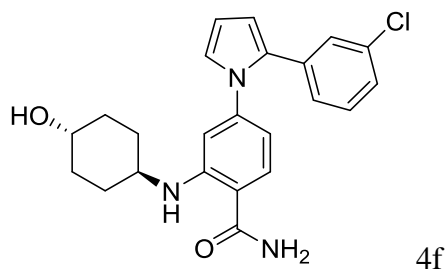
2-(((1r,4r)-4-hydroxycyclohexyl)amino)-4-(2-(p-tolyl)-1H-pyrrol-1-yl)benzamide (4d): 50% yield, white solid. ^1H NMR (400 MHz, CDCl_3) δ 7.92 (s, 1H), 7.38 (d, $J = 8.3$ Hz, 1H), 7.11 (s, 4H), 7.00 (m, 1H), 6.51 (m, 1H), 6.43 – 6.37 (m, 2H), 6.27 (s, 1H), 5.73-5.41 (s, 2H), 3.63 (s, 1H),

2.88 (s, 1H), 2.33 (s, 3H), 1.89 (d, $J = 10.3$ Hz, 2H), 1.70 (d, $J = 11.0$ Hz, 2H), 1.18 (q, $J = 12.3$ Hz, 4H). ^{13}C NMR (126 MHz, CDCl_3) δ 171.52, 149.80, 144.61, 136.22, 133.81, 130.28, 129.51, 128.93, 128.45, 123.42, 111.03, 110.12, 109.53, 109.43, 69.92, 50.09, 42.69, 33.87, 30.12, 21.18. HRMS (ESI) m/z [M-H] for $\text{C}_{24}\text{H}_{26}\text{N}_3\text{O}_2$: 388.2025, found 388.2028.



4-(2-(2-chlorophenyl)-1H-pyrrol-1-yl)-2-(((1r,4r)-4-hydroxycyclohexyl)amino)benzamide

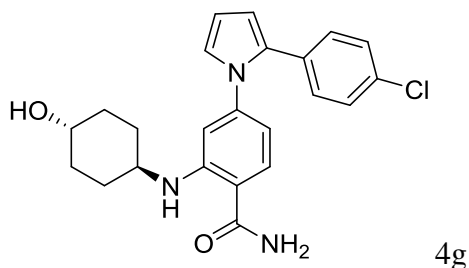
(4e): 55% yield, white solid. ^1H NMR (500 MHz, CDCl_3) δ 8.07 – 8.11 (m, 1H), 7.50 – 7.60 (m, 2H), 7.46 – 7.49 (m, 1H), 7.40 – 7.43 (m, 2H), 7.24 (dd, $J = 2.9, 1.8$ Hz, 1H), 6.67 (dd, $J = 8.4, 2.1$ Hz, 1H), 6.57 – 6.64 (m, 2H), 6.35 (d, $J = 2.1$ Hz, 1H), 5.78 (s, 2H), 3.81 (m, 1H), 2.95 (d, $J = 6.6$ Hz, 1H), 2.05 – 2.13 (m, 2H), 1.81 – 1.91 (m, 2H), 1.32 (m, 4H). ^{13}C NMR (126 MHz, CDCl_3) δ 171.47, 149.73, 144.55, 134.32, 132.78, 132.39, 130.05, 129.76, 129.57, 128.72, 126.64, 122.69, 113.14, 110.17, 109.42, 108.02, 69.92, 50.15, 41.02, 33.94, 30.12. HRMS (ESI) m/z [M-H] for $\text{C}_{23}\text{H}_{23}\text{ClN}_3\text{O}_2$: 408.1479, found 408.1461.



4-(2-(3-chlorophenyl)-1H-pyrrol-1-yl)-2-(((1r,4r)-4-hydroxycyclohexyl)amino)benzamide

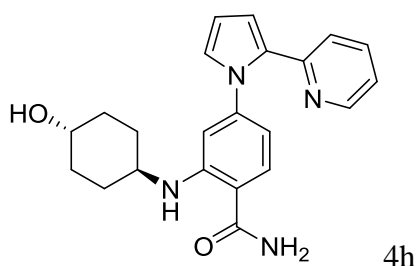
(4f): 59% yield, white solid. ^1H NMR (500 MHz, CDCl_3) δ 7.88 (s, 1H), 7.31 (d, $J = 8.4$ Hz, 1H), 7.12 – 7.08 (m, 2H), 6.95 – 6.91 (m, 2H), 6.42 – 6.36 (m, 2H), 6.30 (dd, $J = 3.6, 2.8$ Hz,

1H), 6.19 (d, $J = 2.0$ Hz, 1H), 5.54 (s, 2H), 3.54 (m, 1H), 2.83 (d, $J = 11.0$ Hz, 1H), 1.84 (m, 2H), 1.66 (m, 2H), 1.17 – 1.06 (m, 4H). ^{13}C NMR (126 MHz, CDCl_3) δ 171.34, 149.77, 144.17, 134.94, 134.10, 132.16, 129.69, 129.42, 128.16, 126.62, 126.42, 124.41, 112.17, 110.28, 109.83, 109.52, 69.84, 50.30, 41.03, 33.78, 30.01. HRMS (ESI) m/z [M-H] for $\text{C}_{23}\text{H}_{23}\text{ClN}_3\text{O}_2$: 408.1479, found 408.1483.



4-(2-(4-chlorophenyl)-1H-pyrrol-1-yl)-2-(((1r,4r)-4-hydroxycyclohexyl)amino)benzamide

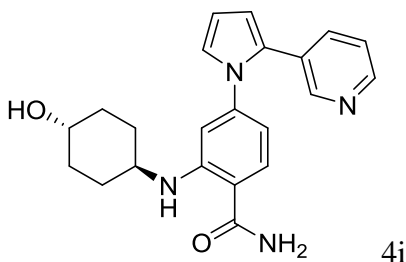
(4g): 55% yield, white solid. ^1H NMR (500 MHz, CDCl_3) δ 7.90 (d, $J = 7.2$ Hz, 1H), 7.37 (d, $J = 8.4$ Hz, 1H), 7.25 – 7.22 (m, 2H), 7.15 – 7.09 (m, 2H), 6.99 (m, 1H), 6.47 – 6.40 (m, 2H), 6.37 (m, 1H), 6.21 (d, $J = 2.0$ Hz, 1H), 3.63 (m, 1H), 2.89 (m, 1H), 1.95 – 1.88 (m, 2H), 1.69 (m, 2H), 1.23 – 1.12 (m, 4H). ^{13}C NMR (126 MHz, CDCl_3) δ 171.35, 149.87, 144.25, 132.42, 131.62, 129.67, 129.64, 128.43, 124.15, 111.69, 110.64, 110.09, 109.76, 109.33, 69.83, 50.15, 41.02, 33.78, 30.09. HRMS (ESI) m/z [M+H] for $\text{C}_{23}\text{H}_{25}\text{ClN}_3\text{O}_2$: 410.1635, found 410.1633.



2-(((1r,4r)-4-hydroxycyclohexyl)amino)-4-(2-(pyridin-2-yl)-1H-pyrrol-1-yl)benzamide (4h):

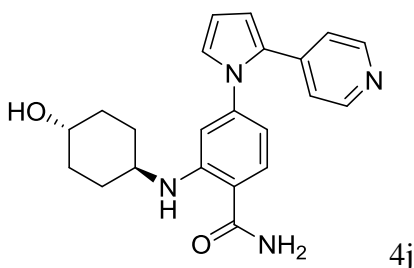
55% yield, white solid. ^1H NMR (500 MHz, CDCl_3) δ 8.55 (d, $J = 4.9$ Hz, 1H), 7.93 (d, $J = 7.3$ Hz, 1H), 7.59 (s, 1H), 7.38 (d, $J = 8.4$ Hz, 1H), 7.12 (m, 2H), 7.06 – 7.01 (m, 1H), 6.49 – 6.39 (m, 2H), 6.33 (d, $J = 1.7$ Hz, 1H), 5.54 (d, $J = 64.2$ Hz, 2H), 3.62 (m, 1H), 3.05 – 2.91 (m, 1H),

1.95 – 1.73 (m, 4H), 1.25 – 1.15 (m, 4H). ^{13}C NMR (126 MHz, CDCl_3) δ 171.42, 171.41, 150.04, 141.86, 129.72, 122.87, 120.96, 120.85, 114.95, 111.00, 110.41, 110.30, 109.19, 109.10, 77.28, 69.81, 60.43, 50.02, 33.68, 30.07. HRMS (ESI) m/z $[\text{M}+\text{H}]$ for $\text{C}_{22}\text{H}_{25}\text{N}_4\text{O}_2$: 377.1978, found 377.1979.



2-(((1r,4r)-4-hydroxycyclohexyl)amino)-4-(2-(pyridin-3-yl)-1H-pyrrol-1-yl)benzamide (4i):

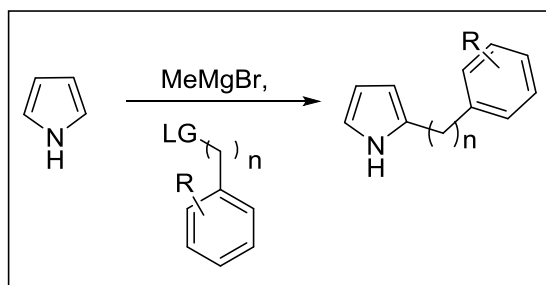
59 % yield, white solid. ^1H NMR (500 MHz, CDCl_3) δ 8.52 – 8.40 (m, 2H), 7.95 (d, $J = 7.3$ Hz, 1H), 7.53 (m, 1H), 7.38 (d, $J = 8.4$ Hz, 1H), 7.24 (dd, $J = 8.0, 4.9$ Hz, 1H), 7.06 (dd, $J = 2.9, 1.7$ Hz, 1H), 6.55 (dd, $J = 3.6, 1.7$ Hz, 1H), 6.45 – 6.38 (m, 2H), 6.32 (d, $J = 2.0$ Hz, 1H), 5.62 (s, 2H), 3.65 (dd, $J = 9.8, 5.6$ Hz, 1H), 2.99 (m, 1H), 1.94 (m, 2H), 1.84 – 1.72 (m, 2H), 1.27 – 1.18 (m, 4H). ^{13}C NMR (126 MHz, CDCl_3) δ 171.26, 150.08, 148.50, 146.78, 144.03, 135.48, 129.81, 129.77, 129.28, 125.07, 123.17, 112.44, 111.20, 110.56, 110.06, 109.11, 69.74, 50.11, 33.69, 29.98. HRMS (ESI) m/z $[\text{M}-\text{H}]$ for $\text{C}_{22}\text{H}_{23}\text{N}_4\text{O}_2$: 375.1821, found 375.1834.



2-(((1r,4r)-4-hydroxycyclohexyl)amino)-4-(2-(pyridin-4-yl)-1H-pyrrol-1-yl)benzamide (4j):

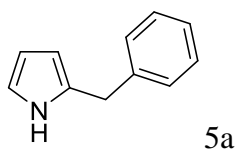
48% yield, white solid. ^1H NMR (500 MHz, CDCl_3) δ 8.45 (s, 2H), 7.98 (d, $J = 7.2$ Hz, 1H), 7.38 (d, $J = 8.4$ Hz, 1H), 7.13 – 7.00 (m, 3H), 6.64 (dd, $J = 3.7, 1.7$ Hz, 1H), 6.44 – 6.36 (m, 2H), 6.32 (d, $J = 2.0$ Hz, 1H), 5.63 (s, 2H), 3.63 (td, $J = 9.6, 4.5$ Hz, 1H), 3.06 – 2.94 (m, 1H), 1.92

(dt, $J = 7.0, 4.3$ Hz, 2H), 1.77 (dt, $J = 10.9, 2.6$ Hz, 2H), 1.27 – 1.17 (m, 4H). ^{13}C NMR (126 MHz, CDCl_3) δ 171.24, 150.11, 149.16, 144.05, 140.58, 130.62, 129.83, 128.72, 126.39, 122.09, 113.74, 111.27, 110.47, 110.32, 109.14, 69.69, 60.42, 50.18, 33.66, 30.02. HRMS (ESI) m/z [M-H] for $\text{C}_{22}\text{H}_{23}\text{N}_4\text{O}_2$: 375.1821, found 375.1823.



General procedure C: Alkylation of pyrrole (preparation of intermediates 5a-n).⁴⁰

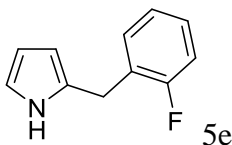
MeMgBr (4.5 mmol, 3N solution in diethyl ether) was added dropwise to a solution of pyrrole (4.47 mmol) in 5mL THF:dichloromethane (1:1) at 0°C followed by quick addition of the corresponding benzyl bromide (to obtain corresponding intermediates)/tosylate **8,12a-c** (4.4 mmol) as solution in 2ml THF. The reaction was left stirring at room temperature overnight after which it was poured in 50mL saturated solution of ammonium chloride and extracted thrice with ethyl acetate. The combined organic extracts were dried over sodium sulfate and adsorbed onto silica for column chromatography which was performed using 15 % ethyl acetate in hexanes as eluent.



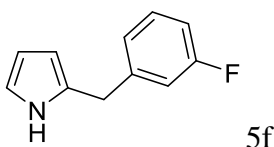
2-benzyl-1H-pyrrole (5a): 49 % yield, colorless oil. ^1H NMR (500 MHz, CDCl_3) δ 7.86 – 7.65 (s, 1H), 7.26 – 7.21 (m, 2H), 7.18 – 7.11 (m, 3H), 6.60 (m, 1H), 6.08 (q, $J = 2.9$ Hz, 1H), 5.93 (m, 1H), 3.92 (s, 2H). ^{13}C NMR (126 MHz, CDCl_3) δ 139.47, 128.69, 128.62, 128.53, 126.43,

116.96, 108.37, 106.46, 34.08. HRMS (ESI) m/z [M+H] for $C_{11}H_{12}N$: 158.0970, found 158.0965.

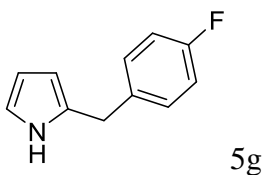
5b-d, h were used as crude for further reaction.



2-(2-fluorobenzyl)-1H-pyrrole (5e): 40% yield, white solid. 1H NMR (500 MHz, $CDCl_3$) δ 7.94 (s, 1H), 7.16 – 7.06 (m, 2H), 7.03 – 6.91 (m, 3H), 6.61 (td, $J = 2.7, 1.5$ Hz, 1H), 6.06 (d, $J = 2.8$ Hz, 1H), 5.97 – 5.90 (m, 1H), 3.96 – 3.90 (m, 2H). ^{13}C NMR (126 MHz, $CDCl_3$) δ 159.86, 130.76, 128.23, 128.16, 124.34, 117.12, 115.42, 115.25, 108.39, 106.48, 27.31. HRMS (ESI) m/z [M+H] for $C_{11}H_{11}N$: 176.0876, found 176.0880.

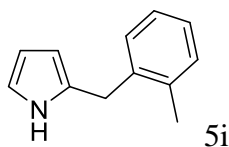


2-(3-fluorobenzyl)-1H-pyrrole (5f): 42% yield, white solid. 1H NMR (500 MHz, $CDCl_3$) δ 7.77 (s, 1H), 7.18 – 7.10 (m, 3H), 6.93 – 6.86 (m, 2H), 6.62 (m, 1H), 6.09 (q, $J = 2.9$ Hz, 1H), 5.81 (d, $J = 2.7$ Hz, 1H), 3.83 (s, 2H). ^{13}C NMR (126 MHz, $CDCl_3$) δ 164.01, 163.98, 142.28, 129.97, 124.17, 124.14, 115.56, 113.38, 108.50, 107.05, 33.88. HRMS (ESI) m/z [M+H] for $C_{11}H_{11}FN$: 176.0876, found 176.0872.

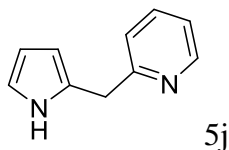


2-(4-fluorobenzyl)-1H-pyrrole (5g): 40% yield, white solid. 1H NMR (500 MHz, $CDCl_3$) δ 7.75 (s, 1H), 7.14 – 7.05 (m, 2H), 6.95 – 6.85 (m, 3H), 6.61 (d, $J = 2.4$ Hz, 1H), 6.08 (q, $J = 2.7$ Hz, 1H), 5.91 (d, $J = 3.1$ Hz, 1H), 3.88 (s, 2H). ^{13}C NMR (126 MHz, $CDCl_3$) δ 162.56, 130.11,

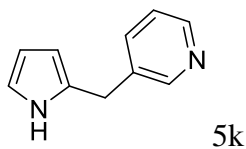
130.04, 129.94, 115.28, 115.02, 108.46, 106.58, 33.28. HRMS (ESI) m/z $[M+H]$ for $C_{11}H_{11}FN$: 176.0876, found 176.0875.



2-(2-methylbenzyl)-1H-pyrrole (5i): 46% yield, white solid. 1H NMR (500 MHz, Chloroform- d) δ 7.35 – 7.31 (m, 1H), 7.08 (m, 3H), 6.98 (m, 1H), 6.78 (dd, $J = 2.9, 1.8$ Hz, 1H), 6.46 – 6.40 (m, 2H), 6.19 (t, $J = 3.2$ Hz, 1H), 5.87 (m, 1H), 3.80 (s, 2H), 2.12 (s, 3H). ^{13}C NMR (126 MHz, $CDCl_3$) δ 136.00, 130.08, 129.49, 128.86, 126.45, 126.13, 121.44, 110.05, 108.71, 69.74, 30.69, 19.44. HRMS (ESI) m/z $[M+Na]$ for $C_{12}H_{13}NNa$: 194.0946, found 194.091.

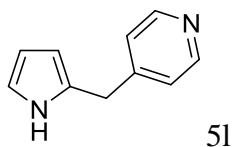


2-((1H-pyrrol-2-yl)methyl)pyridine (5j): 36% yield, white solid. 1H NMR (400 MHz, $CDCl_3$) δ 9.1-8.96(s, 1H), 8.57 (d, $J = 4.9$ Hz, 1H), 7.68 (t, $J = 7.7$ Hz, 1H), 7.27 – 7.18 (m, 2H), 6.75 (m, 1H), 6.14 (d, $J = 2.9$ Hz, 1H), 6.06 (s, 1H), 4.17 (s, 2H). ^{13}C NMR (126 MHz, $CDCl_3$) δ 136.73, 133.11, 132.56, 125.40, 125.12, 121.81, 121.70, 119.91, 109.13, 35.14. HRMS (ESI) m/z $[M+H]$ for $C_{10}H_{11}N_2$: 159.0947, found 159.0922.

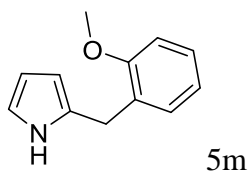


3-((1H-pyrrol-2-yl)methyl)pyridine (5k): 43% yield, white solid. 1H NMR (500 MHz, $CDCl_3$) δ 8.44 – 8.40 (m, 2H), 7.88 (s, 1H), 7.48 – 7.40 (m, 1H), 7.17 (m, 1H), 6.64 (m, 1H), 6.09 (q, $J = 2.9$ Hz, 1H), 5.91 (m, 1H), 3.92 (s, 2H). ^{13}C NMR (126 MHz, $CDCl_3$) δ 149.77, 147.90, 136.32,

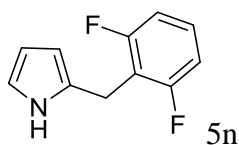
135.09, 129.29, 123.58, 117.50, 108.60, 107.04, 31.33. HRMS (ESI) m/z $[M+H]$ for $C_{10}H_{11}N_2$: 159.0947, found 159.0922.



4-((1H-pyrrol-2-yl)methyl)pyridine (5l): 40% yield, white solid. 1H NMR (500 MHz, $CDCl_3$) δ 8.46 – 8.41 (m, 2H), 7.88 (s, 1H), 7.06 (m, 2H), 6.66 (m, 1H), 6.10 (q, $J = 2.9$ Hz, 1H), 5.95 (m, 1H), 3.92 (s, 2H). ^{13}C NMR (126 MHz, $CDCl_3$) δ 149.80, 149.79, 148.91, 123.93, 117.64, 108.68, 107.46, 33.49. HRMS (ESI) m/z $[M+H]$ for $C_{10}H_{11}N_2$: 159.0947, found 159.0936.

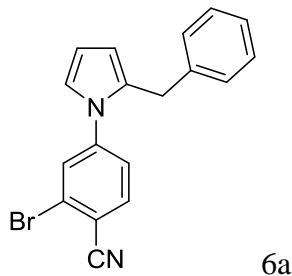


2-(2-methoxybenzyl)-1H-pyrrole (5m): 42 % yield, white solid. 1H NMR (500 MHz, $CDCl_3$) δ 8.21 (s, 1H), 7.22 – 7.08 (m, 2H), 6.93 – 6.81 (m, 2H), 6.65 (m, 1H), 6.14 – 6.06 (m, 1H), 5.99 (t, $J = 3.0$ Hz, 1H), 3.91 (s, 2H), 3.85 (s, 3H). ^{13}C NMR (126 MHz, $CDCl_3$) δ 157.02, 130.27, 129.76, 128.89, 127.68, 120.99, 116.57, 110.61, 107.99, 105.60, 55.46, 28.83. HRMS (ESI) m/z $[M+H]$ for $C_{12}H_{14}NO$: 188.1075, found 188.1074.

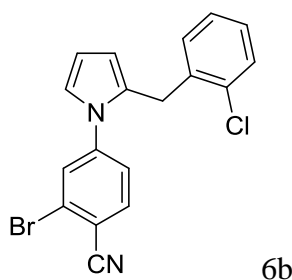


2-(2,6-difluorobenzyl)-1H-pyrrole (5n): 43% yield, white solid. 1H NMR (500 MHz, $CDCl_3$) δ 7.95 (s, 1H), 7.19 – 7.08 (m, 2H), 6.94 – 6.79 (m, 3H), 6.55 (t, $J = 2.8$ Hz, 1H), 5.95 (t, $J = 3.0$ Hz, 1H), 4.08 (d, $J = 1.5$ Hz, 2H). ^{13}C NMR (126 MHz, $CDCl_3$) δ 169.72, 135.78, 132.40, 129.34, 121.32, 116.21, 111.30, 110.99, 33.06. HRMS (ESI) m/z $[M+H]$ for $C_{11}H_{10}F_2N$: 194.0781, found 194.0785.

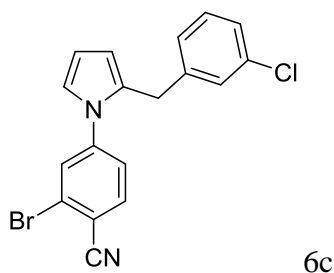
Intermediates **6a-n, 10** have been synthesized using **general procedure A**.



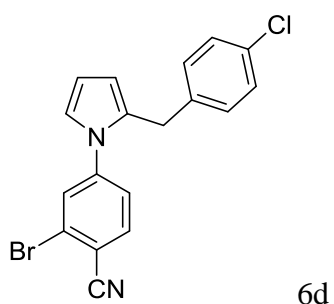
4-(2-benzyl-1H-pyrrol-1-yl)-2-bromobenzonitrile (6a): 81% yield, white solid. ^1H NMR (400 MHz, CDCl_3) δ 7.65 (dd, $J = 8.3, 1.6$ Hz, 1H), 7.52 (t, $J = 1.8$ Hz, 1H), 7.34 – 7.15 (m, 4H), 7.12 – 6.99 (m, 2H), 6.80 (m, 1H), 6.32 (t, $J = 3.2$ Hz, 1H), 6.16 (dd, $J = 3.5, 1.8$ Hz, 1H), 3.96 (s, 2H). ^{13}C NMR (126 MHz, CDCl_3) δ 149.06, 135.23, 128.86, 126.67, 126.35, 125.04, 122.75, 117.96, 112.33, 110.91, 109.13, 103.84, 102.96, 99.40, 98.31, 20.88. HRMS (ESI) m/z $[\text{M}+\text{H}]$ for $\text{C}_{29}\text{H}_{25}\text{BrN}_3$: 337.0340, found 337.0336.



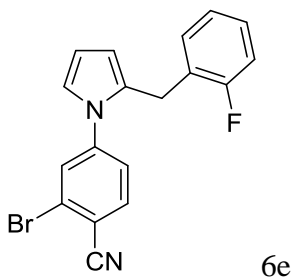
2-bromo-4-(2-(2-chlorobenzyl)-1H-pyrrol-1-yl)benzonitrile (6b): 71% yield, white solid. ^1H NMR (500 MHz, Chloroform- d) δ 7.58 (d, $J = 8.3$ Hz, 1H), 7.46 (d, $J = 2.0$ Hz, 1H), 7.28 – 7.24 (m, 2H), 7.09 (dd, $J = 5.8, 3.5$ Hz, 2H), 6.89 (s, 1H), 6.73 (dd, $J = 3.0, 1.8$ Hz, 1H), 6.23 (t, $J = 3.2$ Hz, 1H), 5.99 (m, 1H), 3.96 (s, 2H). ^{13}C NMR (126 MHz, CDCl_3) δ 141.62, 138.52, 135.63, 134.79, 130.22, 129.72, 129.53, 128.04, 127.00, 126.27, 124.26, 115.03, 110.25, 103.91, 103.01, 98.95, 89.06, 29.71. HRMS (ESI) m/z $[\text{M}+\text{H}]$ for $\text{C}_{18}\text{H}_{13}\text{BrClN}_2$: 370.9951, found 370.9966.



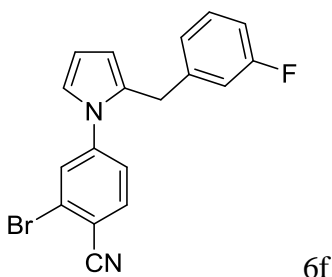
2-bromo-4-(2-(3-chlorobenzyl)-1H-pyrrol-1-yl)benzonitrile (6c): 76 % yield, beige solid. ^1H NMR (500 MHz, CDCl_3) δ 7.58 (d, $J = 8.3$ Hz, 1H), 7.42 (d, $J = 2.1$ Hz, 1H), 7.15 (dd, $J = 8.3$, 2.1 Hz, 1H), 7.12 – 7.08 (m, 2H), 6.95 (m, 1H), 6.87 – 6.81 (m, 1H), 6.71 (dd, $J = 3.0$, 1.7 Hz, 1H), 6.23 (t, $J = 3.2$ Hz, 1H), 6.08 (m, 1H), 3.84 (s, 2H). ^{13}C NMR (126 MHz, CDCl_3) δ 144.40, 140.97, 137.99, 134.73, 132.84, 130.04, 129.78, 128.61, 128.51, 126.76, 126.52, 124.55, 122.07, 116.65, 111.93, 110.19, 100.38, 32.81. HRMS (ESI) m/z $[\text{M}+\text{Na}]$ for $\text{C}_{18}\text{H}_{12}\text{BrClN}_2\text{Na}$: 392.9770, found 392.9771.



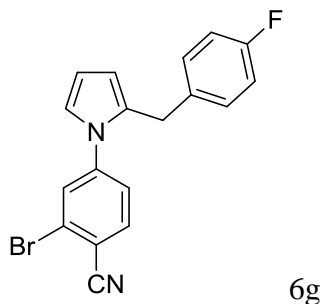
2-bromo-4-(2-(4-chlorobenzyl)-1H-pyrrol-1-yl)benzonitrile (6d): 70 % yield, beige solid. ^1H NMR (500 MHz, CDCl_3) δ 7.58 (d, $J = 8.3$ Hz, 1H), 7.43 (d, $J = 2.0$ Hz, 1H), 7.18 – 7.12 (m, 3H), 6.92 – 6.89 (m, 2H), 6.71 (dd, $J = 3.0$, 1.7 Hz, 1H), 6.22 (t, $J = 3.2$ Hz, 1H), 6.04 (ddt, $J = 3.4$, 1.6, 0.8 Hz, 1H), 3.83 (s, 2H). ^{13}C NMR (126 MHz, CDCl_3) δ 144.43, 137.38, 134.75, 132.33, 131.33, 129.95, 129.68, 128.68, 125.84, 124.48, 122.02, 116.66, 113.89, 111.80, 110.16, 32.56. HRMS (ESI) m/z $[\text{M}+\text{H}]$ for $\text{C}_{18}\text{H}_{13}\text{BrClN}_2$: 370.9951, found 370.9946.



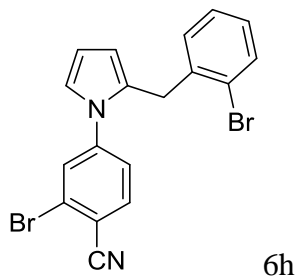
2-bromo-4-(2-(2-fluorobenzyl)-1H-pyrrol-1-yl)benzonitrile (6e): 81 % yield, beige solid. ^1H NMR (500 MHz, CDCl_3) δ 7.59 (d, $J = 8.3$ Hz, 1H), 7.47 (d, $J = 2.0$ Hz, 1H), 7.21 (dd, $J = 8.3$, 2.1 Hz, 1H), 7.15 – 7.07 (m, 1H), 6.97 – 6.86 (m, 3H), 6.71 (dd, $J = 3.0$, 1.8 Hz, 1H), 6.21 (t, $J = 3.2$ Hz, 1H), 6.03 (m, 1H), 3.88 (s, 2H). ^{13}C NMR (126 MHz, CDCl_3) δ 161.37, 144.46, 134.76, 130.60, 130.43, 129.91, 128.41, 125.86, 124.46, 124.13, 121.92, 116.73, 115.39, 113.87, 111.68, 110.13, 25.87, 25.84. HRMS (ESI) m/z $[\text{M}+\text{H}]$ for $\text{C}_{18}\text{H}_{13}\text{BrFN}_2$: 355.0246, found 355.0202.



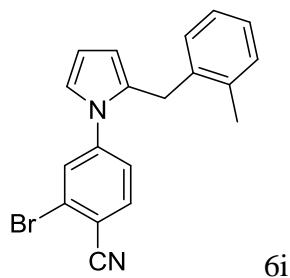
2-bromo-4-(2-(3-fluorobenzyl)-1H-pyrrol-1-yl)benzonitrile (6f): 75% yield, beige solid. ^1H NMR (500 MHz, CDCl_3) δ 7.57 (d, $J = 8.4$ Hz, 1H), 7.42 (d, $J = 2.0$ Hz, 1H), 7.18 – 7.10 (m, 2H), 6.82 (m, 3H), 6.74 – 6.69 (m, 1H), 6.24 (t, $J = 3.2$ Hz, 1H), 6.08 (m, 1H), 3.87 (s, 2H). ^{13}C NMR (126 MHz, CDCl_3) δ 163.97, 144.42, 134.73, 129.96, 125.82, 124.47, 123.95, 122.04, 116.66, 115.33, 115.16, 113.88, 113.58, 113.42, 111.96, 110.19, 109.02, 32.83. HRMS (ESI) m/z $[\text{M}+\text{Na}]$ for $\text{C}_{18}\text{H}_{12}\text{BrFN}_2\text{Na}$: 377.0066, found 377.0114.



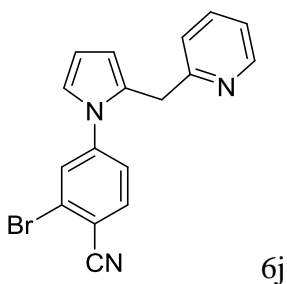
2-bromo-4-(2-(4-fluorobenzyl)-1H-pyrrol-1-yl)benzonitrile (6g): 71% yield, white solid. ^1H NMR (500 MHz, CDCl_3) δ 7.57 (d, $J = 8.3$ Hz, 1H), 7.43 (d, $J = 2.0$ Hz, 1H), 7.16 (dd, $J = 8.3$, 2.0 Hz, 1H), 6.95 – 6.83 (m, 4H), 6.71 (dd, $J = 3.0$, 1.8 Hz, 1H), 6.22 (t, $J = 3.2$ Hz, 1H), 6.04 (ddt, $J = 3.4$, 1.7, 0.8 Hz, 1H), 3.83 (s, 2H). ^{13}C NMR (126 MHz, CDCl_3) δ 162.49, 144.50, 134.72, 134.52, 131.75, 129.94, 129.81, 125.80, 124.47, 121.96, 116.68, 115.29, 113.82, 111.70, 110.12, 32.41. HRMS (ESI) m/z $[\text{M}+\text{H}]$ for $\text{C}_{18}\text{H}_{13}\text{BrFN}_2$: 355.0246, found 355.0202.



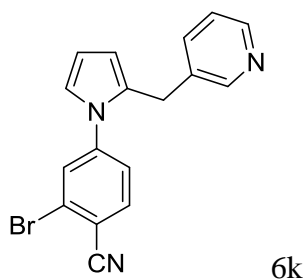
2-bromo-4-(2-(2-bromobenzyl)-1H-pyrrol-1-yl)benzonitrile (6h): 72 % yield, white solid. ^1H NMR (500 MHz, CDCl_3) δ 7.58 (d, $J = 8.3$ Hz, 1H), 7.48 – 7.45 (m, 1H), 7.40 – 7.37 (m, 1H), 7.16 – 7.07 (m, 2H), 7.03 – 6.96 (m, 2H), 6.74 (dd, $J = 3.0$, 1.7 Hz, 1H), 6.23 (t, $J = 3.2$ Hz, 1H), 5.98 (m, 1H), 3.96 (s, 2H). ^{13}C NMR (126 MHz, CDCl_3) δ 144.43, 138.37, 135.97, 134.81, 132.86, 130.30, 129.70, 128.29, 127.56, 124.23, 121.86, 121.34, 121.13, 115.78, 115.60, 112.02, 110.28, 33.38. HRMS (ESI) m/z $[\text{M}+\text{Na}]$ for $\text{C}_{18}\text{H}_{12}\text{Br}_2\text{N}_2\text{Na}$: 436.9228, found 436.9265.



2-bromo-4-(2-(2-methylbenzyl)-1H-pyrrol-1-yl)benzonitrile (6i): 76% yield, red oil. ^1H NMR (400 MHz, CDCl_3) δ 7.69 – 7.66 (m, 1H), 7.57 (q, $J = 4.4, 3.2$ Hz, 1H), 7.17 – 7.11 (m, 4H), 6.99 (d, $J = 7.1$ Hz, 1H), 6.85 – 6.77 (m, 1H), 6.31 (t, $J = 3.6$ Hz, 1H), 5.99 (s, 1H), 3.89 (s, 2H), 2.19 (d, $J = 2.4$ Hz, 3H). ^{13}C NMR (126 MHz, CDCl_3) δ 144.63, 137.17, 135.87, 134.75, 131.48, 130.30, 129.57, 128.86, 126.72, 126.15, 124.15, 121.55, 116.75, 115.60, 113.61, 111.74, 110.26, 30.80, 19.43. HRMS (ESI) m/z $[\text{M}+\text{H}]$ for $\text{C}_{19}\text{H}_{16}\text{BrN}_2$: 351.0483, found 351.0497.

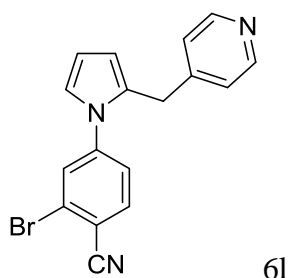


2-bromo-4-(2-(pyridin-2-ylmethyl)-1H-pyrrol-1-yl)benzonitrile (6j): 72% yield, white solid. ^1H NMR (500 MHz, CDCl_3) δ 8.41 (m, 1H), 7.57 (d, $J = 8.3$ Hz, 1H), 7.27 (dd, $J = 8.3, 2.1$ Hz, 2H), 7.06 (m, 1H), 7.01 – 6.96 (m, 1H), 6.72 (dd, $J = 3.0, 1.7$ Hz, 1H), 6.24 (t, $J = 3.2$ Hz, 1H), 6.08 (m, 1H), 4.08 (d, $J = 1.0$ Hz, 2H). ^{13}C NMR (126 MHz, CDCl_3) δ 158.92, 149.27, 144.43, 136.79, 134.74, 130.46, 130.02, 125.79, 124.56, 122.88, 121.95, 121.69, 116.73, 113.77, 111.79, 110.37, 35.77. HRMS (ESI) m/z $[\text{M}+\text{H}]$ for $\text{C}_{17}\text{H}_{13}\text{BrN}_3$: 338.0293, found 338.0300.



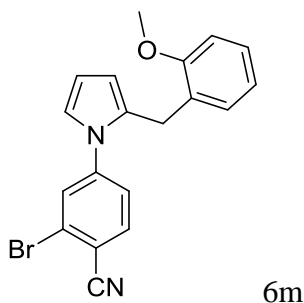
2-bromo-4-(2-(pyridin-3-ylmethyl)-1H-pyrrol-1-yl)benzonitrile (6k): 74% yield, white solid.

^1H NMR (500 MHz, CDCl_3) δ 8.30 (d, $J = 55.8$ Hz, 2H), 7.92 (d, $J = 7.5$ Hz, 1H), 7.39 – 7.27 (m, 2H), 6.74 (dd, $J = 2.9, 1.8$ Hz, 1H), 6.37 (d, $J = 2.0$ Hz, 1H), 6.28 (dd, $J = 8.3, 2.0$ Hz, 1H), 6.19 (dd, $J = 3.5, 2.9$ Hz, 1H), 5.99 (m, 1H), 3.88 (s, 2H). ^{13}C NMR (126 MHz, CDCl_3) δ 150.16, 149.80, 147.54, 144.36, 136.11, 135.33, 130.44, 129.50, 126.01, 123.35, 122.20, 111.70, 111.54, 109.89, 109.12, 108.54, 30.41. HRMS (ESI) m/z $[\text{M}+\text{H}]$ for $\text{C}_{17}\text{H}_{13}\text{BrN}_3$: 338.0293, found 338.0319.



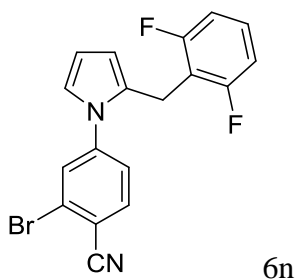
2-bromo-4-(2-(pyridin-4-ylmethyl)-1H-pyrrol-1-yl)benzonitrile (6l): 70 % yield, white solid.

^1H NMR (500 MHz, CDCl_3) δ 8.43 – 8.39 (m, 2H), 7.58 (d, $J = 8.3$ Hz, 1H), 7.43 (d, $J = 2.0$ Hz, 1H), 7.14 (dd, $J = 8.3, 2.1$ Hz, 1H), 6.93 (m, 2H), 6.74 (dd, $J = 3.0, 1.7$ Hz, 1H), 6.25 (t, $J = 3.3$ Hz, 1H), 6.10 (m, 1H), 3.88 (s, 2H). ^{13}C NMR (126 MHz, CDCl_3) δ 150.31, 149.77, 148.35, 144.19, 134.88, 129.92, 129.48, 126.00, 124.46, 123.66, 122.39, 122.36, 116.54, 114.15, 112.29, 110.34, 32.55. HRMS (ESI) m/z $[\text{M}+\text{H}]$ for $\text{C}_{17}\text{H}_{13}\text{BrN}_3$: 338.0293, found 338.0319. HRMS (ESI) m/z $[\text{M}+\text{H}]$ for $\text{C}_{17}\text{H}_{13}\text{BrN}_3$: 338.0293, found 338.0306.



2-bromo-4-(2-(2-methoxybenzyl)-1H-pyrrol-1-yl)benzonitrile (6m): 93% yield, white solid.

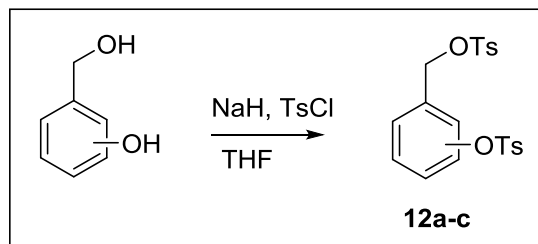
^1H NMR (400 MHz, CDCl_3) δ 7.64 (dd, $J = 8.3, 1.0$ Hz, 1H), 7.59 (d, $J = 2.1$ Hz, 1H), 7.23 – 7.17 (m, 1H), 6.98 (dd, $J = 7.5, 1.8$ Hz, 1H), 6.89 – 6.81 (m, 3H), 6.80 (dd, $J = 3.1, 1.8$ Hz, 1H), 6.31 (t, $J = 3.2$ Hz, 1H), 6.14 – 6.10 (m, 1H), 3.94 (s, 2H), 3.79 (s, 3H). ^{13}C NMR (126 MHz, CDCl_3) δ 156.58, 144.74, 134.59, 131.89, 129.72, 129.59, 127.75, 127.41, 125.62, 124.28, 121.40, 120.50, 116.88, 113.34, 111.56, 110.15, 110.12, 55.31, 26.47. HRMS (ESI) m/z [M+H] for $\text{C}_{19}\text{H}_{16}\text{BrN}_2\text{O}$: 367.0446, found 367.0455.



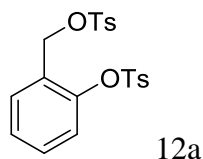
2-bromo-4-(2-(2,6-difluorobenzyl)-1H-pyrrol-1-yl)benzonitrile (6n): 83% yield, white solid.

^1H NMR (500 MHz, CDCl_3) δ 7.77 (dd, $J = 8.2, 2.1$ Hz, 1H), 7.71 (d, $J = 2.0$ Hz, 1H), 7.45 (dd, $J = 8.3, 2.0$ Hz, 1H), 7.23 – 7.16 (m, 2H), 6.89 – 6.84 (m, 2H), 6.75 (dd, $J = 2.9, 1.8$ Hz, 1H), 6.24 (t, $J = 3.2$ Hz, 1H), 5.96 (m, 1H), 3.99 – 3.92 (m, 2H). ^{13}C NMR (126 MHz, CDCl_3) δ 162.18, 144.50, 134.87, 130.30, 128.46, 125.97, 124.95, 121.86, 116.77, 114.13, 111.36, 111.16, 110.52, 110.06, 108.17, 20.20, 20.17. HRMS (ESI) m/z [M+Na] for $\text{C}_{18}\text{H}_{11}\text{BrF}_2\text{N}_2\text{Na}$: 394.9976, found 394.9971.

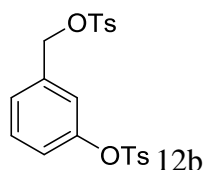
Tosyl protection of benzyl alcohols. General procedure D (preparation of 12a-c):



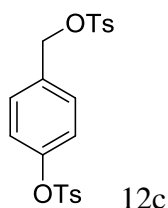
Benzyl alcohol (16.1 mmol) was dissolved in 50 mL THF, the solution was cooled to 0°C and sodium hydride (37 mmol) was added slowly while stirring. The reaction was stirred at 0°C for 20 minutes followed by addition of tosyl chloride (35.42 mmol) as a solution in 20 ml THF. After stirring the reaction overnight at room temperature 50ml water and 50 ml ethyl acetate were added. The organic layer was washed with brine and dried over sodium sulfate. A quick column chromatography was performed using 20% ethyl acetate in hexanes as eluent.



2-(tosyloxy)benzyl 4-methylbenzenesulfonate (12a): 92 % yield, pale yellow oil. ¹H NMR (500 MHz, CDCl₃) δ 7.81 – 7.76 (m, 2H), 7.71 – 7.67 (m, 2H), 7.38 – 7.33 (m, 5H), 7.30 (dd, J = 7.6, 1.9 Hz, 1H), 7.25 (td, J = 7.5, 1.5 Hz, 1H), 7.06 (dd, J = 8.0, 1.4 Hz, 1H), 4.91 (s, 2H), 2.48 (d, J = 5.1 Hz, 6H). ¹³C NMR (126 MHz, CDCl₃) δ 147.17, 145.94, 144.95, 132.81, 132.08, 130.28, 130.13, 130.00, 129.89, 128.42, 127.99, 127.33, 127.31, 122.59, 66.04, 21.80, 21.70. HRMS (ESI) m/z [M+H] for C₂₀H₁₉O₆S₂: 419.0623, found 419.0605.

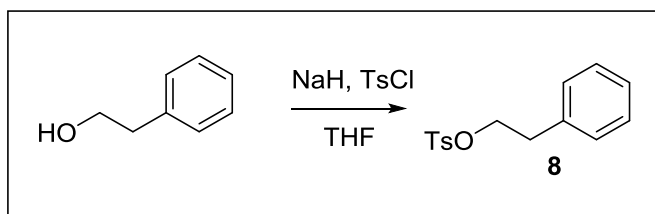


3-(tosyloxy)benzyl 4-methylbenzenesulfonate (12b): 80 % yield, pale yellow oil. ^1H NMR (500 MHz, CDCl_3) δ 7.81 – 7.77 (m, 2H), 7.72 – 7.68 (m, 2H), 7.39 – 7.32 (m, 5H), 7.26 (d, $J = 8.0$ Hz, 1H), 7.19 – 7.15 (m, 1H), 6.96 (m, 1H), 6.89 (t, $J = 2.0$ Hz, 1H), 4.97 (s, 2H), 2.48 (d, $J = 2.4$ Hz, 7H). ^{13}C NMR (126 MHz, CDCl_3) δ 149.62, 145.69, 145.12, 135.35, 132.88, 132.08, 129.96, 129.91, 129.86, 128.48, 127.95, 126.89, 122.94, 122.32, 70.53, 21.77, 21.70. HRMS (ESI) m/z $[\text{M}+\text{H}]$ for $\text{C}_{20}\text{H}_{19}\text{O}_6\text{S}_2$: 419.0623, found 419.0620.



4-(tosyloxy)benzyl 4-methylbenzenesulfonate (12c): 94 % yield, pale yellow oil. ^1H NMR (500 MHz, CDCl_3) δ 7.72 – 7.69 (m, 2H), 7.63 – 7.59 (m, 2H), 7.29 – 7.22 (m, 4H), 7.13 – 7.09 (m, 2H), 6.88 – 6.85 (m, 2H), 4.93 (s, 2H), 2.38 (s, $J = 3.9, 1.1$ Hz, 6H). ^{13}C NMR (126 MHz, CDCl_3) δ 149.91, 145.57, 145.09, 132.98, 132.34, 132.17, 129.92, 129.85, 129.78, 128.49, 127.94, 122.68, 70.73, 21.76, 21.69. HRMS (ESI) m/z $[\text{M}+\text{H}]$ for $\text{C}_{20}\text{H}_{19}\text{O}_6\text{S}_2$: 419.0623, found 419.0620.

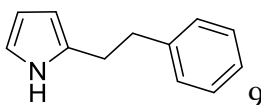
Tosyl protection of phenylethyl alcohol.



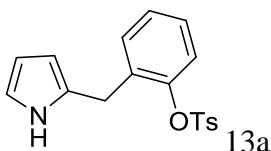
phenethyl 4-methylbenzenesulfonate (8): phenyl ethyl alcohol (16.1 mmol) was dissolved in 50 mL THF, the solution was cooled to 0°C and sodium hydride (16.1 mmol) was added slowly while stirring. The reaction was stirred at 0°C for 20 minutes followed by addition of tosyl

chloride (17 mmol) as a solution in 20 ml THF. After stirring the reaction overnight at room temperature 50ml water and 50 ml ethyl acetate were added. The organic layer was washed with brine and dried over sodium sulfate. A quick column chromatography was performed using 20% ethyl acetate in hexanes as eluent. 4 g, yellow solid, 90% yield. ^1H NMR (500 MHz, CDCl_3) δ 7.74 – 7.68 (m, 2H), 7.32 – 7.22 (m, 7H), 7.17 – 7.10 (m, 2H), 4.23 (t, $J = 7.1$ Hz, 2H), 2.98 (t, $J = 7.1$ Hz, 2H), 2.46 (s, 3H). ^{13}C NMR (126 MHz, CDCl_3) δ 144.65, 136.19, 132.93, 129.78, 128.91, 128.60, 127.84, 126.88, 70.61, 35.35, 21.65. HRMS (ESI) m/z $[\text{M}+\text{Na}]$ for $\text{C}_{15}\text{H}_{16}\text{O}_3\text{SNa}$: 299.0718, found 299.0730.

Intermediates 9, 13a-c have been synthesized using general procedure C

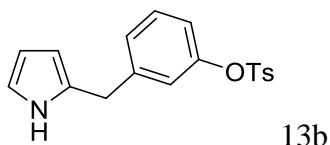


2-phenethyl-1H-pyrrole (9): 42% yield, colorless oil. ^1H NMR (500 MHz, CDCl_3) δ 7.78 (s, 1H), 7.35 – 7.16 (m, 5H), 6.69 – 6.62 (m, 1H), 6.15 (p, $J = 3.1$ Hz, 1H), 5.98 (m, 1H), 3.00 – 2.82 (m, 5H). ^{13}C NMR (126 MHz, CDCl_3) δ 141.60, 128.51, 128.47, 128.44, 128.42, 128.28, 126.12, 116.26, 108.23, 105.26, 36.15, 29.62. HRMS (ESI) m/z $[\text{M}+\text{Na}]$ for $\text{C}_{12}\text{H}_{13}\text{NNa}$: 194.0946, found 194.0941.

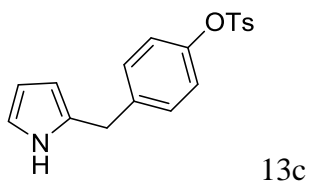


2-((1H-pyrrol-2-yl)methyl)phenyl 4-methylbenzenesulfonate (13a): 24% yield, white solid. ^1H NMR (500 MHz, CDCl_3) δ 8.36 (s, 1H), 7.82 – 7.78 (m, 2H), 7.38 – 7.35 (m, 2H), 7.20 – 7.14 (m, 2H), 7.12 – 7.08 (m, 2H), 6.89 (dd, $J = 8.0, 1.3$ Hz, 1H), 6.67 (m, 1H), 6.11 (q, $J = 2.9$ Hz, 1H), 6.02 (m, 1H), 3.89 (s, 2H), 2.48 (s, 3H). ^{13}C NMR (126 MHz, CDCl_3) δ 147.15, 145.72,

133.86, 132.78, 131.28, 129.98, 128.50, 127.89, 127.50, 127.48, 122.21, 117.49, 107.92, 106.92, 27.70, 21.79. HRMS (ESI) m/z [M+H] for $C_{25}H_{20}BrN_2O_3S$: 507.0378, found 507.0385.

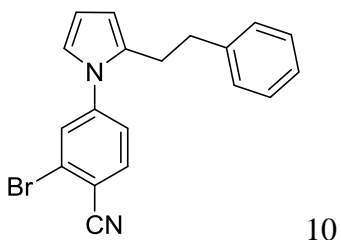


3-((1H-pyrrol-2-yl)methyl)phenyl 4-methylbenzenesulfonate (13b): 27 % yield, white solid. 1H NMR (500 MHz, $CDCl_3$) δ 7.71 – 7.57 (m, 3H), 7.24 – 7.20 (m, 2H), 7.14 (t, $J = 7.9$ Hz, 1H), 7.01 (m, 1H), 6.81 – 6.77 (m, 1H), 6.74 (dd, $J = 2.4, 1.4$ Hz, 1H), 6.59 (m, 1H), 6.05 (q, $J = 2.9$ Hz, 1H), 5.80 (m, 1H), 3.83 (s, 2H), 2.38 (s, 3H). ^{13}C NMR (126 MHz, $CDCl_3$) δ 149.79, 145.31, 141.64, 132.39, 129.76, 129.74, 129.69, 128.50, 127.36, 122.55, 120.38, 117.24, 108.46, 106.80, 33.70, 21.76. HRMS (ESI) m/z [M+H] for $C_{25}H_{20}BrN_2O_3S$: 507.0378, found 507.0362.

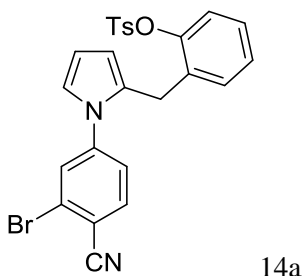


4-((1H-pyrrol-2-yl)methyl)phenyl 4-methylbenzenesulfonate (13c): 25% yield, white solid. 1H NMR (500 MHz, $CDCl_3$) δ 7.75 (s, 1H), 7.64 (m, 2H), 7.27 – 7.21 (m, 2H), 7.05 – 7.01 (m, 2H), 6.85 – 6.82 (m, 2H), 6.62 (m, 1H), 6.07 (q, $J = 2.9$ Hz, 1H), 5.88 (m, 1H), 3.87 (s, 2H), 2.38 (s, 3H). ^{13}C NMR (126 MHz, $CDCl_3$) δ 148.14, 145.32, 138.59, 132.47, 129.76, 129.73, 128.53, 128.50, 128.04, 122.49, 122.46, 117.26, 108.46, 106.83, 33.42, 21.75.

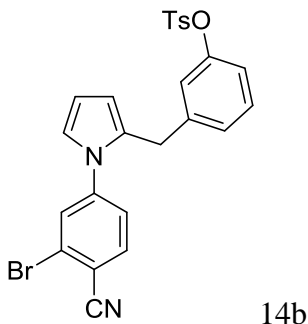
HRMS (ESI) m/z [M+H] for $C_{25}H_{20}BrN_2O_3S$: 507.0378, found 507.0362.



2-bromo-4-(2-phenethyl-1H-pyrrol-1-yl)benzotrile (10): 80 % yield, white solid. ^1H NMR (500 MHz, CDCl_3) δ 7.69 (d, $J = 8.3$ Hz, 1H), 7.50 (d, $J = 2.0$ Hz, 1H), 7.28 – 7.21 (m, 4H), 7.09 – 7.03 (m, 2H), 6.72 (dd, $J = 3.0, 1.7$ Hz, 1H), 6.31 (t, $J = 3.2$ Hz, 1H), 6.22 (m, 1H), 2.94 – 2.82 (m, 4H). ^{13}C NMR (126 MHz, CDCl_3) δ 144.63, 140.85, 134.72, 133.04, 129.83, 128.44, 128.33, 126.27, 125.92, 124.52, 121.33, 116.78, 113.64, 110.08, 109.48, 36.00, 28.88. HRMS (ESI) m/z [M+H] for $\text{C}_{19}\text{H}_{16}\text{BrN}_2$: 351.0497, found 351.0498.

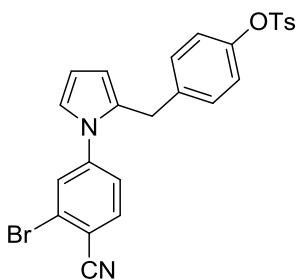


2-((1-(3-bromo-4-cyanophenyl)-1H-pyrrol-2-yl)methyl)phenyl 4-methylbenzenesulfonate (14a): 81% yield, white solid. ^1H NMR (500 MHz, CDCl_3) δ 7.64 – 7.58 (m, 2H), 7.54 (d, $J = 8.3$ Hz, 1H), 7.36 (d, $J = 2.0$ Hz, 1H), 7.28 – 7.21 (m, 2H), 7.13 (dd, $J = 8.3, 2.1$ Hz, 1H), 7.09 – 7.02 (m, 2H), 6.96 – 6.90 (m, 1H), 6.82 – 6.78 (m, 1H), 6.69 (dd, $J = 3.0, 1.7$ Hz, 1H), 6.20 (t, $J = 3.2$ Hz, 1H), 5.95 (m, 1H), 3.78 (s, 2H), 2.40 (s, 3H). ^{13}C NMR (126 MHz, CDCl_3) δ 147.41, 145.55, 144.30, 134.79, 132.90, 132.74, 130.49, 130.35, 129.88, 129.73, 128.33, 127.85, 127.19, 125.80, 124.37, 122.22, 121.89, 116.75, 113.75, 112.00, 110.16, 27.18, 21.79. HRMS (ESI) m/z [M+H] for $\text{C}_{25}\text{H}_{20}\text{BrN}_2\text{O}_3\text{S}$: 507.0372, found 507.0378.



3-((1-(3-bromo-4-cyanophenyl)-1H-pyrrol-2-yl)methyl)phenyl 4-methylbenzenesulfonate

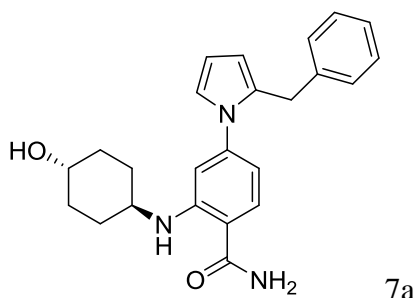
(14b): 82% yield, white solid. ^1H NMR (500 MHz, CDCl_3) δ 7.68 – 7.62 (m, 4H), 7.43 (d, J = 2.1 Hz, 1H), 7.31 – 7.26 (m, 3H), 7.20 (dd, J = 8.3, 2.0 Hz, 1H), 7.14 (t, J = 7.9 Hz, 1H), 6.92 (m, 1H), 6.78 – 6.76 (m, 1H), 6.28 (t, J = 3.2 Hz, 1H), 6.03 (m, 1H), 3.88 (d, J = 1.0 Hz, 2H), 2.43 (s, 3H). ^{13}C NMR (126 MHz, CDCl_3) δ 149.81, 145.30, 144.32, 141.14, 134.77, 129.88, 129.75, 129.58, 128.55, 128.51, 128.47, 128.45, 126.99, 124.52, 122.45, 122.06, 120.33, 116.66, 113.90, 111.98, 110.16, 32.73, 21.75. HRMS (ESI) m/z $[\text{M}+\text{H}]$ for $\text{C}_{25}\text{H}_{20}\text{BrN}_2\text{O}_3\text{S}$: 507.0372, found 507.0362.



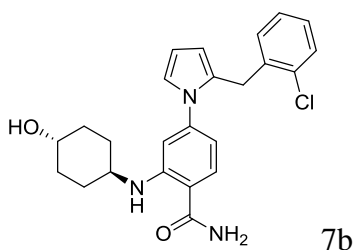
4-((1-(3-bromo-4-cyanophenyl)-1H-pyrrol-2-yl)methyl)phenyl 4-methylbenzenesulfonate

(14c): 71% yield, white solid. ^1H NMR (500 MHz, CDCl_3) δ 7.69 – 7.65 (m, 2H), 7.60 (d, J = 8.3 Hz, 1H), 7.44 (d, J = 2.1 Hz, 1H), 7.31 – 7.27 (m, 2H), 7.16 (dd, J = 8.3, 2.1 Hz, 1H), 6.95 – 6.90 (m, 2H), 6.86 – 6.82 (m, 2H), 6.75 (dd, J = 3.0, 1.7 Hz, 1H), 6.26 (t, J = 3.2 Hz, 1H), 6.06 (m, 1H), 3.87 (s, 2H), 2.43 (s, 3H). ^{13}C NMR (126 MHz, CDCl_3) δ 148.15, 145.39, 144.38, 137.94, 134.74, 132.43, 131.17, 129.87, 129.76, 129.45, 128.48, 125.79, 124.46, 122.49, 122.04, 116.63, 113.85, 111.88, 110.16, 32.55, 21.76. HRMS (ESI) m/z $[\text{M}+\text{Na}]$ for $\text{C}_{25}\text{H}_{19}\text{BrN}_2\text{O}_3\text{SNa}$: 529.0197, found 529.0177.

Following Compounds (7a-n, 11, 15a-c, 16) have been synthesized using general procedure B

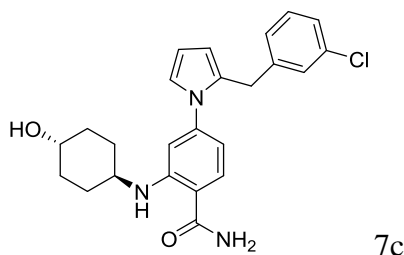


4-(2-benzyl-1H-pyrrol-1-yl)-2-(((1r,4r)-4-hydroxycyclohexyl)amino)benzamide (7a): 44 % yield, white solid. ^1H NMR (500 MHz, CDCl_3) δ 7.87 (d, $J = 7.6$ Hz, 1H), 7.32 – 7.26 (m, 1H), 7.21 (q, $J = 1.3$ Hz, 0H), 7.18 (q, $J = 1.2, 0.8$ Hz, 1H), 7.15 – 7.10 (m, 1H), 7.08 – 7.01 (m, 2H), 6.75 (dd, $J = 2.9, 1.8$ Hz, 1H), 6.34 (d, $J = 7.0$ Hz, 2H), 6.20 (t, $J = 3.2$ Hz, 1H), 6.00 (m, 1H), 5.58 (s, 2H), 3.88 (s, 2H), 3.63 – 3.54 (m, 1H), 2.90 – 2.80 (m, 1H), 1.93 – 1.81 (m, 4H), 1.28 – 1.12 (m, 4H). ^{13}C NMR (126 MHz, CDCl_3) δ 170.40, 149.06, 143.59, 139.05, 130.50, 128.32, 127.37, 125.14, 120.60, 110.62, 110.05, 108.83, 108.13, 107.44, 68.75, 48.65, 32.44, 31.86, 29.12, 28.67. HRMS (ESI) m/z [M-H] for $\text{C}_{24}\text{H}_{26}\text{N}_3\text{O}_2$: 388.2025, found 388.2025.



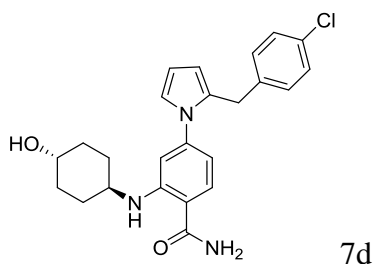
4-(2-(2-chlorobenzyl)-1H-pyrrol-1-yl)-2-(((1r,4r)-4-hydroxycyclohexyl)amino)benzamide (7b): 51 % yield, white solid. ^1H NMR (500 MHz, CDCl_3) δ 7.91 (d, $J = 7.6$ Hz, 1H), 7.33 – 7.25 (m, 2H), 7.13 – 7.01 (m, 3H), 6.78 (dd, $J = 2.9, 1.8$ Hz, 1H), 6.43 – 6.35 (m, 2H), 6.21 (t, $J = 3.2$ Hz, 1H), 5.94 (m, 1H), 5.46 (d, $J = 55.2$ Hz, 2H), 3.97 (s, 2H), 3.60 (s, 1H), 2.94 (s, 1H), 1.90 (m, 4H), 1.27 – 1.13 (m, 4H). ^{13}C NMR (126 MHz, CDCl_3) δ 171.41, 150.18, 144.51, 137.78, 133.76, 130.31, 129.98, 129.54, 129.37, 127.73, 126.83, 121.77, 111.34, 111.09, 110.20,

108.67, 108.65, 69.76, 49.85, 33.52, 30.68, 30.17. HRMS (ESI) m/z $[M-H]$ for $C_{24}H_{25}ClN_3O_2$: 422.1635, found 422.1642.



4-(2-(3-chlorobenzyl)-1H-pyrrol-1-yl)-2-(((1r,4r)-4-hydroxycyclohexyl)amino)benzamide

(7c): 53% yield, white solid. 1H NMR (500 MHz, $CDCl_3$) δ 7.97 (d, $J = 7.6$ Hz, 1H), 7.38 (d, $J = 8.8$ Hz, 1H), 7.20 – 7.16 (m, 2H), 7.07 (td, $J = 1.8, 0.9$ Hz, 1H), 7.01 – 6.97 (m, 1H), 6.83 (dd, $J = 2.9, 1.8$ Hz, 1H), 6.41 – 6.36 (m, 2H), 6.32 – 6.25 (m, 1H), 6.14 – 6.07 (m, 1H), 5.63 (s, 2H), 3.93 (s, 2H), 3.68 (m, 1H), 3.02 – 2.91 (m, 1H), 2.04 – 1.90 (m, 4H), 1.35 – 1.20 (m, 4H). ^{13}C NMR (126 MHz, $CDCl_3$) δ 171.40, 150.10, 144.46, 142.18, 134.20, 130.60, 129.60, 129.39, 128.49, 126.58, 126.37, 121.95, 111.72, 111.32, 110.03, 109.22, 108.53, 69.75, 49.83, 33.50, 32.60, 30.14. HRMS (ESI) m/z $[M-H]$ for $C_{24}H_{25}ClN_3O_2$: 422.1635, found 422.1645.

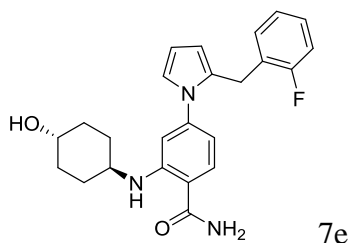


4-(2-(4-chlorobenzyl)-1H-pyrrol-1-yl)-2-(((1r,4r)-4-hydroxycyclohexyl)amino)benzamide

(7d): 44% yield, white solid. 1H NMR (500 MHz, $CDCl_3$) δ 7.95 (d, $J = 7.6$ Hz, 1H), 7.36 (d, $J = 8.3$ Hz, 1H), 7.24 – 7.18 (m, 2H), 7.06 – 6.98 (m, 2H), 6.81 (dd, $J = 2.9, 1.8$ Hz, 1H), 6.38 (dd, $J = 8.3, 2.0$ Hz, 1H), 6.34 (d, $J = 2.0$ Hz, 1H), 6.27 (dd, $J = 3.5, 2.9$ Hz, 1H), 6.08 (m, 1H), 5.61 (s, 2H), 3.91 (s, 2H), 3.64 (m, 1H), 2.89 (m, 1H), 2.01 – 1.89 (m, 4H), 1.27 – 1.22 (m, 4H). ^{13}C NMR (126 MHz, $CDCl_3$) δ 171.37, 150.07, 144.48, 138.68, 131.79, 130.83, 129.73, 129.41,

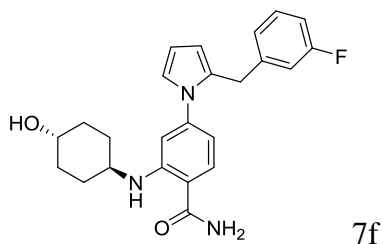
128.52, 121.89, 111.62, 111.21, 109.99, 109.07, 108.53, 69.76, 49.84, 33.62, 32.28, 30.21.

HRMS (ESI) m/z $[M-H]$ for $C_{24}H_{25}ClN_3O_2$: 422.1635, found 422.1642.



4-(2-(2-fluorobenzyl)-1H-pyrrol-1-yl)-2-(((1R,4R)-4-hydroxycyclohexyl)amino)benzamide

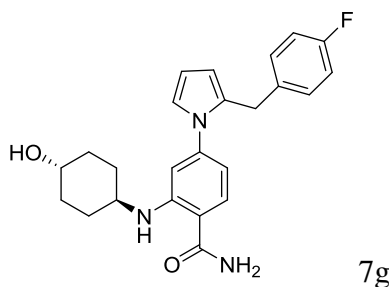
(7e): 48% yield, white solid. 1H NMR (500 MHz, $CDCl_3$) δ 8.08 (s, 1H), 7.40 (d, $J = 8.3$ Hz, 1H), 7.21 – 7.15 (m, 1H), 7.08 – 6.95 (m, 3H), 6.82 (dd, $J = 2.9, 1.8$ Hz, 1H), 6.52 (d, $J = 2.0$ Hz, 1H), 6.46 (dd, $J = 8.3, 2.0$ Hz, 1H), 6.26 (t, $J = 3.2$ Hz, 1H), 6.04 (dd, $J = 3.6, 1.7$ Hz, 1H), 5.69 (s, 2H), 3.97 (s, 2H), 3.67 (m, 1H), 3.04 (m, 1H), 2.10 – 1.90 (m, 4H), 1.37 – 1.23 (m, 4H). ^{13}C NMR (126 MHz, $CDCl_3$) δ 171.38, 161.61, 159.65, 144.53, 130.50, 130.11, 129.48, 127.95, 126.89, 124.03, 121.84, 115.19, 115.02, 112.01, 109.98, 109.42, 108.61, 69.73, 50.24, 33.51, 30.08, 25.89. HRMS (ESI) m/z $[M+H]$ for $C_{24}H_{27}FN_3O_2$: 408.2087, found 408.2086.



4-(2-(3-fluorobenzyl)-1H-pyrrol-1-yl)-2-(((1R,4R)-4-hydroxycyclohexyl)amino)benzamide

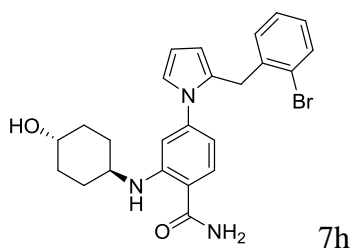
(7f): 42% yield, white solid. 1H NMR (500 MHz, $CDCl_3$) δ 8.08 (s, 1H), 7.38 (d, $J = 8.3$ Hz, 1H), 7.20 (m, 1H), 6.90 – 6.87 (m, 2H), 6.81 (m, 2H), 6.47 – 6.39 (m, 2H), 6.29 – 6.24 (m, 1H), 6.10 (dd, $J = 3.5, 1.7$ Hz, 1H), 5.68 (s, 2H), 3.95 (s, 2H), 3.65 (m, 1H), 2.99 (m, 1H), 2.03 – 1.93 (m, 4H), 1.36 – 1.21 (m, 4H). ^{13}C NMR (126 MHz, $CDCl_3$) δ 171.31, 163.91, 161.95, 144.50, 142.70, 130.69, 129.80, 129.73, 129.41, 123.99, 121.92, 115.36, 115.19, 113.17, 113.01, 110.13,

108.63, 69.70, 50.23, 33.47, 32.62, 30.03. HRMS (ESI) m/z $[M+H]$ for $C_{24}H_{27}FN_3O_2$: 408.2087, found 408.2101.



4-(2-(4-fluorobenzyl)-1H-pyrrol-1-yl)-2-(((1R,4R)-4-hydroxycyclohexyl)amino)benzamide

(7g): 42% yield, white solid. 1H NMR (500 MHz, $CDCl_3$) δ 8.00 (s, 1H), 7.37 (d, $J = 8.1$ Hz, 1H), 7.04 (dd, $J = 8.4, 5.4$ Hz, 2H), 6.97 – 6.88 (m, 2H), 6.80 (t, $J = 2.4$ Hz, 1H), 6.44 – 6.36 (m, 2H), 6.26 (t, $J = 3.2$ Hz, 1H), 6.06 (dd, $J = 3.3, 1.8$ Hz, 1H), 5.84 – 5.44 (m, 2H), 3.91 (s, 2H), 3.67 (m, 1H), 2.97 (t, $J = 8.0$ Hz, 1H), 1.97 (t, $J = 5.5$ Hz, 4H), 1.37 – 1.18 (m, 4H). ^{13}C NMR (126 MHz, $CDCl_3$) δ 171.38, 162.31, 160.37, 149.91, 144.57, 135.64, 131.47, 129.77, 129.37, 121.87, 115.23, 111.89, 109.82, 109.37, 108.48, 69.71, 50.01, 33.55, 32.21, 30.13. HRMS (ESI) m/z $[M-H]$ for $C_{24}H_{25}FN_3O_2$: 406.1931, found 406.1923.

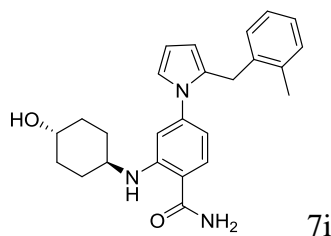


4-(2-(2-bromobenzyl)-1H-pyrrol-1-yl)-2-(((1R,4R)-4-hydroxycyclohexyl)amino)benzamide

(7h): 41% yield, white solid. 1H NMR (500 MHz, $CDCl_3$) δ 7.62 – 7.54 (m, 1H), 7.52 (dd, $J = 7.9, 1.3$ Hz, 1H), 7.25 – 7.18 (m, 2H), 7.12 – 7.02 (m, 2H), 6.92 – 6.81 (m, 2H), 6.75 (d, $J = 8.4$ Hz, 1H), 6.30 (t, $J = 3.2$ Hz, 1H), 6.04 (dd, $J = 3.5, 1.7$ Hz, 1H), 4.05 (s, 2H), 3.71 – 3.63 (m, 1H), 3.09 – 3.03 (m, 1H), 1.99 (t, $J = 14.8$ Hz, 4H), 1.46 – 1.31 (m, 2H). ^{13}C NMR (126 MHz, $CDCl_3$) δ 170.55, 170.55, 162.20, 144.60, 144.60, 139.19, 133.52, 132.66, 130.36, 130.01,

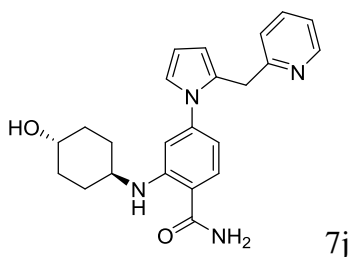
129.67, 128.09, 127.59, 124.25, 121.92, 111.11, 109.40, 69.41, 53.45, 31.60, 29.71, 29.17.

HRMS (ESI) m/z [M-H] for $C_{24}H_{26}BrN_3O_2$: 466.1130, found 466.1123.



2-(((1r,4r)-4-hydroxycyclohexyl)amino)-4-(2-(2-methylbenzyl)-1H-pyrrol-1-yl)benzamide

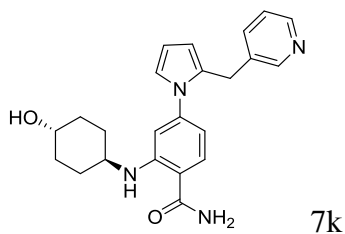
(7i): 45% yield, white solid. 1H NMR (500 MHz, $CDCl_3$) δ 8.20 – 7.76 (m, 1H), 7.35 – 7.31 (m, 1H), 7.08 (m, 3H), 6.98 (m, 1H), 6.78 (dd, $J = 2.9, 1.8$ Hz, 1H), 6.46 – 6.40 (m, 2H), 6.19 (t, $J = 3.2$ Hz, 1H), 5.87 (m, 1H), 5.68 (d, $J = 57.1$ Hz, 2H), 3.80 (s, 2H), 3.68 – 3.52 (m, 1H), 2.87 (s, 1H), 2.12 (s, 3H), 1.94 – 1.81 (m, 4H), 1.26 – 1.15 (m, 4H). ^{13}C NMR (126 MHz, $CDCl_3$) δ 171.37, 144.69, 144.69, 138.29, 136.00, 131.09, 130.08, 130.00, 129.49, 129.21, 128.86, 126.48, 126.45, 126.13, 121.44, 120.38, 110.05, 108.71, 69.74, 50.20, 33.44, 30.69, 30.05, 19.44. HRMS (ESI) m/z [M+H] for $C_{25}H_{30}N_3O_2$: 404.2338, found 404.2350.



2-(((1r,4r)-4-hydroxycyclohexyl)amino)-4-(2-(pyridin-2-ylmethyl)-1H-pyrrol-1-

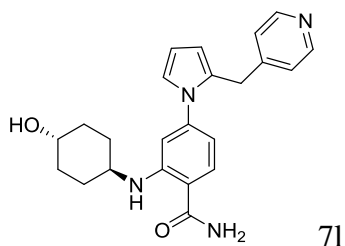
yl)benzamide (7j): 48% yield, white solid. 1H NMR (400 MHz, $CDCl_3$) δ 8.52 (d, $J = 5.0$ Hz, 1H), 7.95 (s, 1H), 7.69 (s, 1H), 7.43 (d, $J = 8.4$ Hz, 1H), 7.24 – 7.10 (m, 2H), 6.87 (s, 1H), 6.47 (d, $J = 7.3$ Hz, 2H), 6.31 (t, $J = 3.2$ Hz, 1H), 6.17 (s, 1H), 5.32 (s, 2H), 4.27 (s, 2H), 3.70 (s, 1H), 3.08 (s, 1H), 1.99 (s, 4H), 1.37 – 1.26 (m, 4H). ^{13}C NMR (126 MHz, $CDCl_3$) δ 171.47, 159.98, 150.15, 149.08, 144.48, 136.73, 129.53, 128.34, 122.82, 121.87, 121.39, 111.66, 111.23, 110.07,

109.07, 108.77, 69.74, 49.81, 35.60, 33.52, 30.11. HRMS (ESI) m/z $[M+H]$ for $C_{23}H_{25}N_4O_2$: 389.1978, found 389.1969.



2-(((1r,4r)-4-hydroxycyclohexyl)amino)-4-(2-(pyridin-3-ylmethyl)-1H-pyrrol-1-yl)

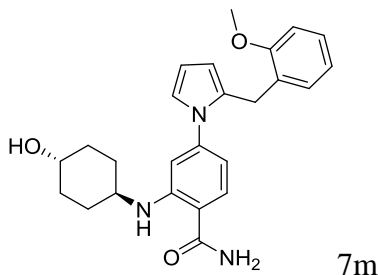
benzamide (7k): 44% yield, white solid. 1H NMR (500 MHz, $CDCl_3$) δ 8.38 (d, $J = 55.8$ Hz, 2H), 8.00 (d, $J = 7.5$ Hz, 1H), 7.43 (m, 1H), 7.38 (d, $J = 8.3$ Hz, 1H), 7.19 (dd, $J = 7.8, 4.8$ Hz, 1H), 6.82 (dd, $J = 2.9, 1.8$ Hz, 1H), 6.44 (d, $J = 2.0$ Hz, 1H), 6.36 (dd, $J = 8.3, 2.0$ Hz, 1H), 6.26 (dd, $J = 3.5, 2.9$ Hz, 1H), 6.07 (m, 1H), 5.78 (d, $J = 111.9$ Hz, 2H), 3.96 (s, 2H), 3.69 (m, 1H), 3.09 (m, 1H), 2.05 – 1.96 (m, 4H), 1.37 – 1.29 (m, 4H). ^{13}C NMR (126 MHz, $CDCl_3$) δ 171.36, 150.16, 149.80, 147.54, 144.36, 136.11, 135.33, 130.44, 129.50, 123.35, 122.20, 111.70, 111.54, 109.89, 109.12, 108.54, 69.70, 49.97, 33.55, 30.41, 30.15. HRMS (ESI) m/z $[M+H]$ for $C_{23}H_{25}N_4O_2$: 389.1978, found 389.1970.



2-(((1r,4r)-4-hydroxycyclohexyl)amino)-4-(2-(pyridin-4-ylmethyl)-1H-pyrrol-1-

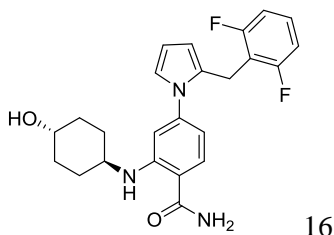
yl)benzamide (7l): 48% yield, white solid. 1H NMR (500 MHz, $CDCl_3$) δ 8.52 – 8.44 (m, 2H), 8.01 (s, 1H), 7.34 (d, $J = 8.3$ Hz, 1H), 7.14 (d, $J = 5.4$ Hz, 2H), 6.84 (dd, $J = 2.9, 1.8$ Hz, 1H), 6.36 (d, $J = 2.0$ Hz, 1H), 6.31 – 6.25 (m, 2H), 6.16 (dd, $J = 3.4, 1.8$ Hz, 1H), 5.54 (d, $J = 99.5$ Hz, 2H), 4.02 (s, 2H), 3.66 (dd, $J = 10.4, 4.8$ Hz, 1H), 2.98 (d, $J = 10.2$ Hz, 1H), 2.02 – 1.94 (m,

4H), 1.34 – 1.27 (m, 4H). ^{13}C NMR (126 MHz, CDCl_3) δ 171.20, 171.20, 150.14, 147.37, 144.12, 129.58, 128.50, 124.40, 122.58, 111.54, 110.60, 109.24, 109.00, 108.78, 69.63, 50.00, 33.56, 32.68, 30.15. HRMS (ESI) m/z $[\text{M}-\text{H}]$ for $\text{C}_{23}\text{H}_{25}\text{N}_4\text{O}_2$: 389.1978, found 389.1983.



2-(((1r,4r)-4-hydroxycyclohexyl)amino)-4-(2-(2-methoxybenzyl)-1H-pyrrol-1-yl)benzamide

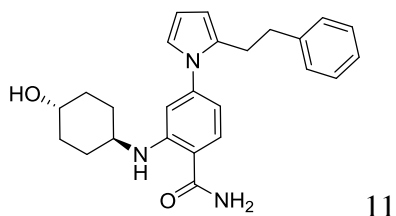
(7m): 51% yield, white solid. ^1H NMR (500 MHz, CDCl_3) δ 7.93 (d, $J = 7.4$ Hz, 1H), 7.35 (d, $J = 8.3$ Hz, 1H), 7.19 (m, 1H), 6.99 (m, 1H), 6.89 – 6.80 (m, 3H), 6.51 – 6.41 (m, 2H), 6.26 (dd, $J = 3.4, 2.9$ Hz, 1H), 6.03 (m, 1H), 5.53 (s, 2H), 3.91 (s, 2H), 3.75 (s, 3H), 3.71 – 3.58 (m, 1H), 2.95 (d, $J = 30.9$ Hz, 1H), 1.99 – 1.88 (m, 4H), 1.30 – 1.16 (m, 4H). ^{13}C NMR (126 MHz, CDCl_3) δ 171.51, 156.91, 150.08, 144.75, 131.25, 129.55, 129.36, 128.73, 127.42, 121.32, 120.48, 111.52, 110.85, 110.01, 109.86, 108.83, 108.55, 69.79, 55.30, 49.72, 33.47, 30.16, 26.77. HRMS (ESI) m/z $[\text{M}+\text{H}]$ for $\text{C}_{25}\text{H}_{30}\text{N}_3\text{O}_3$: 420.2287, found 420.2292.



4-(2-(2,6-difluorobenzyl)-1H-pyrrol-1-yl)-2-(((1r,4r)-4-hydroxycyclohexyl)amino)benzamide

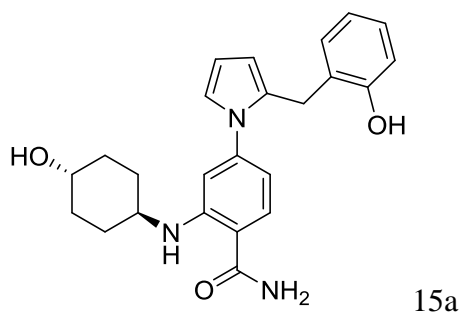
(16): 55% yield, white solid. ^1H NMR (500 MHz, CDCl_3) δ 8.01 (s, 1H), 7.38 (d, $J = 8.3$ Hz, 1H), 7.16 – 7.06 (m, 1H), 6.82 – 6.77 (m, 2H), 6.70 (dd, $J = 2.9, 1.8$ Hz, 1H), 6.61 (d, $J = 2.0$ Hz, 1H), 6.49 (dd, $J = 8.3, 2.0$ Hz, 1H), 6.11 (t, $J = 3.2$ Hz, 1H), 5.85 – 5.38 (m, 3H), 3.88 (d, $J = 1.4$ Hz, 2H), 3.64 (m, 1H), 3.24 (s, 1H), 2.10 – 1.90 (m, 4H), 1.39 – 1.26 (m, 4H). ^{13}C NMR (126

MHz, CDCl₃) δ 171.47, 162.48, 160.51, 150.17, 144.59, 130.97, 129.95, 129.51, 128.11, 121.80, 112.00, 111.44, 111.28, 111.07, 109.56, 108.50, 108.40, 69.84, 50.22, 33.65, 30.24, 20.18. HRMS (ESI) m/z [M-H] for C₂₄H₂₄F₂N₃O: 424.1837, found 424.1838.



2-(((1r,4r)-4-hydroxycyclohexyl)amino)-4-(2-phenethyl-1H-pyrrol-1-yl)benzamide (11):

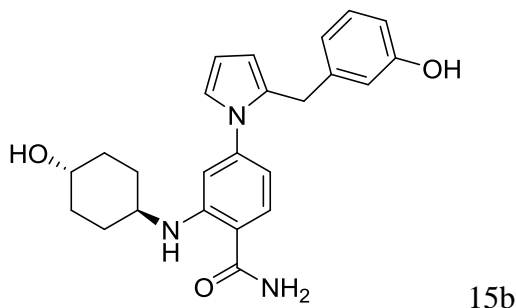
45% yield, white solid. ¹H NMR (500 MHz, CDCl₃) δ 8.10 (s, 1H), 7.41 (d, *J* = 8.2 Hz, 1H), 7.24 (d, *J* = 7.5 Hz, 2H), 7.20 – 7.14 (m, 1H), 7.13 – 7.07 (m, 2H), 6.79 (t, *J* = 2.3 Hz, 1H), 6.62 (s, 1H), 6.47 (dd, *J* = 8.4, 2.1 Hz, 1H), 6.25 (t, *J* = 3.1 Hz, 1H), 6.15 (dd, *J* = 3.4, 1.7 Hz, 1H), 5.67 (s, 2H), 3.70 (m, 1H), 3.26 (m, 1H), 2.97 – 2.81 (m, 4H), 2.14 – 1.95 (m, 4H), 1.42 – 1.29 (m, 4H). ¹³C NMR (126 MHz, CDCl₃) δ 171.39, 149.99, 144.79, 141.55, 133.06, 129.48, 128.36, 128.27, 126.02, 121.43, 111.81, 111.33, 109.20, 108.37, 107.69, 69.75, 50.39, 35.47, 33.62, 30.17, 29.26. HRMS (ESI) m/z [M-H] for C₂₅H₂₈N₃O₂: 402.2181, found 402.2176.



4-(2-(2-hydroxybenzyl)-1H-pyrrol-1-yl)-2-(((1r,4r)-4-hydroxycyclohexyl)amino)benzamide

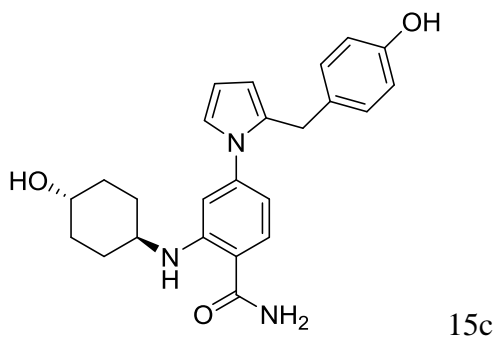
(15a) 46% yield, white solid. ¹H NMR (500 MHz, CDCl₃) δ 7.31 (d, *J* = 8.4 Hz, 1H), 7.03 – 6.97 (m, 1H), 6.89 (dd, *J* = 7.6, 1.7 Hz, 1H), 6.78 – 6.76 (m, 1H), 6.74 – 6.68 (m, 2H), 6.47 (d, *J* = 2.0 Hz, 1H), 6.40 (dd, *J* = 8.3, 2.0 Hz, 1H), 6.21 – 6.15 (m, 1H), 6.02 – 5.95 (m, 1H), 5.53 (s,

2H), 3.88 (s, 2H), 3.57 (tt, $J = 10.1, 4.2$ Hz, 1H), 2.91 (m, 1H), 1.95 – 1.82 (m, 4H), 1.26 – 1.12 (m, 4H). ^{13}C NMR (126 MHz, CDCl_3) δ 172.86, 161.06, 159.17, 148.66, 130.08, 129.49, 127.47, 126.26, 121.92, 120.07, 115.19, 111.67, 109.15, 108.47, 106.83, 102.07, 99.99, 69.67, 60.50, 33.24, 30.18, 27.34. HRMS (ESI) m/z $[\text{M}+\text{Na}]$ for $\text{C}_{24}\text{H}_{27}\text{N}_3\text{O}_3\text{Na}$: 428.1950, found 428.1949.



4-(2-(3-hydroxybenzyl)-1H-pyrrol-1-yl)-2-(((1R,4R)-4-hydroxycyclohexyl)amino)benzamide

(15b): 42% yield, white solid. ^1H NMR (400 MHz, CDCl_3) δ 7.80 (d, $J = 7.9$ Hz, 1H), 7.38 (d, $J = 8.3$ Hz, 1H), 7.12 (t, $J = 7.8$ Hz, 1H), 6.83 (dd, $J = 2.9, 1.8$ Hz, 1H), 6.74 – 6.63 (m, 3H), 6.44 (dd, $J = 8.4, 2.0$ Hz, 1H), 6.35 – 6.28 (m, 2H), 6.19 (dd, $J = 3.4, 1.8$ Hz, 1H), 3.91 (s, 2H), 5.61–5.90 (s, 2H) 3.64 (q, $J = 10.8$ Hz, 1H), 2.65 (s, 1H), 1.89 (d, $J = 11.3$ Hz, 4H), 1.24 – 1.10 (m, 4H). ^{13}C NMR (126 MHz, CDCl_3) δ 168.64, 166.43, 162.90, 157.79, 152.71, 148.84, 141.58, 119.49, 117.65, 115.39, 113.27, 109.31, 106.40, 99.52, 94.41, 90.08, 86.38, 68.98, 61.90, 46.01, 31.76, 28.83. HRMS (ESI) m/z $[\text{M}+\text{Na}]$ for $\text{C}_{24}\text{H}_{27}\text{N}_3\text{O}_3\text{Na}$: 428.1950, found 428.1974.



4-(2-(4-hydroxybenzyl)-1H-pyrrol-1-yl)-2-(((1r,4r)-4-hydroxycyclohexyl)amino)benzamide

(15c): 42% yield, white solid. ^1H NMR (400 MHz, CDCl_3) δ 7.82 (d, $J = 8.5$ Hz, 1H), 7.38 (d, $J = 8.4$ Hz, 1H), 7.01 (d, $J = 8.2$ Hz, 2H), 6.89 (d, $J = 8.5$ Hz, 1H), 6.82 (dd, $J = 2.9, 1.8$ Hz, 1H), 6.81 – 6.74 (m, 2H), 6.68 (d, $J = 8.2$ Hz, 1H), 6.44 (dd, $J = 8.4, 2.0$ Hz, 1H), 6.32 – 6.29 (m, 2H), 6.16 (d, $J = 3.6$ Hz, 1H), 5.45-5.80 (s, 2H), 3.89 (s, 2H), 3.61 (s, 1H), 2.62 (s, 1H), 1.88 (m, 4H), 1.19 (m, 4H). ^{13}C NMR (126 MHz, CDCl_3) δ 171.93, 154.50, 144.57, 132.16, 131.00, 129.49, 129.34, 128.94, 121.36, 115.87, 111.30, 110.41, 108.72, 108.61, 108.42, 70.03, 55.99, 33.12, 31.52, 30.28. HRMS (ESI) m/z $[\text{M}+\text{H}]$ for $\text{C}_{24}\text{H}_{28}\text{N}_3\text{O}_3$: 406.2131, found 406.2135.

6. References

1. Hartl, F. U. Molecular chaperones in cellular protein folding. *Nature* **1996**, *381*, 571-579.
2. Hartl, F.U. Molecular chaperones in protein folding and proteostasis. *Nature* **2011**, *475*, 324-332.
3. Donnelly, A.; Blagg, B. S. J., Novobiocin and Additional Inhibitors of the Hsp90 C-Terminal Nucleotide-binding Pocket. *Curr. Med. Chem.* **2008**, *15*, 2702-2717.
4. Powers MV, Workman P. Inhibitors of the heat shock response :biology and pharmacology. *FEBS Lett* **2007**, *581*, 3758–69.
5. Whitesell, L.; Bagatell, R.; Falsey, R. The stress response: implications for the clinical development of Hsp90 inhibitors. *Curr. Cancer Drug Targets* **2003**, *3*, 349-358.
6. Whitesell, L.; Lindquist, S. L. Hsp90 and the chaperoning of cancer. *Nat. Rev. Cancer* **2005**, *5*, 761-772.
7. Zhang, H.; Burrows, F. Targeting multiple signal transduction pathways through inhibition of Hsp90. *J. Mol. Med.* **2004**, *82*, 488-499.
8. Yu, X.M.; Shen, G.; Neckers, L.; Blake, H.; Holzbeierlein, J.; Cronk, B.; Blagg, B.S.J. Hsp90 inhibitors identified from a library of novobiocin analogues. *J. Am. Chem. Soc.* **2005**, *127*, 12778-12779.
9. Burlison, J.A.; Blagg, B.S.J. Synthesis and evaluation of coumermycin A1 analogues that inhibit the Hsp90 protein folding machinery. *Org. Lett.* **2006**, *8*, 4855-4858.
10. Burlison, J.A.; Neckers, L.; Smith, A.B.; Maxwell, A.; Blagg, B.S.J. Novobiocin: redesigning a DNA gyrase inhibitor for selective inhibition of Hsp90. *J. Am. Chem. Soc.* **2006**, *128*, 15529-15536.
11. Burlison, J.A.; Avila, C.; Vielhauer, G.; Lubbers, D.J.; Holzbeierlein, J.; Blagg, B.S.J. Development of novobiocin analogues that manifest anti-proliferative activity against several cancer cell lines. *J. Org. Chem.* **2008**, *73*, 2130-2137.
12. Donnelly, A.C.; Mays, J.R.; Burlison, J.A.; Nelson, J.T.; Vielhauer, G.; Holzbeierlein, J.; Blagg, B.S.J. The design, synthesis, and evaluation of coumarin ring derivatives of the novobiocin scaffold that exhibit antiproliferative activity. *J. Org. Chem.*, **2008**, *73*, 8901-8920.
13. Picard D, Khursheed B, Garabedian MJ, Fortin MG, Lindquist S, Yamamoto KR. Reduced levels of hsp90 compromise steroid receptor action in vivo. *Nature* **1990**, *348*, 166-8.
14. Stancato LF, Chow YH, Hutchison KA, Perdew GH, Jove R, Pratt WB. Raf exists in a native heterocomplex with hsp90 and p50 that can be reconstituted in a cell-free system. *J Biol Chem* **1993**, *268*, 21711-6.
15. Sreedhar, A.S.; Kalmar, E.; Csermely, P.; Shen, Y.F. Hsp90 isoforms: functions, expression and clinical importance. *FEBS Lett.*, **2004**, *562*, 11-15.
16. Pearl, L.H.; Prodromou, C. Structure and in vivo function of Hsp90. *Curr. Opin. Struct. Biol.* **2000**, *10*, 46-51.
17. Prodromou, C., Pearl, L.H. Structure and functional relationships of Hsp90. *Curr. Cancer Drug Targets* **2003**, *3*, 301-323.
18. DeBoer C, Meulman PA, Wnuk RJ, Peterson DH., Geldanamycin, a new antibiotic. *J Antibiot* **1970**, *23*, 442-7.
19. Whitesell, L.; Mimnaugh, E. G.; De Costa, B.; Myers, C. E.; Neckers, L. M., Inhibition of heat shock protein HSP90-pp60v-src heteroprotein complex formation by benzoquinone ansamycins: essential role for stress proteins in oncogenic transformation *Proc. Natl. Acad. Sci. USA* **1994**, *91*, 8324-8.

20. Messaoudi, S.; Peyrat, J. F.; Brion, J. D.; Alami, M., Recent advances in Hsp90 inhibitors as antitumor agents. *Anti-cancer agents med. chem.* **2008**, *8*, 761-82.
21. Kim, Y. S.; Alarcon, S. V.; Lee, S.; Lee, M. J.; Giaccone, G.; Neckers, L.; Trepel, J. B. Update on Hsp90 inhibitors in clinical trial. *Curr. Top. Med. Chem.* **2009**, *9*, 1479-1492.
22. Biamonte, M. A.; Van de Water, R.; Arndt, J. W.; Scannevin, R. H.; Perret, D.; Lee, W. Heat shock protein 90: inhibitors in clinical trials. *J. Med. Chem.* **2010**, *53*, 3-17.
23. Peterson, L.B.; Esker, J.D.; Vielhauer, G.A.; Blagg, B.S. The hERG channel is dependent upon the Hsp90 α isoform for maturation and trafficking. *Mol. Pharm.*, **2012**, *9*, 1841-1846.
24. Sreedhar, A.S.; Kalmar, E.; Csermely, P.; Shen, Y.F. Hsp90 isoforms: functions, expression and clinical importance. *FEBS Lett.*, **2004**, *562*, 11-15.
25. Kozutsumi, Y.; Segal, M.; Normington, K.; Gething, M.; Sambrook, J. The presence of malformed proteins in the endoplasmic reticulum signals the induction of glucose-regulated proteins. *Nature* **1988**, *332*, 462-464.
26. Li, Z.; Srivastava, P. K., Tumor rejection antigen gp96/grp94 is an ATPase: implications for protein folding and antigen presentation. *EMBO J*, **1993**, *12*, 3143-51.
27. Goodman, S.L.; Picard, M. Integrins as therapeutic targets. *Trends Pharmacol. Sci.*, **2012**, *33*, 405-412.
28. Dejeans, N.; Glorieux, C.; Guenin, S.; Beck, R.; Sid, B.; Rousseau, R.; Bisig, B.; Delvenne, P.; Buc Calderon, P.; Verrax, J. Overexpression of Grp94 in breast cancer cells resistant to oxidative stress promotes high levels of cancer cell proliferation and migration: implications for tumor recurrence. *Free Radic. Biol. Med.*, **2012**, *52*, 993-1002.
29. Suntharalingam, A.; Abisambra, J.F.; O'Leary, J.C. III; Koren, J. III; Zhang, B.; Joe, M.K.; Blair, L.J.; Hill, S.E.; Jinwal, U.K.; Cockman, M.; Duerfeldt, A.S.; Tomarev, S.; Blagg, B.S.; Lieberman, R.L.; Dickey, C.A. Glucose-regulated protein 94 triage of mutant myocilin through endoplasmic reticulum-associated degradation subverts a more efficient autophagic clearance mechanism. *J. Biol. Chem.*, **2012**, *287*, 40661-40669.
30. Gullo, C.A.; Teoh, G. Heat shock protein: to present or not, that is the question. *Immunol. Lett.*, **2004**, *94*, 1-10.
31. Obeng, E.A.; Carlson, L.M.; Gutman, D.M.; Harrington, W.J.; Lee, K.P.; Boise, L.H. Proteasome inhibitors induce a terminal unfolded protein response in myeloma cells. *Blood*, **2006**, *107*, 4907-4916.
32. Hua, Y.; White-Gilbertson, S.; Kellner, J.; Rachidi, S.; Usmani, S.Z.; Chiosis, G.; DePinho, R.; Li, Z.; Liu, B. Molecular chaperone gp96 is a novel therapeutic target for multiple myeloma. *Clin. Cancer Res.*, **2013**, *19*, 6242-6251.
33. Barta, T.; Veal, J.; Rice, J.; Partridge, J.; Fadden, R.; Ma, W.; Jenks, M.; Geng, L.; Hanson, G.; Huang, K. et al. Discovery of benzamide tetrahydro-4H-carbazol-4-ones as novel small molecule inhibitors of Hsp90. *Bioorg. Med. Chem. Lett.*, **2008**, *18*, 3517-3521.
34. Huang, K.; Veal, J.; Fadden, R.; Rice, J.; Eaves, J.; Strachan, J.; Barabasz, A.; Foley, B.; Barta, T.; Ma, W. et al. Discovery of Novel 2-Aminobenzamide Inhibitors of Heat Shock Protein 90 as Potent, Selective and Orally Active Antitumor Agents. *J. Med. Chem.*, **2009**, *52*, 4288-4305.
35. Ernst, J. T.; Liu, M.; Zuccola, H.; Neubert, T.; Beaumont, K.; Turnbull, A.; Kallel, A.; Vought, B.; Stamos, D., Correlation between chemotype-dependent binding conformations of HSP90 α/β and isoform selectivity—Implications for the structure-based design of HSP90 α/β selective inhibitors for treating neurodegenerative diseases. *Bioorg. Med. Chem. Lett.*, **2014**, *24*, 204-208.
36. Gilow, H.; Burton, D. Bromination and chlorination of pyrrole and some reactive 1-substituted pyrroles. *J. Org. Chem.* **1981**, *46*, 2221-2225.

37. Chen, W.; Stephenson, E. K.; Cava, M. P.; Jackson, Y. A., 2-Substituted Pyrroles from N-tert-Butoxycarbonyl-2-Bromopyrrole: N-tert-Butoxycarbonyl-2-Trimethylsilylpyrrole. In *Organic Syntheses*, John Wiley & Sons, Inc.: 2003.
38. Chakrabarty, M.; Kundu, T.; Harigaya, Y. Mild Deprotection Of Tert -Butyl Carbamates Of NH-Heteroarenes Under Basic Conditions. *Synthetic Communications*, **2006**, *36*, 2069-2077.
39. Bohm, H. J.; Banner, D.; Bendels, S.; Kansy, M.; Kuhn, B.; Muller, K.; Obst-Sander, U.; Stahl, M., Fluorine in medicinal chemistry. *Chembiochem* **2004**, *5*, 637-43.
40. Clark, D. L.; Egbertson, M.; Guare, J. P.; Hazuda, D. J.; Medina, J. C.; Selnick, H. G.; Wai, J. S.; Young, S. D., Hiv integrase inhibitors. WO1999062513, Dec 09, **1999**.